The Thesis Committee for Leandro Sebastian Montagna
Certifies that this is the approved version of the following thesis:

Two-way Shear Strength of Reinforced Concrete Slab-Column Connections: Influence of Testing Conditions in Isolated Specimens

APPROVED BY
SUPERVISING COMMITTEE:

Supervisor:

Trevor D Hrynyk

Juan Murcia-Delso

Two-way Shear Strength of Reinforced Concrete Slab-Column Connections: Influence of Testing Conditions in Isolated Specimens

by

Leandro Sebastian Montagna

Thesis

Presented to the Faculty of the Graduate School of

The University of Texas at Austin

in Partial Fulfillment

of the Requirements

for the Degree of

Master of Science in Engineering

The University of Texas at Austin

May 2018

Acknowledgements

Only a few times in my life have I felt the support and encouragement to pursue my goals that I found while studying and researching here at the University of Texas at Austin. For that reason, I would like to thank my supervisor, Dr. Trevor D Hrynyk, for the opportunity to join his research team and his relentless dedication and teachings that shape this Thesis. I would also like to express my gratitude to Dr. Juan Murcia-Delso for taking the time to read this Thesis and Ph.D. candidate Gabriel Polo, with whom I worked at the Ferguson Structural Eng. Laboratory (FSEL), for his companionship in this journey.

Nobody is a self-made man, we all need help eventually and, when needed, they all were there for us. Therefore, I would like to thank all the Staff at FSEL and all other students at FSEL that help us make of the experimental program a starling success.

Because I would not be here if it were not for their unconditional love and support, I would like to express my deepest gratitude to my spouse, family, especially my parents, and friends that made it all possible.

I would like to share this accomplishment with all the people at the Fulbright program who believed in me and grant me the opportunity of a life time.

I owe a debt of gratitude to the University of Texas at Austin that took me in and make me feel I am home.

Finally, I would like to thank the American people for believing that the "international educational exchange is the most significant […] designed to continue the process of humanizing mankind to the point, we would hope, that men can learn to live in peace--eventually even to cooperate in constructive activities rather than compete in a mindless contest of mutual destruction" [Senator J. Fulbright].

Abstract

Two-way Shear Strength of Reinforced Concrete Slab-Column Connections: Influence of Testing Conditions in Isolated Specimens

Leandro Sebastian Montagna M.S.E.

The University of Texas at Austin, 2018

Supervisor: Trevor D Hrynyk

To assess the two-way shear resistance, or punching shear strength, of reinforced concrete slabs, code provisions fitted from experimental data are typically employed. The experimental data forming the bases of these provisions have generally consisted of isolated slab-column connection tests that seek to represent the negative moment region of a flat plate slab.

This research is focused on exploring the variation in the punching performance of slab-column connections when the typical testing conditions used to investigate isolated slab specimen are varied in a manner that produces alternative sectional loading conditions within the column connection region. To accomplish this, an innovative testing apparatus is introduced that permits alternative combinations of slab bending moment to out-of-plane shear force ratios to be applied to the slab-column connection.

Results are presented from an experimental program conducted at the Ferguson Structural Engineering Laboratory (FSEL) of The University of Texas at Austin and an analysis is presented comparing the results from the tests with estimations made from

current standards, the Critical Crack Shear Theory (CSCT), and also from numerical models. The data obtained from the experimental program are used to scrutinize current design and analysis procedures, and to shed light on the significance of the sectional loading conditions in the light of flat plate connection shear resisting performance.

Table of Contents

List of Tables

List of Figures

Chapter 1: Introduction

SCOPE

Flat slabs and flat plates are nonprestressed reinforced concrete (RC) slabs that contain flexural reinforcement in two directions, but are constructed without beams between supports (i.e., columns). Examples of flat slab and flat plate systems are presented in Figure 1-1.

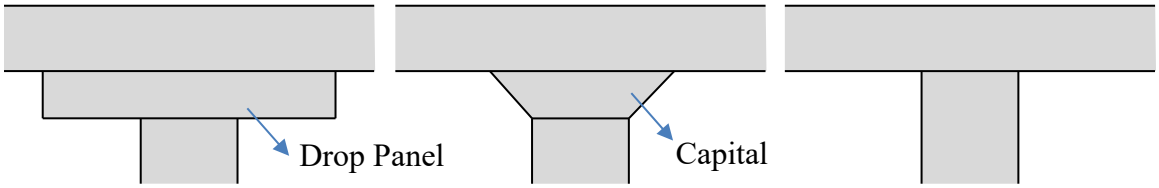

Figure 1-1: Flat slab systems (left and center) and flat plate systems (right)

The applications of these slab systems, for a wide variety of uses, are becoming more popular mainly due to their ease of construction and their architectural appeal which permits more economical and esthetically sound buildings as compared to many other conventional slabs systems. For these types of slab systems, particularly in the case of flat plates, the punching resistance, or the two-way shear strength, of the slabs in the vicinities of the column-supported regions has been the focus of extensive investigation since for several decades. This research has been largely motivated by the fact that punching failures involve typically brittle failure mechanisms and, as such, can propagate the partial, or even total, collapse of a structure (Hawkins and Mitchell 1979).

To experimentally assess the punching shear strength of RC flat plates, isolated slab elements loaded by way of some form of integrated column stub are commonly considered. These specimens seek to represent the negative moment region comprising the slab-column connection region. In Figure 1-2, the isolated RC element representing the negative

moment region of the slab-column connection is illustrated as a square slab element but others (e.g., Muttoni 2008) have also used circular or polygonal shapes to investigate connection shear capacity.

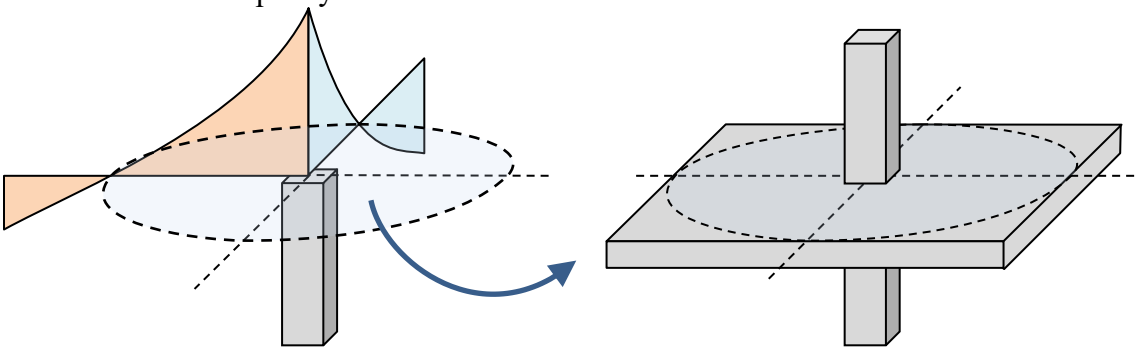

Figure 1-2: Negative moment region of the slab-column connection.

Phenomena such as moment redistribution between negative bending moment regions (located within connection regions) and positive bending moments (located outside of the connection regions) flexural moments and compressive membrane action do not occur in isolated specimens and are likely to increase the actual punching shear strength of RC flat plate systems (Einpaul et al. 2016; Goh and Hrynyk 2018). Thus, punching shear strength design provisions that have typically been derived on the basis of data obtained from experiments done on isolated specimens, typically provide conservative estimations.

This research focuses on exploring the variation in the punching shear strength of RC slab-column connections when the applied loading is changed from concentrated loading conditions, which are typical to these types of tests, to the application of loads that are distributed over the slab surface, as illustrated in Figure 1-3. This change influences the combination of bending moment and out-of-plane shear applied to the slab-column connection. Additionally, the results obtained from the experiments will be contrasted with shear strength estimates obtained from current European and American building codes: i) ACI 318-14 (American Concrete Institute Committee 318 2014), ii) Eurocode 2 (European

Committee for Standardization 2004), and other formulations such as iii) *fib* Model Code 2010 (International Federation for Structural Concrete 2010), and iv) Critical Shear Crack Theory (CSCT) (Muttoni 2008).

Finally, it should also be note that the research presented in this thesis is limited to the investigation of slab-column connections constructed without shear reinforcement.

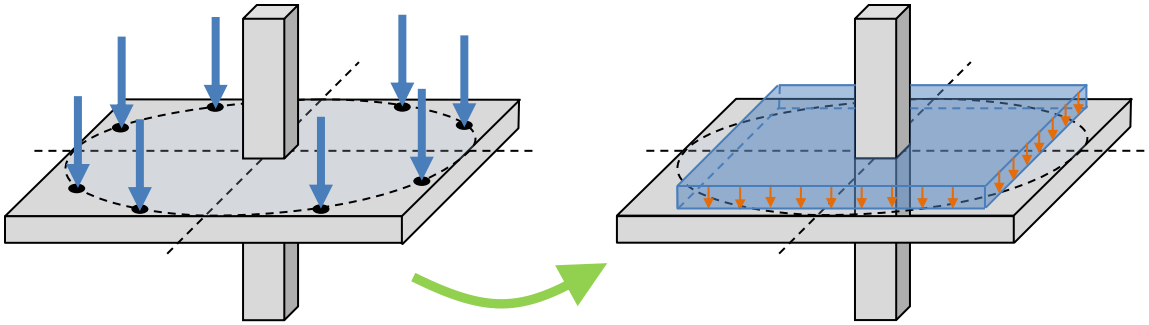

Figure 1-3: Isolated RC element with concentrated loading conditions (left) and with loads distributed over the slab surface (right).

MOTIVATION AND OBJECTIVES

Current North-American two-way shear design provisions are generally very simple to use and practical; however, it has been noted that, in some cases, they can tend to produce highly-conservative designs but, in others, may produce designs with little-to-no conservatism (Moehle et al. 1988; Joint ACI-ASCE Committee 352 1988). The current specifications provided in these codes (ACI 318-14 and CSA A23.3) are primarily based on research conducted between the 1960s and 1970s (Bayrak and Jirsa 2009), and much has been unveiled since.

The main goal of this thesis is to compose a comparative analysis between different known assessment models for punching shear strength, understanding their foundations and fundamental concepts, to examine their performance when compared to data obtained from full-scale tests and numerical models. Additionally, it is also of interest to review the

influence of key design parameters on the shear resisting performance of RC slabs in the context of what is employed in existing North-American provisions.

ORGANIZATION

This thesis is divided into *three* main parts.

The *first* part of the thesis involves an overview of the main formulations given in building codes and know analytical models to estimate the punching shear strength of slab-column connections. A comparison between the different provisions is presented noting the strengths and weaknesses of each method and the two-way shear capacity is estimated for the slab-column connections included in the experimental program, detailed in chapter 3, according to all the discussed documents.

The *second* stage comprehends a detailed description of the experimental program carried out showing the main characteristics of the testing apparatus and the specimens as well as the implemented instrumentation, materials used and their properties, and a summary of the obtained results, including measured deflections, relationship between the shear resistance and the rotation of the slab, strains in the steel reinforcement and pictures showing the failure mode. A comparison is made between the results obtained from the experiments and conclusions are drawn considering the variation on the punching shear strength produced by the change in loading conditions.

In the *third* and last stage are gathered the results from numerical models, computer simulations using finite element method of the tested specimens. The results are contrasted with the experiments to analyze their validity and a discussion of the results is presented to describe differences in the results obtained from the numerical models and the experiments.

This thesis contains 5 chapters. Beyond the introduction and background material provided in Chapters 1 and 2, the experimental program and the obtained results are

detailed in Chapter 3, the results from computer simulations and the comparative analysis with the experimental data are compiled in Chapter 4, and the conclusions drawn from the research study are noted in the final chapter.

Chapter 2: Formulations to estimate punching shear strength

In this chapter, current code provisions and analytical models used to estimate punching shear strength of RC flat plate slab-column connections are summarized and discussed. The scope of this section is limited to the following standards and models:

(1) ACI Committee 318 (2014). "318-14: Building Code Requirements for Structural Concrete and Commentary".

(2) European Committee for Standardization (2004). "Eurocode 2: Design of Concrete Structures".

(3) International Federation for Structural Concrete (2010). "The *fib* Model Code for Concrete Structures 2010".

(4) Critical Shear Crack Theory (CSCT) by Muttoni (2008)

Sample calculations to estimate the punching shear strength of a slab-column connection according to each set of provisions/models noted above can be found in Appendix A of this thesis.

ACI 318-14 BUILDING CODE

The following subsection of this thesis presents an overview of the ACI 318-14 two-way shear design provisions. In these provisions, the nominal shear stress resistance (v_n) for two-way members shall be calculated by:

$$v_n = v_c + v_s \quad \text{Eq. 2-1}$$

Where v_c is the shear stress resistance provided by concrete, and v_s is the shear strength provided by shear reinforcement, if provided (e.g., stirrups or headed studs).

For the calculation of v_c and v_s, d shall be the average of the effective depths in the two orthogonal directions, the value of $\sqrt{f'_c}$ shall not exceed 100 psi, and the value of f_{yt} shall not exceed 60,000 psi.

Critical sections for two-way members

The critical sections shall be located so that the perimeter b_o is minimized, but need not be taken closer than $d/2$ to (a) and (b):

(a) edges or corners of columns, concentrated loads, or reaction areas

(b) changes in slab thickness, such as edges of capitals, drop panels, or shear caps

The critical sections considered in flat plates systems are illustrated in Figure 2-1. In the case shear reinforcement is provided, a critical section with perimeter b_o located at a distance $d/2$ beyond the outermost peripheral line of shear reinforcement shall also be considered.

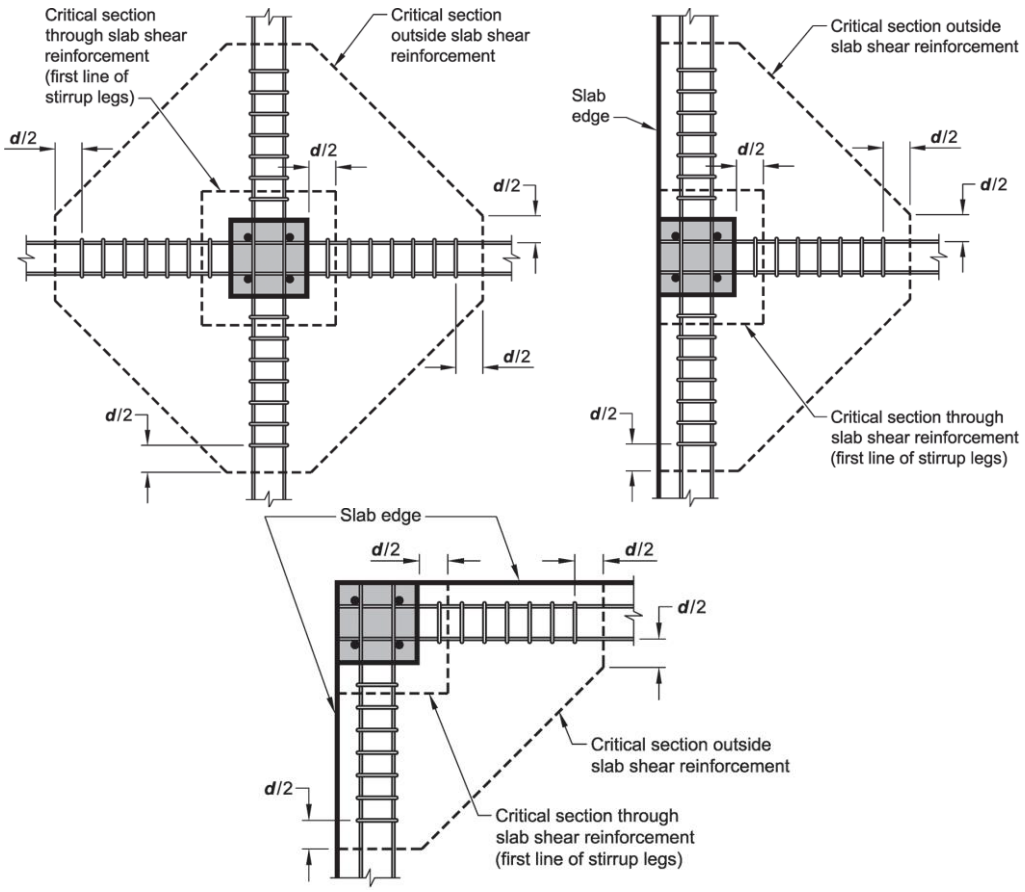

Figure 2-1: Critical sections for interior column, edge column, and corner columns respectively. (Adapted from ACI 318-14 22.6.4.2)

Two-way shear strength provided by concrete

The shear strength provided by concrete (v_c) shall be calculated in accordance with:

Table 2-1: Shear strength provided by concrete for nonprestressed two-way members (Adapted from ACI 318-14 22.6.5).

v_c to be taken as the least of (a), (b), and (c):	$4\lambda\sqrt{f_c'}$	(a)
	$(2+4/\beta)\lambda\sqrt{f_c'}$	(b)
	$(2+\alpha_s d/b_0)\lambda\sqrt{f_c'}$	(c)

Where λ is a modification factor used to reflect the reduced mechanical properties of lightweight concretes relative to normal weight concretes of the same compressive strength (*λ=1.0 for normal weight concrete)*, β is the ratio of long side to short side of the column if rectangular, for other shapes, β is taken to be the ratio of the longest overall dimension to the largest overall perpendicular dimension of the effective loaded area, and α_s is a factor equal to 40 for interior columns, 30 for edge columns, and 20 for corner columns.

For square columns, the stress corresponding to the nominal two-way shear strength provided by concrete in slabs subjected to bending in two directions is limited to $4\lambda\sqrt{f_c'}$. However, tests have indicated that this value is unconservative when the ratio β is larger than 2.0 (Joint ACI-ASCE Committee 426 1974). In such cases, the actual shear stress on the critical section at punching shear failure varies from a maximum of approximately $4\lambda\sqrt{f_c'}$ around the corners of the column or loaded area, down to $2\lambda\sqrt{f_c'}$, or less, along the long sides between the two end sections. Data obtained from other tests have shown that v_c decreases as the ratio b_o/d increases (Vanderbilt 1972). Expressions 22.6.5.2(*b*) and (*c*) are intended to account for these two effects.

Maximum concrete shear resistance for two-way members with shear reinforcement

The value of v_c calculated at critical sections shall not exceed the following limits:

Table 2-2: Maximum vc for two-way members with shear reinforcement (Adapted from ACI 318-14 22.6.6).

Type of shear reinf.	Maximum v_c at critical section located at:			
	d/2 from edges or corners of columns, loaded area, etc.		*d/2* beyond the outermost peripheral line of shear reinf.	
Stirrups	$2\lambda\sqrt{f_c'}$	(a)	$2\lambda\sqrt{f_c'}$	(b)
Headed studs	$3\lambda\sqrt{f_c'}$	(c)	$2\lambda\sqrt{f_c'}$	(d)

The effective depth shall be selected such that v_u calculated at critical sections does not exceed the following values:

Table 2-3: Maximum v_u for two-way members with shear reinforcement (Adapted from ACI 318-14 22.6.6).

Type of shear reinf.	Maximum v_u at critical section located at *d/2* from edges or corners of columns, loaded area, etc.	
Stirrups	$\phi 6\sqrt{f_c'}$	(*a*)
Headed studs	$\phi 8\sqrt{f_c'}$	(*b*)

Two-way shear strength provided by shear reinforcement (v_s)

When stirrups or headed shear stud reinforcement is present, the shear strength provided by shear reinforcement (v_s) shall be calculated by:

$$v_s = \frac{A_v f_{yt}}{b_0 s} \qquad \text{Eq. 2-2}$$

Where A_v is the sum of the area of all legs of reinforcement or the sum of the area of all shear studs, on one peripheral line that is geometrically similar to the perimeter of the column section, f_{yt} is the yield strength of the shear reinforcing steel, b_0 is the critical section as defined previously, and s is the spacing of the peripheral lines of headed shear stud reinforcement in the direction perpendicular to the column face.

If headed shear stud reinforcement is provided, A_v/s shall satisfy:

$$\frac{A_v}{s} \geq 2\sqrt{f_c'}\frac{b_0}{f_{yt}} \qquad \text{Eq. 2-3}$$

Single or multiple-leg stirrups fabricated from bars or wires shall be permitted to be used as shear reinforcement in slabs satisfying (*a*) and (*b*):

(*a*) *d* is at least *6 in*.

(*b*) *d* is at least $16d_b$, where d_b is the diameter of the stirrups.

EUROCODE 2

Basic control perimeter

The following subsection of this thesis presents an overview of the Eurocode 2 (EC2) two-way shear design provisions. In these provisions, the shear resistance should be checked at the face of the column and at the basic control perimeter u_1, and may normally be taken to be at a distance *2d* from the loaded area. Further, if shear reinforcement is provided in the slab, an additional control perimeter $u_{out,ef}$ must also be also be considered in slab region where shear reinforcement is no longer required.

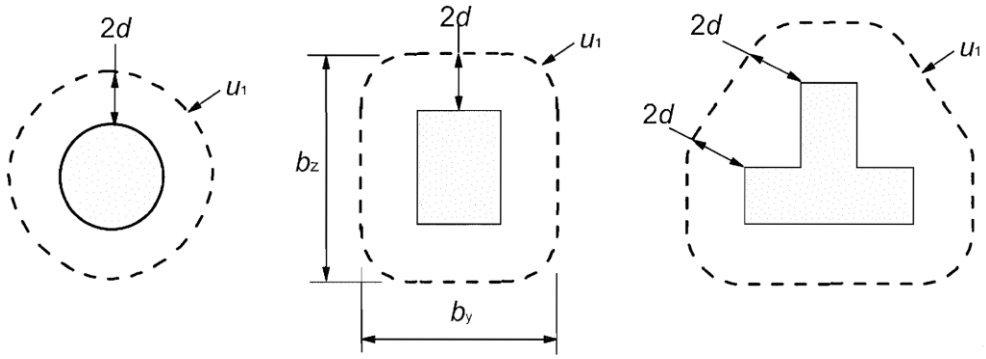

Figure 2-2: Basic control perimeter around loaded areas (Adapted from EC2 6.4.3)

For a loaded area situated near an edge or a corner, the control perimeter should be:

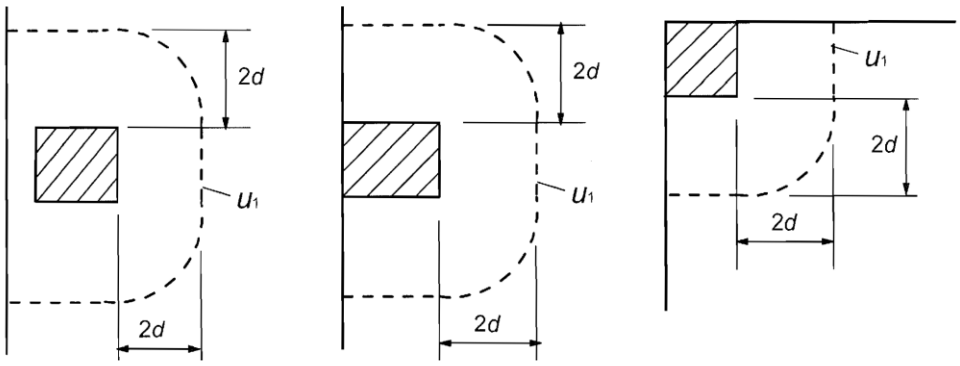

Figure 2-3: Basic control perimeters for loaded areas close to or at edge or corner. (Adapted from EC2 6.4.3)

The effective depth of the slab (d_{eff}) is assumed constant and may be taken as:

$$d_{eff} = \frac{d_y + d_z}{2} \qquad \text{Eq. 2-4}$$

Where d_y and d_z are the effective depths in the *y*- and *z*-directions, respectively.

Punching shear calculation

The following checks should be carried out:

(a) At the column perimeter, or the perimeter of the loaded area, the maximum punching shear stress should not be exceeded: $v_{Rd,max} \geq v_{Ed}$

(b) Punching shear reinforcement is not necessary if: $v_{Rd,c} \geq v_{Ed}$

(c) Where v_{Ed} exceeds the value $v_{Rd,c}$ for the control section considered, punching shear reinforcement should be provided.

Punching shear resistance of slabs and column bases without shear reinforcement

The punching shear resistance of a slab should be assessed for the basic control section according to 6.4.2. The design punching shear stress resistance [MPa] shall be:

$$v_{Rd,c} = C_{Rd,c} k \cdot (100 \rho_l f_{ck})^{1/3} + k_1 \sigma_{cp} \geq v_{min} + k_1 \sigma_{cp} \qquad \text{Eq. 2-5}$$

In the latter expression:

a) f_{ck} is the characteristic compressive strength of concrete in MPa

b) k is a factor that can be obtained as $k = 1 + \sqrt{200/d}$ with d in mm

c) $\rho_l = \sqrt{\rho_{ly} \cdot \rho_{lz}}$ where ρ_{ly}, ρ_{lz} relate to the bonded tension steel in y- and z-directions. The values ρ_{ly} and ρ_{lz} should be calculated as mean values taking into account a slab width equal to the column width plus *3d* each side.

d) $\sigma_{cp} = (\sigma_{cy} + \sigma_{cz})/2$, where $\sigma_{cy} = N_{Ed,y}/A_{cy}$, $\sigma_{cz} = N_{Ed,z}/A_{cz}$ are the normal concrete stresses in the critical section in y- and z-directions (MPa, positive if compression), and where $N_{Ed,y}$, $N_{Ed,z}$ are the longitudinal forces

across the full bay for internal columns or across the control section for edge columns. The force may be from a load or prestressing action.

e) A_c is the area of concrete according to the definition of N_{ed}.

f) Recommended values: $C_{Rd\_c} = 0.18/\gamma_c$, v_{min} from Eq. (6.3N) and $k_1 = 0.1$

Note that the European code use a characteristic strength f_{ck} instead of a specified concrete strength f'_c. Gardner (2005) concluded that the two can be related as follows:

$$f_{ck} = f'_c - 1.60 \text{ (MPa)} \qquad \text{Eq. 2-6}$$

Punching shear resistance of slabs and column bases with shear reinforcement

Where shear reinforcement is required, it should be calculated in accordance with:

$$V_{Rd,cs} = 0.75V_{Rd,c} + 1.5\left(\frac{d}{S_r}\right)A_{sw}F_{ywd,ef}\left(\frac{1}{u_1 d}\right)\sin\alpha \qquad \text{Eq. 2-7}$$

In the last expression:

a) A_{sw} is the sum of the area of all legs of reinforcement on one peripheral line that is geometrically similar to the perimeter of the column section [mm^2]

b) S_r is the spacing of the peripheral lines of shear reinforcement in the direction perpendicular to the column face [mm]

c) $f_{ywd,ef}$ is the effective design strength of the punching shear reinforcement, according to $f_{ywd,ef} = 250 + 0.25d \leq f_{ywd}$

d) d is the mean of the effective depths in the orthogonal directions [mm]

e) a is the angle between the shear reinforcement and the plane of the slab

f) If a single line of bent-down bars is provided, the ratio d/S_r may be 0.67

The control perimeter at which shear reinforcement is no longer required, u_{out} (or $u_{out,ef}$ (see Figure 2-4) should be calculated as: $u_{out,ef} = \beta V_{Ed}/V_{Rd,c}d$ and should be placed at a distance not greater than kd within u_{out} (or $u_{out,ef}$). The recommended value for k is 1.5.

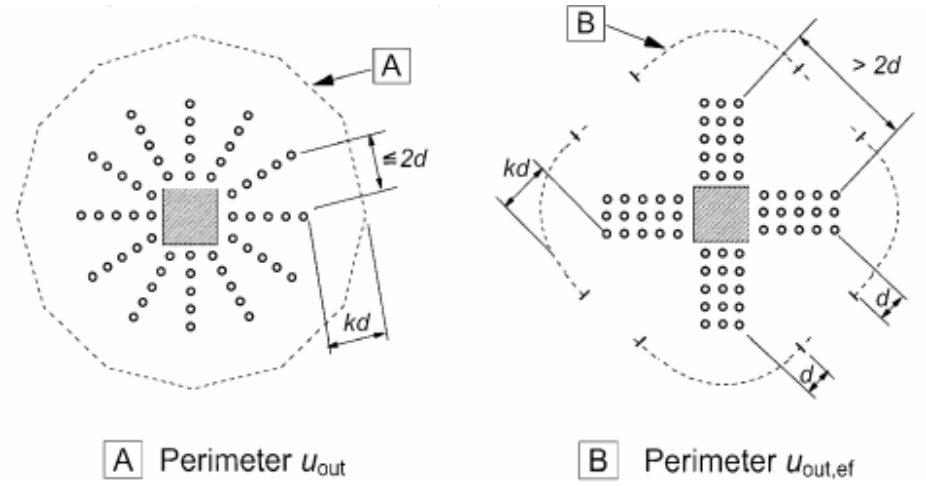

Figure 2-4: Outermost perimeter of shear reinforcement (Adapted from EC2 6.4.5).

The recommended value of $V_{Rd,max}$ is $0.4\nu f_{cd}$ where ν is a strength reduction factor for concrete cracked in shear: $\nu = 0.6(1 - f_{ck}/250)$ and f_{cd} is the design value of concrete compressive strength [MPa].

FIB MODEL CODE 2010

The following subsection of this thesis presents an overview of the *fib* Model Code 2010 (MC2010) two-way shear design provisions. In these provisions, punching shear design provisions for slab-column connections are based on the Critical Shear Crack Theory (CSCT) (Muttoni 2008).

Fundamental concepts

The design shear force with respect to punching (V_{Ed}) is calculated as the sum of design shear forces acting on a basic control perimeter (b_1).

The basic control perimeter (b_1) may be taken at a distance 0.5 d_v from the supported area, where dv is the shear-resisting effective depth.

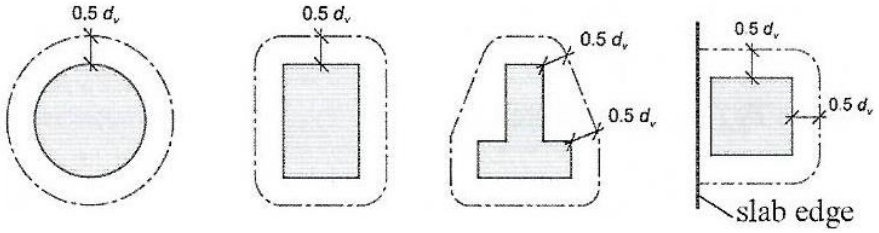

Figure 2-5: Basic control perimeters around supported areas (Adapted from *fib* MC 2010 7.3.5.2)

The shear-resisting effective depth of the slab (d_v) is the distance from the centroid of the longitudinal tension reinforcement layers to the supported area.

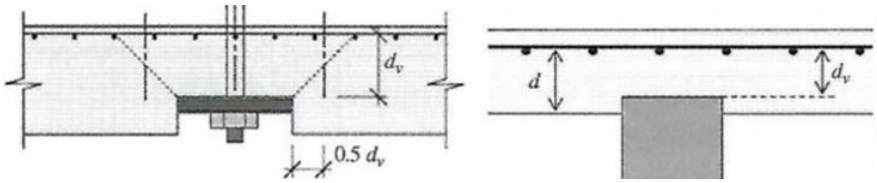

Figure 2-6: Effective depth of the slab (Adapted from *fib* MC 2010 7.3.5.2)

The shear-resisting control perimeter (b_0) accounts for the non-uniform distribution of shear forces along the basic control perimeter and can be obtained on the basis of a detailed shear field analysis as:

$$b_0 = \frac{V_{Ed}}{v_{perp,d,max}} \qquad \text{Eq. 2-8}$$

Where $v_{perp.d.max}$ is the maximum shear force per unit length perpendicular to the basic control perimeter (b_1).

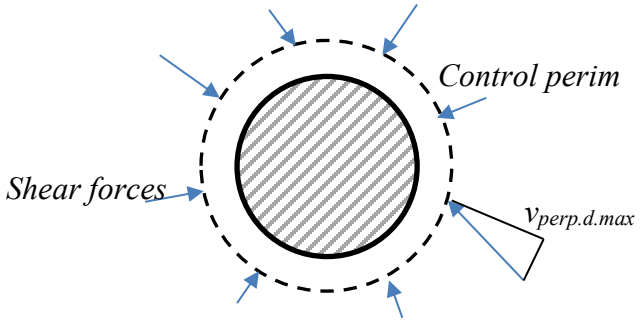

Figure 2-7: Maximum shear force per unit length perpendicular to the basic control perimeter (adapted from *fib* MC 2010 7.3.5.2)

The shear-resisting control perimeter (b_0) can also be approximately estimated as:

$$b_0 = k_e \cdot b_{1,red} \qquad \text{Eq. 2-9}$$

In the Equation 2-9, the effects of concentrated shear forces at the corners of large supported areas and/or geometrical and statical discontinuities of the slab are approximately taken into account by adopting a reduced basic control perimeter ($b_{1,red}$). The effect of concentrated shear forces due to moment transfer between the slab and the supported area are considered by multiplying the length of the reduced basic control perimeter ($b_{1,red}$) by the coefficient of eccentricity (k_e).

The coefficient of eccentricity (k_e) can be determined as a function of the moment transferred from the column to the slab as:

$$k_e = \frac{1}{1 + e_u/b_u}$$ Eq. 2-9

Where e_u is the eccentricity of the resultant of shear forces with respect to the centroid of the basic control perimeter (b_0), and b_u is the diameter of a circle with the same surface as the region inside the basic control perimeter (b_0). In cases where the lateral stability does not depend on frame action of slabs and columns, and where the adjacent spans do not differ in length by more than 25%, the following approximated values may be adopted for the coefficient of eccentricity (k_e):

- For inner columns: 0.90
- For edge columns: 0.70
- For corner columns: 0.65

Punching shear strength

The punching shear resistance (V_{Rd}) is calculated as:

$$V_{Rd} = V_{Rd,c} + V_{Rd,s} \geq V_{Ed}$$ Eq. 2-10

Where $V_{Rd,c}$ is the design shear resistance provided by concrete and, $V_{Rd,s}$ is the design shear resistance provided by stirrups (if present).

Design shear resistance attributed to concrete

The design shear resistance attributed to the concrete ($V_{Rd,c}$) may be taken as:

$$V_{Rd,c} = k_\psi \cdot \frac{\sqrt{f_{ck}}}{\gamma_c} \cdot b_0 \cdot d_v$$ Eq. 2-11

Where k_ψ is a parameter that depends on the deformations (rotations) of the slab, f_{ck} is the characteristic value of compressive strength, γ_c is the partial safety factor depending on the design scenario, b_0 is the shear-resisting control perimeter as defined previously and, d_v is the shear-resisting effective depth defined previously.

The parameter k_ψ can be obtained as:

$$k_\psi = \frac{1}{1.5 + 0.9 \cdot k_{dg} \cdot \psi \cdot d} \qquad \text{Eq. 2-12}$$

Where d is the mean value (in mm) of the effective depth for the x- and y-directions, k_{dg} is a parameter that depends of the maximum size of aggregate (d_g), and ψ is the rotation of the slab around the supported area.

Provided that the size of the maximum aggregate particles (d_g) is not less than 16 mm, k_{dg} can be taken as 1.0. If concrete with a maximum aggregate size (d_g) smaller than 16 mm is used, k_{dg} is assessed as:

$$k_{dg} = \frac{32}{16 + d_g} \geq 0.75 \qquad \text{Eq. 2-13}$$

Rotation of the slab around supported area

Four different procedures, of varying complexities, may be used to estimate the rotations of the slab surrounding the supported area. These procedures are categorized as *Levels of Approximation I* through *IV*. An illustration of the slab rotations developed within the slab-column connection regions is presented in Figure 2-8.

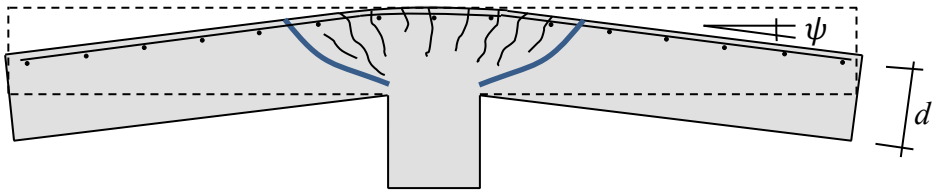

Figure 2-8: Rotation of a slab (Adapted from *fib* MC 2010 7.3.5.3)

Level I approximation

For a regular flat slab designed according to an elastic analysis without significant redistribution of internal forces, a safe estimate of the rotation at failure may be taken as:

$$\psi = 1.5 \cdot \frac{r_s}{d} \cdot \frac{f_{yd}}{E_s} \qquad \text{Eq. 2-14}$$

Where r_s denotes the position where the radial bending moment is zero with respect to the support axis, d is the mean value (in mm) of the effective depth for the x- and y-directions, f_{yd} is the yield strength of the longitudinal steel reinforcing bars and, E_s is the modulus of elasticity of the reinforcing steel.

The value of r_s can be approximated as $0.22L_x$ or $0.22L_y$ for the x- and y-directions respectively, for regular flat slabs where L_x/L_y is between 0.5 and 2.0.*Level II approximation*

In cases where significant bending moment redistribution is considered in the design, the slab rotation can be calculated as:

$$\psi = 1.5 \cdot \frac{r_s}{d} \cdot \frac{f_{yd}}{E_s} \cdot \left(\frac{m_{Ed}}{m_{Rd}}\right)^{1.5} \qquad \text{Eq. 2-15}$$

Where m_{Ed} is the average moment per unit length for calculation of the flexural reinforcement in the support strip and, m_{Rd} is the design average flexural strength per unit length in the support strip which can be obtained as follows:

$$m_{Rd} = \rho_l \cdot f_{yd} \cdot d^2 \cdot \left(1 - \frac{\rho_l \cdot f_{yd}}{2 \cdot f_{ck}}\right) \qquad \text{Eq. 2-16}$$

Note that the term ρ_l refers to the longitudinal steel reinforcement ratio of the slab. Further, slabs designed using this assumption will not necessarily comply with deformation capacity requirements, therefore, additional integrity reinforcement must be provided.

Level III approximation

If r_s is calculated using a linear elastic (uncracked) model and, m_{Ed} is calculated from a linear elastic (uncracked) model as the average value of the moment for design of the flexural reinforcement over the width of the support strip (b_s), then the slab rotation can be obtained as:

$$\psi = 1.2 \cdot \frac{r_s}{d} \cdot \frac{f_{yd}}{E_s} \cdot \left(\frac{m_{Ed}}{m_{Rd}}\right)^{1.5} \quad \text{Eq. 2-17}$$

However, it must be noted that for edge or corner columns, a minimum value of r_s shall be considered according to Eq. (7.3-78) from *fib* Model Code 2010. This level of approximation is recommended for irregular slabs or for flat slabs where L_x/L_y falls outside of 0.5 and 2.0.

Level IV approximation

Finally, it is also permitted to calculate slab rotations on the basis of a nonlinear analysis of the structure that accounts for cracking, post-cracking tension-stiffening effects, yielding of the reinforcement, and any other nonlinear effects relevant for providing an accurate assessment of the structure.

Design shear resistance provided by the shear reinforcement

The design shear resistance provided by the shear reinforcement (e.g., stirrups, studs, inclined reinforcement, or bent-up bars) may be calculated as:

$$V_{Rd,s} = (\sum A_{sw}) \cdot k_e \cdot \sigma_{swd} \cdot \sin\alpha \quad \text{Eq. 2-18}$$

Where ΣA_{sw} is the sum of the cross-sectional area of all shear reinforcement suitably anchored, or developed, and intersected by the potential failure surface (conical surface with angle 45°) within the zone bounded by $0.35d_v$ and d_v from the edge of the supported area (refer to Figure 2-9).

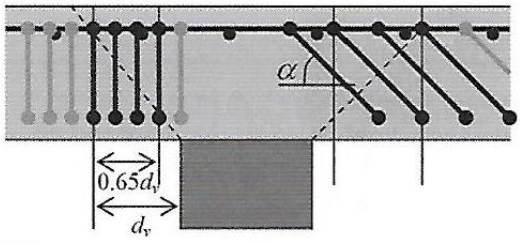

Figure 2-9: Shear reinforcement activated at failure (Adapted from *fib* MC 2010 7.3.5.3)

In Equation 2-18, the term σ_{swd} refers to the activated stress in the shear reinforcement:

$$\sigma_{swd} = \frac{E_s \cdot \psi}{6} \cdot (\sin\alpha + \cos\alpha) \cdot \left(\sin\alpha + \frac{f_{bd}}{f_{ywd}} \cdot \frac{d}{\varphi_w}\right) \leq f_{ywd} \qquad \text{Eq. 2-19}$$

Where φ_w denotes the diameter of the shear reinforcement, f_{ywd} is its yield strength, and f_{bd} is the reinforcement bond strength which is calculated from:

$$f_{bd} = \frac{1}{\gamma_c} \cdot \eta_1 \cdot \eta_2 \cdot \eta_3 \cdot \eta_4 \cdot \sqrt{f_{ck}/_{25}} \qquad \text{Eq. 2-20}$$

Where η_1 to $\eta_4$are coefficients denoting the characteristics of the reinforcing steel.

Shear reinforcement limits

To ensure sufficient deformation capacity in slabs constructed with punching shear reinforcement, a minimum amount of shear reinforcement is required:

$$\sum A_{sw} \cdot k_e \cdot f_{ywd} \geq 0.5\, V_{Ed} \qquad \text{Eq. 2-20}$$

The maximum punching shear resistance is limited by crushing of the concrete struts in the supported area:

$$V_{Rd,max} = k_{sys} \cdot k_\psi \cdot \frac{\sqrt{f_{ck}}}{\gamma_c} \cdot b_0 \cdot d_v \leq \frac{\sqrt{f_{ck}}}{\gamma_c} \cdot b_0 \cdot d_v \qquad \text{Eq. 2-21}$$

In Equation 2-21, the coefficient k_{sys} accounts for the performance of punching shear reinforcing systems to control shear cracking and to suitably confine compression struts at the soffit of the slab. A value of $k_{sys}=2$ can be adopted in absence of other data.

THE CRITICAL SHEAR CRACK THEORY

The failure criterion comprising the Critical Shear Crack Theory (CSCT) (Muttoni 2008) has been derived on the basis of experimental data that have shown the punching shear resistance of RC slabs to decrease with increasing rotation of the slab. It is assumed that the width of the critical shear crack ω is proportional to the product of the slab rotation

and the effective depth ψd. The critical shear crack is defined as the crack that propagates through the slab into the inclined compression strut carrying the shear force to the column:

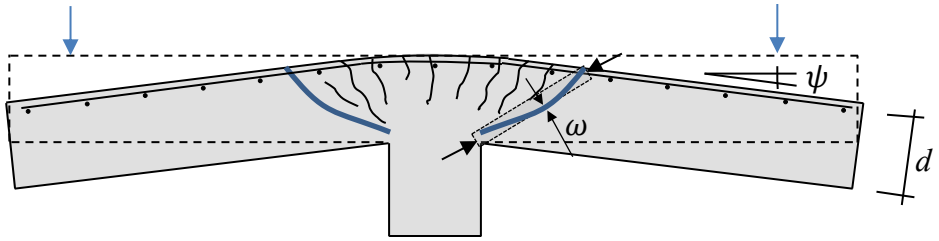

Figure 2-10: Correlation between opening of critical shear crack ω, effective depth d, and rotation ψ (Adapted from Muttoni 2008).

The expression proposed by Muttoni (2008) for the CSCT failure criterion also assumes that the amount of shear that can be transferred across the critical shear crack depends on the roughness of the crack, which is a function of the maximum aggregate size:

$$\frac{V_R}{b_0 d\sqrt{f_c}} = \frac{3/4}{1 + 15\frac{\psi d}{d_{g0} + d_g}} \qquad \text{(SI units: N, mm) Eq. 2-22}$$

$$\frac{V_R}{b_0 d\sqrt{f_c}} = \frac{9}{1 + 15\frac{\psi d}{d_{g0} + d_g}} \qquad \text{(US units: lb, in) Eq. 2-23}$$

Where d_g is the maximum aggregate size, and d_{g0} is a reference size equal to 16 mm (0.63 in). From this expression, it is possible to obtain the punching shear strength once the relationship between the slab rotation ψ and the applied load V is known. This relationship can be obtained from nonlinear numerical simulation or by using other analytical approaches. For example, if one considers an isolated slab specimen that is circular in shape, is loaded by way of a circular supporting column, and has a perimeter of contraflexure located at a distance r_q from the centroid of the column cross section (refer to Figure 2-11), an expression for the relationship between the slab rotation ψ and the applied load V can be derived.

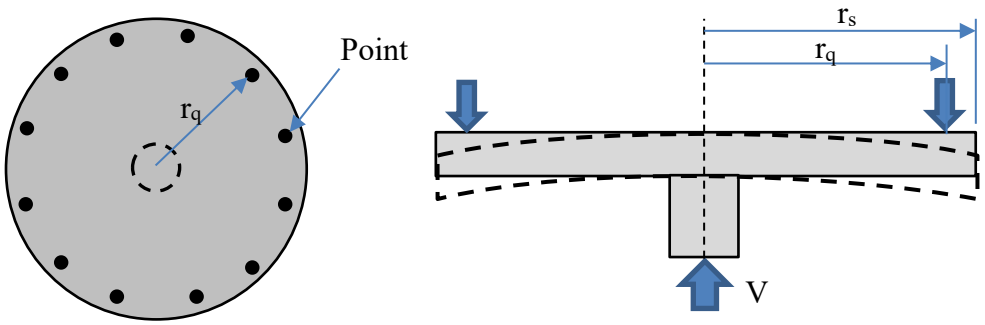

Figure 2-11: Characteristics of isolated slab specimens for derivation of load-rotation relationship in CSCT.

On the basis of the case summarized above, Muttoni (2008) assumed that the slab deforms following a conical shape with constant slab rotation ψ outside the critical shear crack. Considering a quadrilinear moment-curvature relationship for RC slabs as shown Figure 2-12, Equation 2-24 was derived for the purpose of relating applied shear RC slab-column connection shear force to slab rotation.

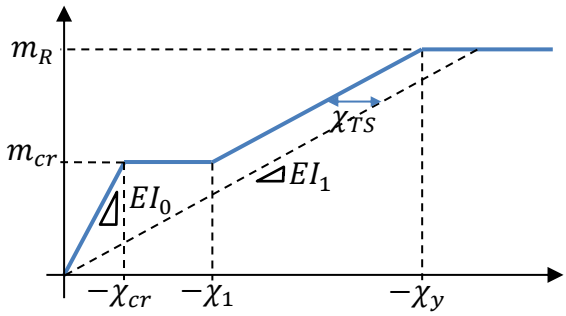

Figure 2-12: Quadrilinear (solid) and bilinear (dashed) moment-curvature relationship for the RC section (Adapted from Muttoni 2008).

$$V = \frac{2\pi}{r_q - r_c}\begin{pmatrix} -m_r r_0 + m_R\langle r_y - r_0\rangle + EI_1\psi\langle \ln(r_1) - \ln(r_y)\rangle + \\ EI_1\chi_{TS}\langle r_1 - r_y\rangle + m_{cr}\langle r_{cr} - r_1\rangle + EI_0\psi\langle \ln(r_s) - \ln(r_{cr})\rangle \end{pmatrix} \quad \text{Eq. 2-24}$$

Where:

a) r_c is the radius of the column cross-section (m).

b) The operator $\langle x\rangle$ is x for $x \geq 0$ and 0 for $x < 0$.

c) m_r is the radial moment per unit length acting in a portion of the slab at a distance from the axis of the column of $r = r_0$ (up to the critical crack) (MNm/m).

d) m_{cr} is the cracking moment determined as follows (MNm/m):

$$m_{cr} = \frac{f_{ct} h^2}{6}$$

-f_{ct} is the tensile strength of concrete (MPa)
-h is the thickness of the slab (m)

e) m_R is the moment capacity (refer to Eq. 2-16) (MNm/m)

f) χ_{TS} is the decrease in curvature caused by tension stiffening and can be accounted for as a constant contribution as follows (rad):

$$\chi_{TS} = \frac{f_{ct}}{\rho \beta E_s 6h}$$

-E_s, the reinforcement's modulus of elasticity (MPa)
-$\beta = 0.6$ is an efficiency factor

g) EI_0 is the stiffness before cracking determined as follows (MNm^3):

$$EI_0 = \frac{E_c h^3}{12}$$

-E_c, the concrete's modulus of elasticity (MPa)

h) EI_1 is the stiffness after cracking determined as follows (MNm^3):

$$EI_1 = \rho \beta E_s d^3 \left(1 - \frac{c}{d}\right)\left(1 - \frac{c}{3d}\right)$$

-c is the depth of the compression zone (m)

$$c = \rho \beta \frac{E_s}{E_c} d \left(\sqrt{1 + \frac{2E_c}{\rho \beta E_s}} - 1\right)$$

i) r_y is the zone within which the reinforcement is yielding, r_1 is zone in which cracking is stabilized and r_{cr} is zone up to which the concrete is cracked, determined as follows (m):

$$r_y = \frac{\psi}{-\chi_y} = \frac{\psi}{\frac{m_R}{EI_1} - \chi_{TS}} \qquad r_1 = \frac{\psi}{-\chi_1} = \frac{\psi}{\frac{m_{cr}}{EI_1} - \chi_{TS}} \qquad r_{cr} = \frac{\psi}{-\chi_{cr}} = \frac{\psi EI_0}{m_{cr}}$$

A correction factor should also be applied when considering square-shape RC slabs. Further, for square columns, r_c should be taken as: $r_c = 2c/\pi$.

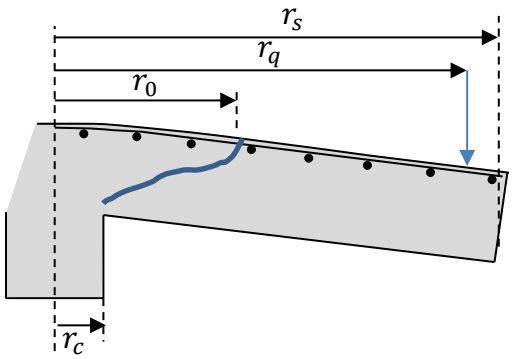

Figure 2-13: Geometrical parameters and rotation of slab (Adapted from Muttoni 2008)

The expression presented in Eq. 2-24 can be simplified, by considering a bilinear moment-curvature relationship that neglects the tensile strength of concrete and the influence of post-cracking concrete tension stiffening. Making a few more assumptions as noted in Muttoni 2008, the following equation is derived:

$$\psi = 1.5 \cdot \frac{r_s}{d} \cdot \frac{f_y}{E_s} \cdot \left(\frac{V}{V_{flex}}\right)^{3/2} \qquad \text{Eq. 2-25}$$

This expression is analogous to the Equation 2-15 of this thesis for a Level II approximation. The flexural strength V_{flex} of the isolated slab specimen can be estimated by the yield-line method. The pattern of the yield-lines will depend on the applied load.

COMPARISON BETWEEN CODES

In light of what has been presented in this section, a brief comparison of the key equations used in each of the codified approaches is shown in the following table. Note that similar comparisons have been made by others (Gardner 2005, Bayrak and Jirsa 2009).

Table 2-4: Comparison between provisions from codes.

Code:	***ACI 318-14***		***EC2***		***fib MC 2010***	
	US [lb,in]	*SI [N,mm]*	*US [lb,in]*	*SI [N,mm]*	*US [lb,in]*	*SI [N,mm]*
v_c	$4\sqrt{f'_c}$	$0.33\sqrt{f'_c}$	$5(f_{ck})^{1/3}$	$0.18(f_{ck})^{1/3}$	$k_\psi\sqrt{f_{ck}}$	
ξ	-	-	$k = 1 + \sqrt{\frac{7.9}{d}}$ $k \le 2$	$k = 1 + \sqrt{\frac{200}{d}}$ $k \le 2$	$k_{dg} = \frac{1.26}{0.63+d_g}$ $k_{dg} \ge 0.75$	$k_{dg} = \frac{32}{16+d_g}$ $k_{dg} \ge 0.75$
ρ_l	-	-	$(100\rho)^{1/3} \quad \therefore \quad \rho \le 0.002$		$k_\psi = f(\psi) \rightarrow \psi = f(\rho)$	
b_0	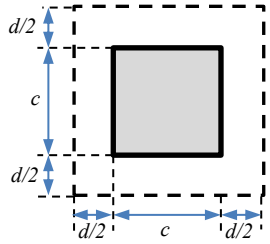 $b_0 = 4 \cdot (c + d)$		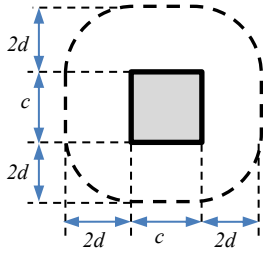 $b_0 = 4 \cdot (c + \pi d)$		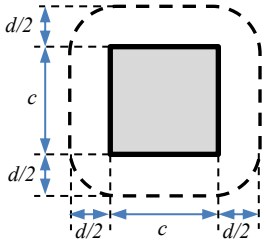 $b_0 = 4c + \pi d$	

v_c; Shear strength
ξ; Size effect
ρ_l ; Longitudinal reinforcement ratio
b_0; Control perimeter, or critical section

Additionally, a comparison is made to determine the variation of the two-way shear strength, obtained according to the provisions discussed in this chapter, with the change of different parameters (i.e., longitudinal reinforcement ratio, compressive strength of

concrete, slab depth, shear span to depth ratio). Consider a reference slab-column connection which contains no shear reinforcement, is constructed with a 16-in. (406-mm) square column, a 10 in. (254 mm) slab thickness, a 8.5 in. (216 mm) effective depth, 1.0 % longitudinal steel reinforcement, and 4000 psi (28 MPa) specified compressive strength of concrete. On the basis of these properties and assumptions, Figures 2-16 to 2-19 presents the estimated punching shear strength for the described connection as a function of several key parameters.

Figure 2-16 shows the variation of the punching shear stress at the critical section of the prototype connection when the hogging reinforcement ratio varies between 0.3 and 1.8 %. Note that the critical section at which the stress is evaluated changes for each code. Since ACI 318-14, as shown in Table 2-4, does not take into account the reinforcement level, the two-way shear stress remains constant with changing reinforcement ratios. The formulation for Eurocode 2 and the *fib* Model Code 2010 follow similar trends to each other, increased capacity with increased reinforcement ratio, but the Eurocode results are more conservative.

Figure 2-17 shows the variation of the two-way shear stress at the critical section of the prototype connection when the slab thickness varies between 5 and 20 inches. The effective depth of the slab has a greater significance in the length of the basic control perimeter in the European standard, Eurocode 2. For this provision, the maximum allowable shear stress at the critical section decreases with increasing slab thickness. The curve describing the influence of the slab thickness in *fib* Model Code 2010 provisions was conceived with the assumption that the relationship shear span to effective depth (r_s/d) is kept constant. In this case the resulting curve remains more or less constant showing a slight reduction in the shear stress as the slab's thickness increases. For slab depths below around 11 in., the slab-column connection failure mode is governed by flexure. ACI 318-

14 does not account for size effect; therefore, as expected, the shear stress at the critical section remains constant with changing slab thickness. For slabs with a slab thickness near 5 in., a deviation from the straight line is observed. Note that equation (c) from Table 2-1, which is a function of the effective depth, comes into play and introduces a cap in the permitted shear stress at the critical section in those cases.

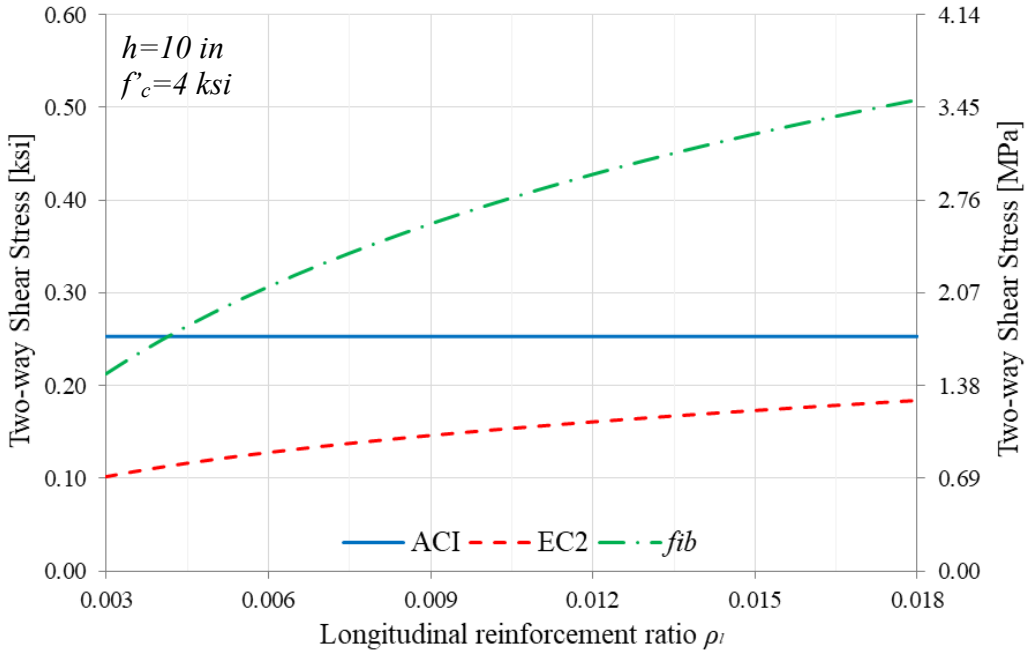

Figure 2-16: Two-way shear strength *vs* longitudinal tension reinforcement ratio.

Figure 2-18 illustrates how the punching shear stress at the critical section of the prototype connection changes as a function of the compressive strength of concrete. Note that in the plot, compressive strength refers to the specified compressive strength (f'_c). All the curves follow the same trend, increasing shear stress at the critical section for increasing compressive strength of concrete. However, *fib* Model Code 2010 always predicts higher resistances for any value of compressive strength, as expected given the nature of the code intended as a modeling tool.

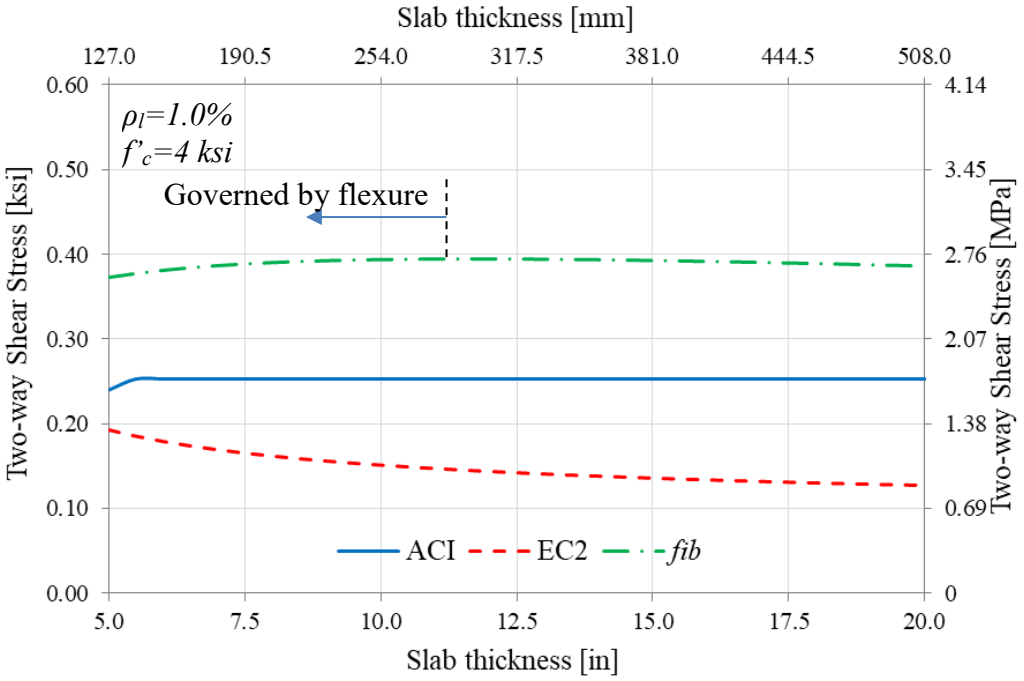

Figure 2-17: Two-way shear stress at the critical section *vs* slab thickness.

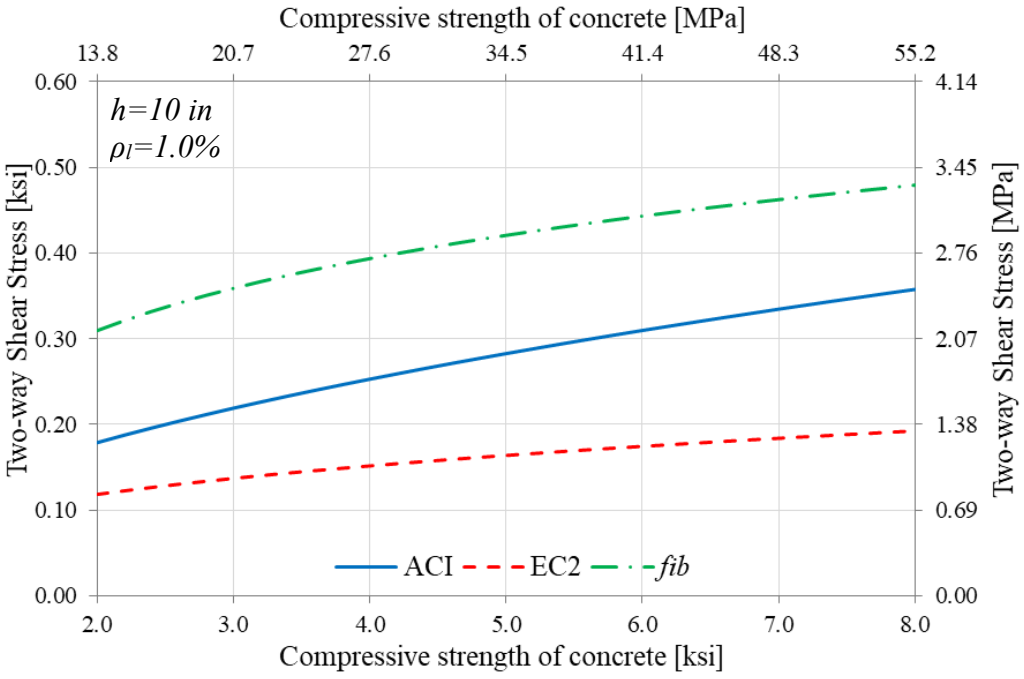

Figure 2-18: Two-way shear stress as a function of compressive strength of concrete.

Figure 2-19 illustrates the variation in the maximum allowable shear stress at the critical section, or basic control perimeter, with the change in the shear span to depth ratio. The only code accounting for this parameter is *fib* Model Code 2010, which shows a lower maximum allowable shear stress with increasing shear span to depth ratio. For the rest of the codes analyzed, the estimated shear stress resistance remains constant.

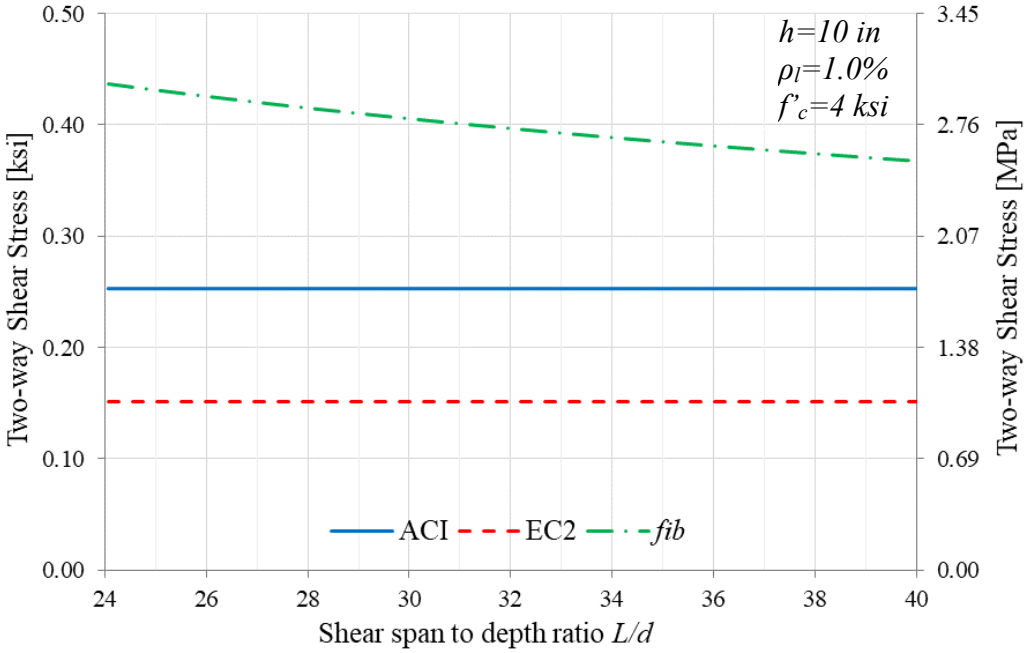

Figure 2-19: Two-way shear stress as a function of the shear span to depth ratio.

Chapter 3: Experimental program

The experimental program presented in this thesis was part of a larger testing program carried-out at the Ferguson Structural Engineering Laboratory of the University of Texas at Austin. Results from other stages of this program are presented in Glikman et al. (2016) and Polo et al. (2018). The program consisted of four full-scale isolated RC slab-column connections, as summarized in Table 3-1. The test specimens were designed as two pairs of nominally-identical specimens.

Current code formulations to evaluate punching shear strength are based on tests of isolated slab elements that are typically tested with slab loads being applied as concentrated forces along the line of moment contraflexure, as mentioned in Chapter 1. This leads to acceptable, but potentially artificial estimations, of the punching shear resistance and makes the testing much simpler and cost-efficient. However, the way the load is applied to the specimens in these tests may be significantly different from real-world cases. Thus, the main purpose of the experimental program presented in this thesis was to examine how the punching shear strength was affected as a result of varied applied loading scenarios.

Two different testing approaches were used to fail the isolated slab-column connection specimens. Half of the specimens were tested using a setup with similar characteristics to those used by others in the past to assess punching shear strength of slab-column connections (Birkle & Dilger 2008, Guandalini et al 2009, Einpaul et al 2016). A vertical force was applied to the intersecting column while the slab was vertically-restrained using a series of rigid struts. In this thesis, this testing procedure is referred to as a Concentrated Load (CL) test setup. The other half of the testing specimens were loaded to failure using an innovative testing approach, designated in this thesis as the Uniform Load (UL) test setup. In the UL testing procedure, loads were applied by way of an

increasing distributed surface pressure applied to the slab using a series of airbags. The slab was restrained vertically using a high-strength rod that passed through the center-point of the specimen (i.e., through the column stub) and was fastened to a stiff reaction frame. Key dimensions of the test specimens used in each testing configuration are shown in Figure 3-1. It should also be noted that different RC column configurations were used for the two slab testing procedures employed.

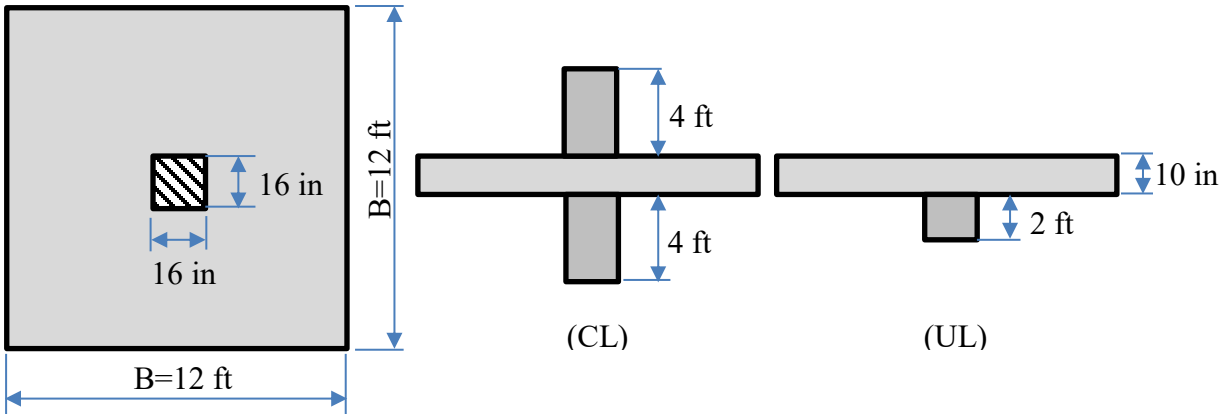

Figure 3-1: Main dimensions of specimens. From left to right: Top view, lateral view of specimen for CL test setup, lateral view of specimen for UL test setup.

The edge boundaries of the slabs were free to rotate and translate laterally. Further, all of the slab-column connection assemblies were constructed without through-thickness slab shear reinforcement. In all cases, a lower and an upper orthogonal grid of longitudinal reinforcement was provided. US No. 6 steel reinforcing bars were provided for the top mat of longitudinal reinforcement, which served as the flexural tension reinforcement. US No. 3 steel reinforcing bars were used for bottom mat of reinforcement which was located near the compressive surface of the slab. Note that the primary difference amongst the test specimens was the amount of longitudinal reinforcement provided in the top layer (i.e., on the flexural tension side). A clear cover of 0.75 in. was provided for all reinforcing bars

comprising the slabs. Given the aforementioned construction details, the mean effective depth was 8.50 in. and was the same for all four slab specimens (refer to Figure 3-2).

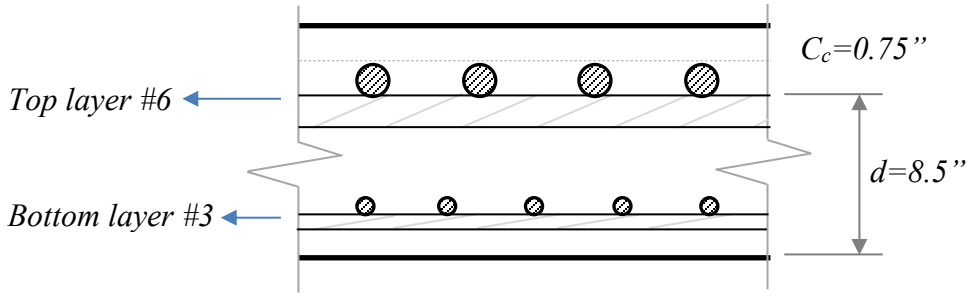

Figure 3-2: Mean effective depth (d) of both orthogonal directions of hogging reinforcement of the specimens.

The negative, or hogging, reinforcement ratio *(ρ_l)* of the slab was defined as the amount of area flexural tension reinforcement placed in the top layer (in one of the two orthogonal directions) divided by the effective area of the slab $B \cdot d$:

$$\rho_l[\%] = \frac{N \cdot A_{\#6}}{B \cdot d} \cdot 100 \qquad \text{Eq. 3-1}$$

Where N is the number of bars placed, $A_{\#6}$ is the nominal area of a US No. 6 bar (0.44 in^2), d is the mean effective depth (8.50”) and B is the width of the slab (144”).

Table 3-1: Summary of the experimental program.

#	slab designation	hogging reinforcement ratio, ρ_l (%)	transverse reinforcement ratio, ρ_v (%)	test method
1	C-1.0	1.00	0	CL [(a)]
2	U-1.0	1.00	0	UL [(b)]
3	C-0.7	0.72	0	CL [(a)]
4	U-0.7	0.72	0	UL [(b)]
(a) Concentrated Load or CL test setup; (b) Uniform Load or UL test setup				

The characteristics of the specimens, the apparatus used to test the specimens as well as the complementary instrumentation used to measured deformations and strains in the steel reinforcement, are described in more detail in this chapter.

EXPERIMENTAL APPARATUS

The following section provides details regarding the two different experimental test frames that were employed to test the RC slab-column connection assemblies under punching shear loading conditions.

Concentrated Loading (CL) Test Setup

Illustrations of the concentrated loading test frame are presented in Figures 3-3 through 3-6. An upward vertical load was applied to the base of the lower column stub comprising slab-column connection C-0.7 and C-1.0 using a 300-ton (2670 kN) capacity hydraulic ram. The applied loading was measured using a 1000-kip (4450 kN) load cell that was placed between the hydraulic ram and a RC strong floor. The slabs comprising the specimens were restrained vertically and intersection column stubs were restrained laterally using steel struts. Eight vertical struts, placed in a circular patter surround the intersecting column at a distance of 61 in (1550 mm) from the centroid of the column cross section, were used to restrain slab vertical translations and serve as the reaction for the shear force applied to column by way of the hydraulic ram. Additionally, to prevent the connection assemblies from rotating globally and/or displacing laterally, three horizontal struts were used to restrain the intersection column stubs, in two orthogonal directions. In each case, one end of lateral struts was fastened to the column stub comprising the specimen and the other was anchored to a reaction structure, consisting of either a stiff steel frame assembly or RC strong wall. Finally, an additional horizontal pin-ended steel bar was used to prevent the slab from rotating during testing. This steel bar element was

fastened to an RC strong wall at one end and was connected to the edge of the RC slab at the other end. It should be noted that the strut used to prevent slab twist was positioned such that it would not restrain the slab laterally.

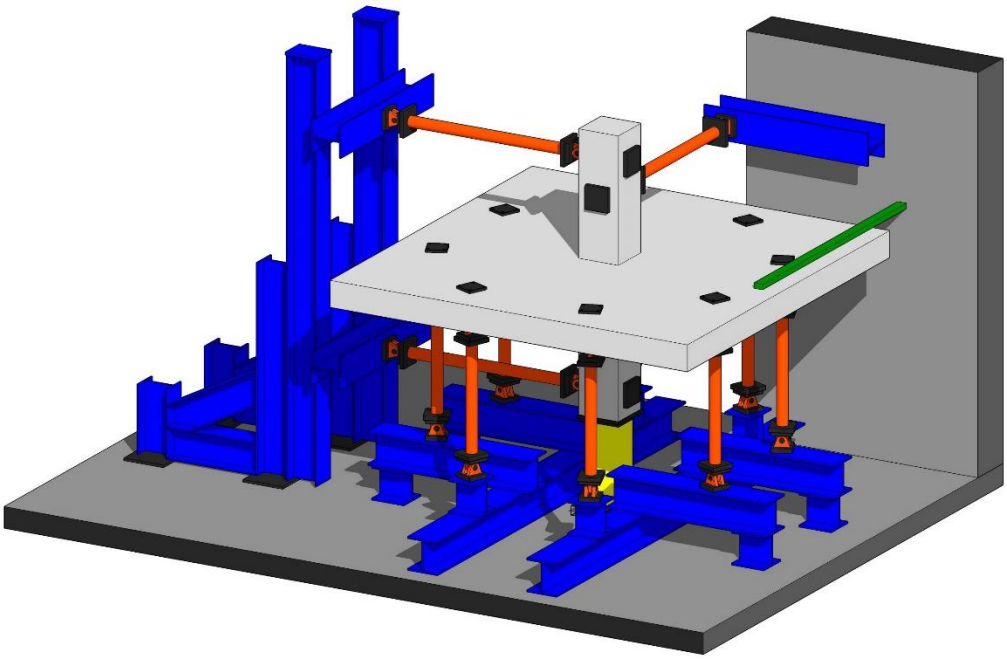

Figure 3-3: Concentrated Load Test Setup. 3d view.

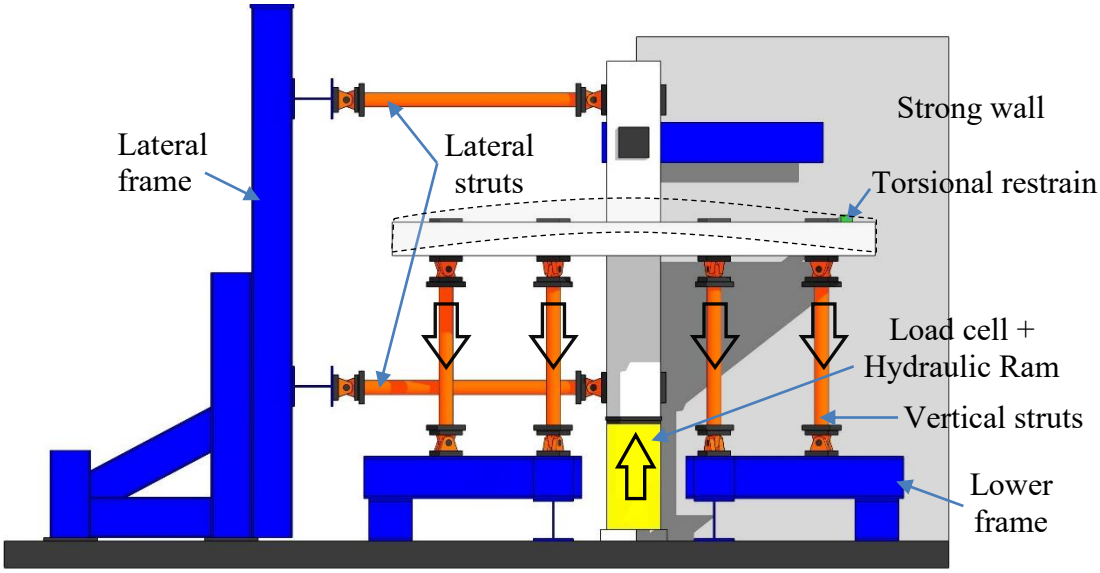

Figure 3-4: Concentrated Load Test Setup. Front view and main parts.

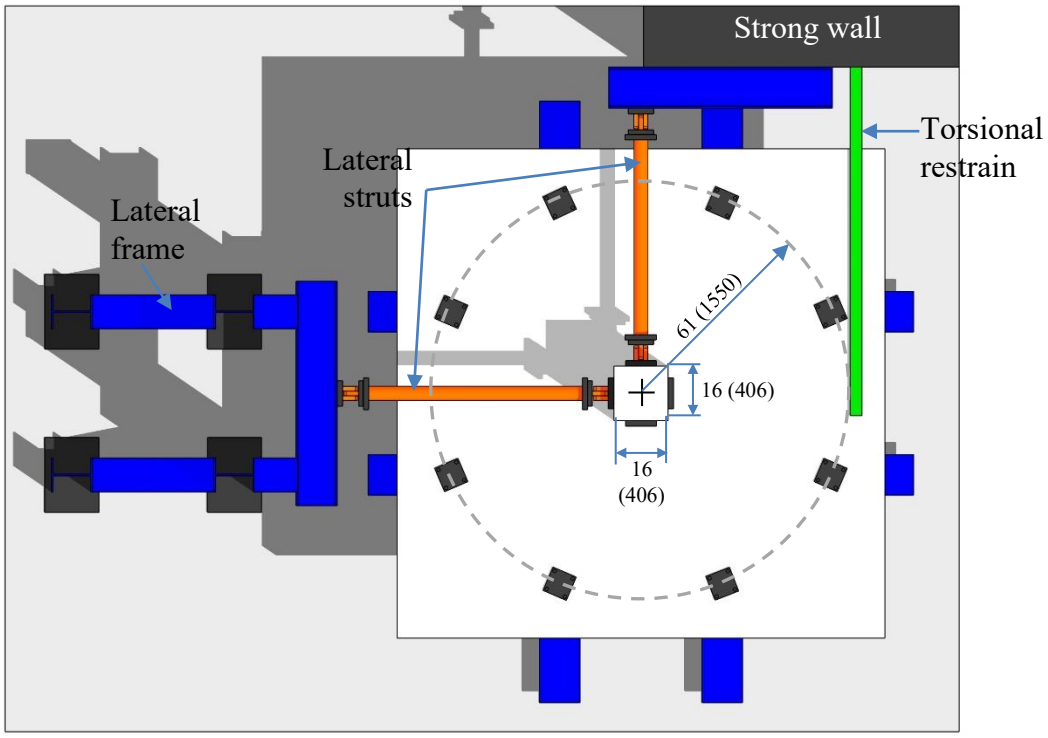

Figure 3-5: Concentrated Load Test Setup. Top view, parts and dimensions [in (mm)].

Figure 3-6: Concentrated Load Test Setup. Photo without specimen in place.

Uniformly distributed Load (UL) Test Setup

Illustrations of the uniform loading test frame are presented in Figures 3-7 through 3-10. Unlike the Concentrated Load test setup where an upward load was applied to the base of column of the specimen and shear forces in the slab were developed using a series of vertical reaction positioned in a circular configuration surrounding the intersecting column, the uniformly distributed load test applied shear forces by way of a distributed slab surface pressure. Upward distributed pressures were applied to the slab using a series of airbags and the vertical force reaction was developed by way of restraining the intersecting column. A high strength steel rod was provided through the center of the column cross-section and slab, and was anchored to the base of a stiff reaction assembly provided beneath the test specimen. The steel rod prevented the column of the test specimen from moving upwards as the airbags were inflated. Additionally the rod was also used to apply a pre-compression force to the column, approximately equal to the self-weight of the slab-column connection specimen, prior to starting the test. The load was measured using a load cell positioned at the top of the specimen, on top of the intersecting column. There was a space of approximately 4” between the metal deck and the face of the slab. Further, the airbags are placed between two sheets of plywood for protection.

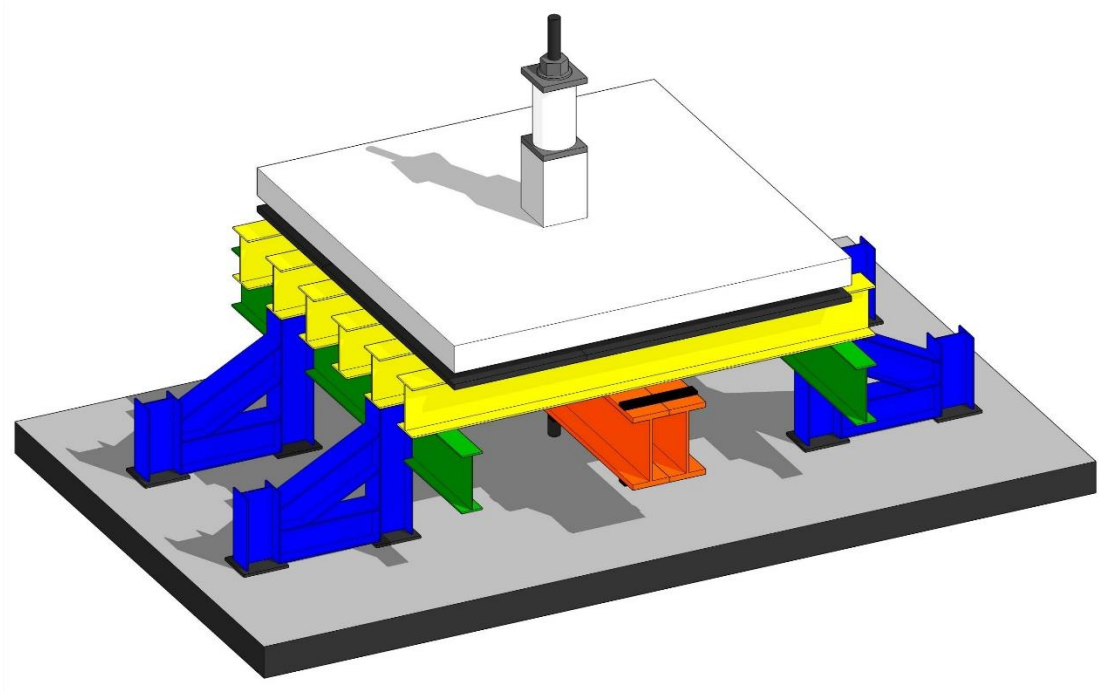

Figure 3-7: Uniform Load Test Setup. 3d view.

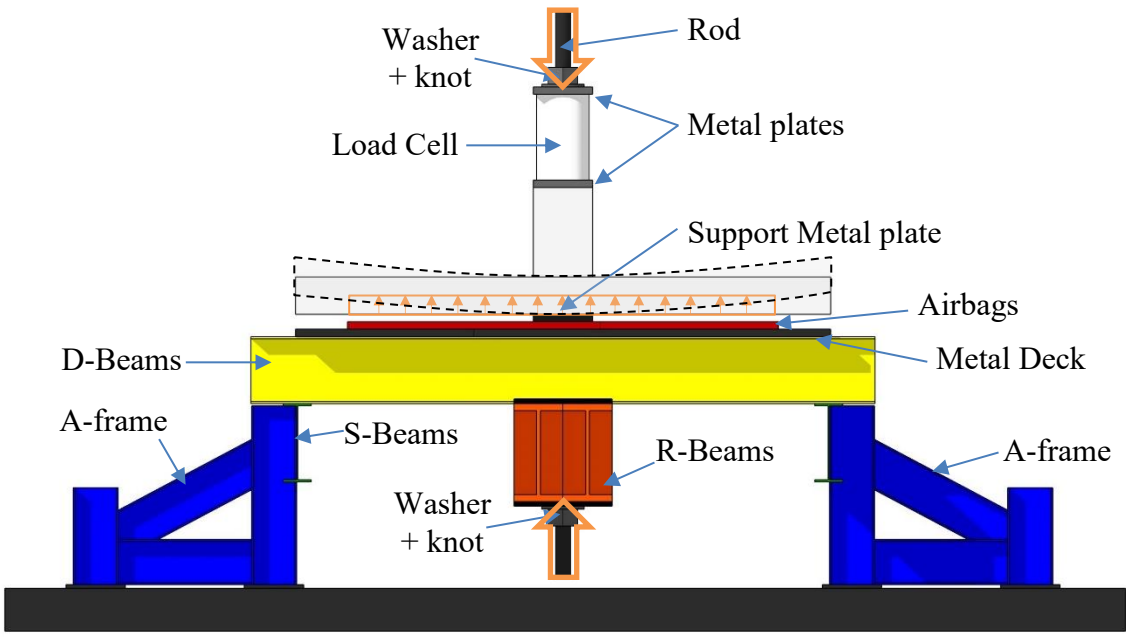

Figure 3-8: Uniform Load Test Setup. Front view, main parts.

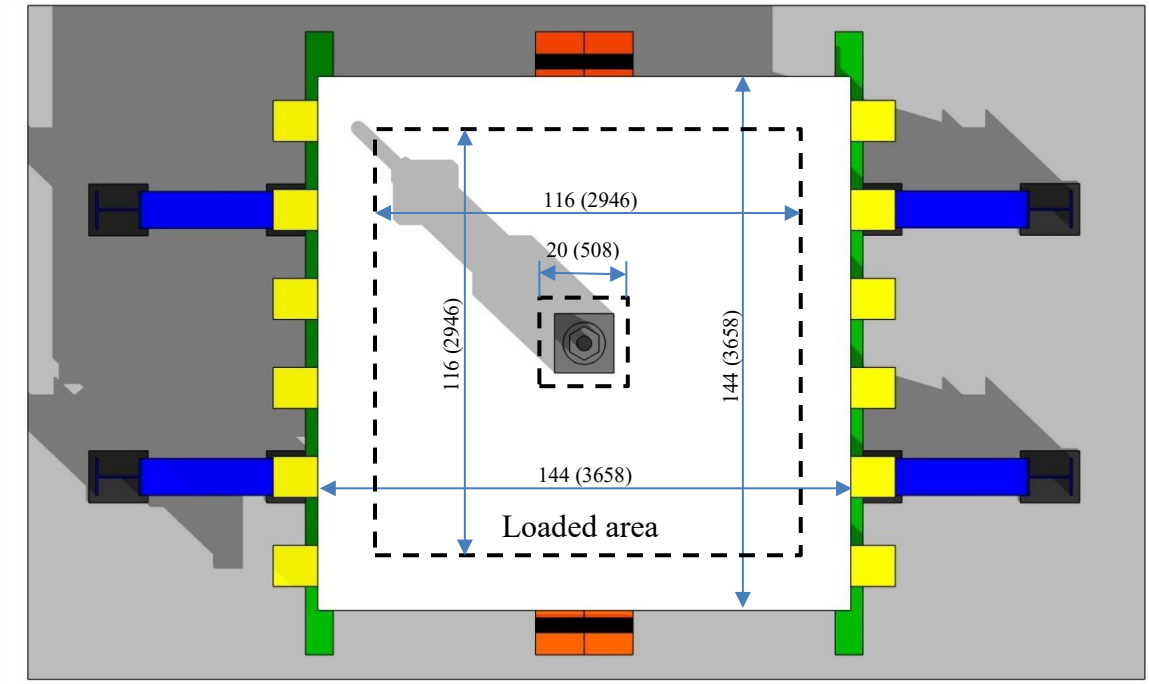

Figure 3-9: Uniform Load Test Setup. Top view, parts and dimensions [in (mm)].

Figure 3-10: Uniform Load Test Setup. Photo with specimen in place, load cell, rod and instrumentation not yet installed.

MATERIAL PROPERTIES

The following section provides an overview of the mechanical properties that were obtained for the materials comprising the RC slab-column connection specimens. More detailed information is provided in the Appendix B of this thesis. Note that mechanical properties for concrete and steel reinforcement are reported separately in Tables 3-2 and 3-3, respectively.

Concrete

Concrete mechanical properties were evaluated using a series of well-established concrete material testing techniques. The concrete compressive strength (*f'c*) was obtained from the testing of three (3) 4 × 8-in. (100 × 200-mm) cylinders for each connection specimen, and at the time of slab testing, in accordance with ASTM C39. The tensile strength of the concretes comprising the test specimens was evaluated using several different test methods. Split tension tests were performed according to ASTM C496. Three (3) 4 × 8-in. (100 × 200-mm) cylinders were subjected to a diametral compression force along the length until failure occurred. Another concrete tension testing method employed was the modulus of rupture test according to ASTM C78. Three (3) prismatic specimens of size 6 × 6 × 18-in (152.4 × 152.4 × 457.2-mm) were tested to determine their flexural strength. The third tension testing method was the direct tension test for which there is no well-established standard available. In these tests, three (3) "dog-bone" shaped specimens with a central cross-section of 4 × 4-in (101.6 × 101.6-mm) were subjected to uniaxial tension until failure occurred.

Key mechanical properties for the concrete used in the construction of each specimen are shown in the Table 3-2. In all cases, the maximum nominal aggregate size specified for the concrete was 1.0 in (25.4 mm).

Table 3-2: Main properties of concrete in each specimen.

#	Designation:	Age [days]	f_c' (a) ksi (MPa)	f_{ct} (b) ksi (MPa)	f_r (c) ksi (MPa)	f_t' (d) ksi (MPa)
1	C-1.0	87	4.29 (29.58)	0.636 (4.38)	0.697 (4.81)	0.341 (2.35)
2	U-1.0	48	4.99 (34.41)	0.781 (5.38)	0.661 (4.56)	0.429 (2.96)
3	C-0.7	51	6.17 (42.54)	0.756 (5.21)	0.601 (4.14)	0.394 (2.72)
4	U-0.7	56	6.24 (43.02)	0.650 (4.48)	0.730 (5.03)	0.430 (2.96)
(a) Compressive Strength Test (ASTM C39); (b) Split Tension Test (ASTM C496); (c) Modulus of Rupture Test (ASTM C78); (d) Direct Tension Test (No standard)						

Steel reinforcing bars

Three (3) steel coupons were tested under uniaxial tension following the specifications of ASTM 370-15. The main material parameters evaluated for the steel reinforcement employed in this testing program are shown in Table 3-3.

Table 3-3: Main properties of steel bars for all specimens

Size	*Diameter* *in. (mm)*	*Area* *in.^{2} (mm^2)*	F_Y *ksi (MPa)*	F_u *ksi (MPa)*	E_S *ksi (MPa)*	ε_{sh} *(x10^{-3})*	ε_u *(x10^{-3})*
US No. 3	0.375 (9.53)	0.11 (71)	64 (441)	97 (669)	28,871 (199,060)	7	100
US No. 6	0.75 (19.05)	0.44 (284)	67 (462)	108 (745)	27,068 (186,630)	7	100

INSTRUMENTATION

The following section of this thesis provides an overview of the instrumentation that was used to monitor and control testing, and to measure specimen response data. For most instrumentation types, typical instrumentation plans are provided.

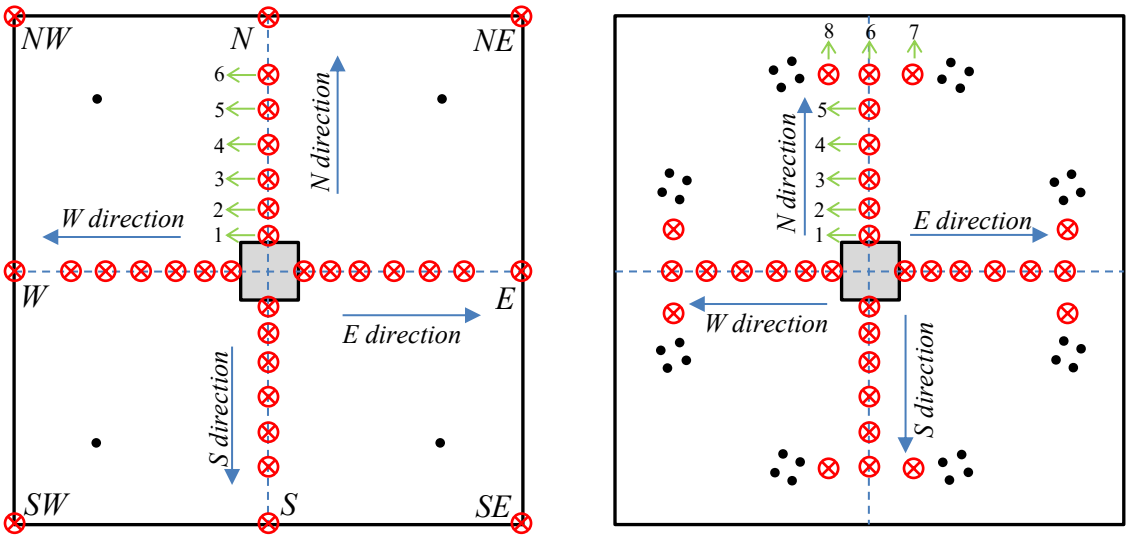

Figure 3-11: Measurement of deflections. Positioning of LPOTs devices for UL (left) and CL (right) test specimens.

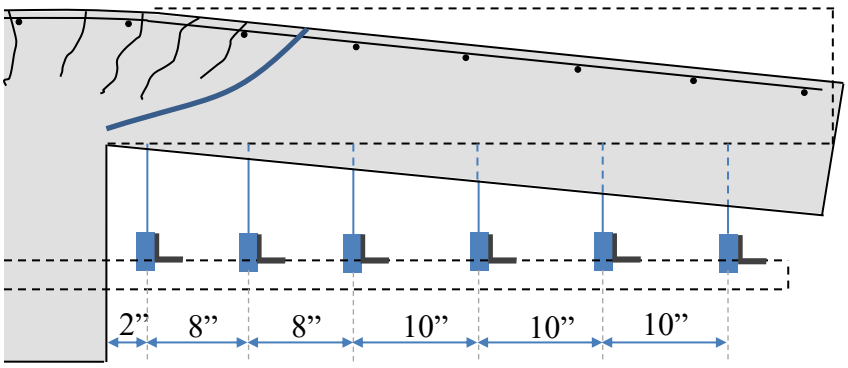

Figure 3-12: Measurement of deflections. Disposition and separation between LPOTs devices in each fabrication direction.

Linear potentiometers, or LPOTs, were installed to record deflections at several points along the four directions of fabrication (N, S, W and E) of the specimens as shown

in Figure 3-11. The LPOTs were fastened to a light instrumentation frame that was attached to the intersecting column stub. The instrumentation frame was installed once the specimen was in place on the apparatus. The LPOTs were mounted to the specimens using high-resistance cable. Further, displacements obtained using this system provided slab displacements that were measured relative to the movement of the intersecting column.

Figure 3-13: Measurement of deflections. Pictures of installed frame with LPOTs for UL (left) and CL (right) test specimens.

Strain gauges were installed at several locations on the longitudinal steel reinforcing bars for the purpose of measuring reinforcing bar strains. The gauges were installed with many insulating layers to ensure that they were protected during the concrete casting process. The outside protective layer, which consisted of yellow electrical tape, can be observed in Figure 3-14.

The approximate location where the strain gauges were placed on the top layer of reinforcement (i.e., on the flexural tension mat of reinforcement) are shown in Figure 3-15. The picture only details the strain gauges in one quarter of slab showing the locations for TN1 to TN5 and TW1 to TW5. The locations for TS1 to TS5 and TE1 to TE5 are directly opposite to those from TN1 to TN5 and TW1 to TW5 respectively. It should also

be noted that there were also strain gauges provided in the lower layer (i.e., the flexural compression mat) of reinforcement. These gauges were denoted as BN1, BS1, BW1 and BE1 and were positioned at the same locations of TN1, TS1, TW1 and TE1 respectively.

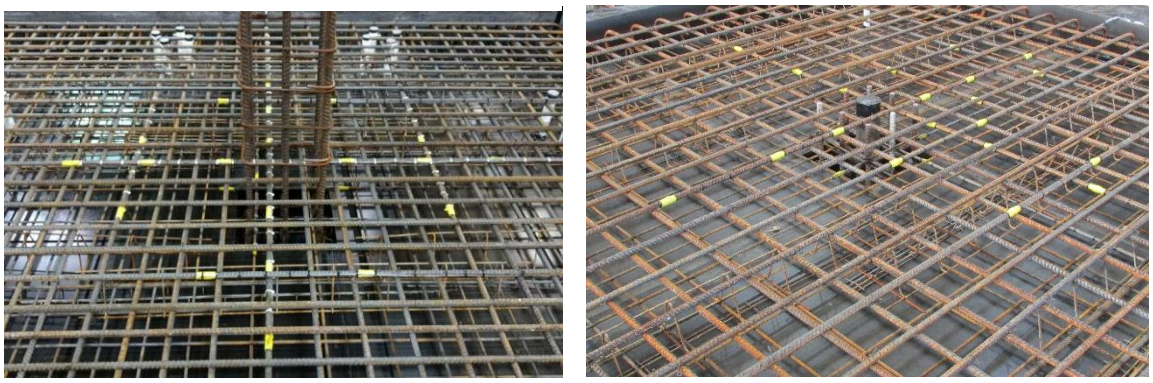

Figure 3-14: Measurement of strains. Pictures showing strain gauges in the steel reinforcement prior casting.

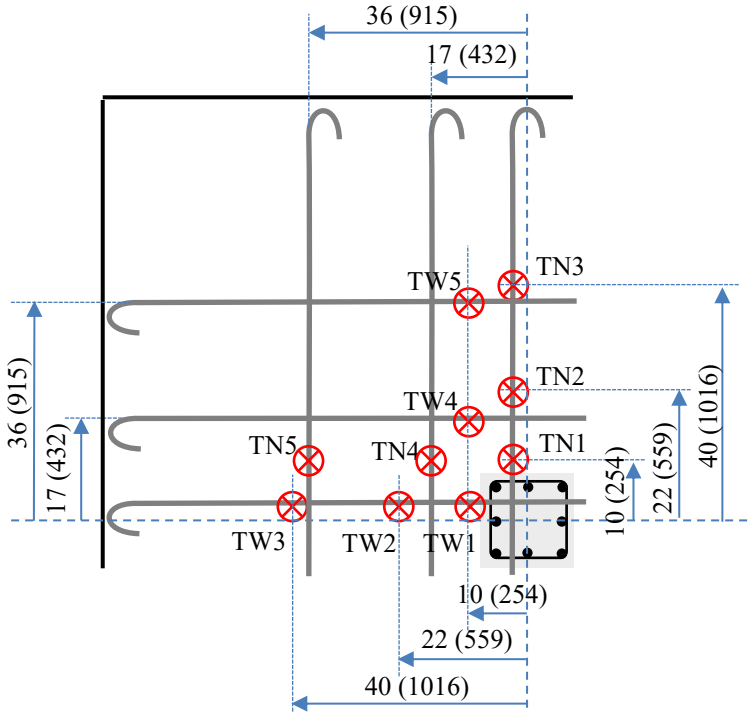

Figure 3-15: Sketch showing locations of strain gauges in the top layer of reinforcement for all specimens.

SPECIMEN #1: C-1.0

Specimen C-1.0 was constructed with a top longitudinal steel reinforcement ratio of 1.00 % and was tested under concentrated loading conditions. Key properties and design details for C-1.0 are shown below in Figure 3-16.

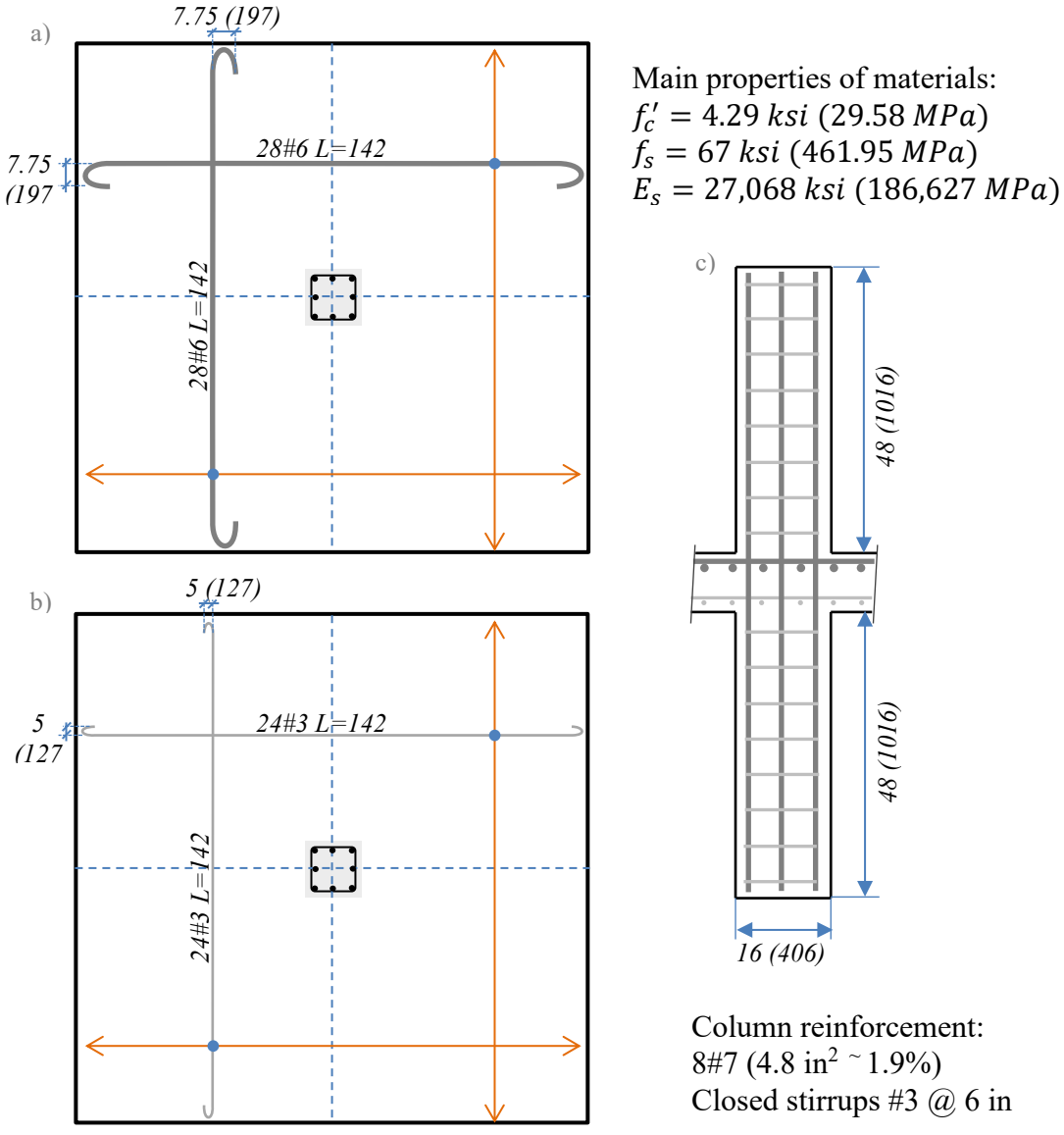

Main properties of materials:
$f_c' = 4.29\ ksi\ (29.58\ MPa)$
$f_s = 67\ ksi\ (461.95\ MPa)$
$E_s = 27{,}068\ ksi\ (186{,}627\ MPa)$

Column reinforcement:
8#7 (4.8 in^2 ~ 1.9%)
Closed stirrups #3 @ 6 in

Figure 3-16: Main characteristics of specimen C-1.0. Detailing of: a) Top reinforcement; b) Bottom reinforcement; c) Column reinforcement.

Summary of test results

Figure 3-17 presents the experimental data coming from the measurement of the deflection of the slab along its four fabrication directions (N, S, E, and W) as shown in Figure 3-11. The information from this plots is used to calculate the rotation of the slab at any given value of shear resistance for each fabrication direction. The rotation is taken as the slope of the trend line, computed using the method of least squares, considering the deflections measured in the LPOT devices 3 to 6.

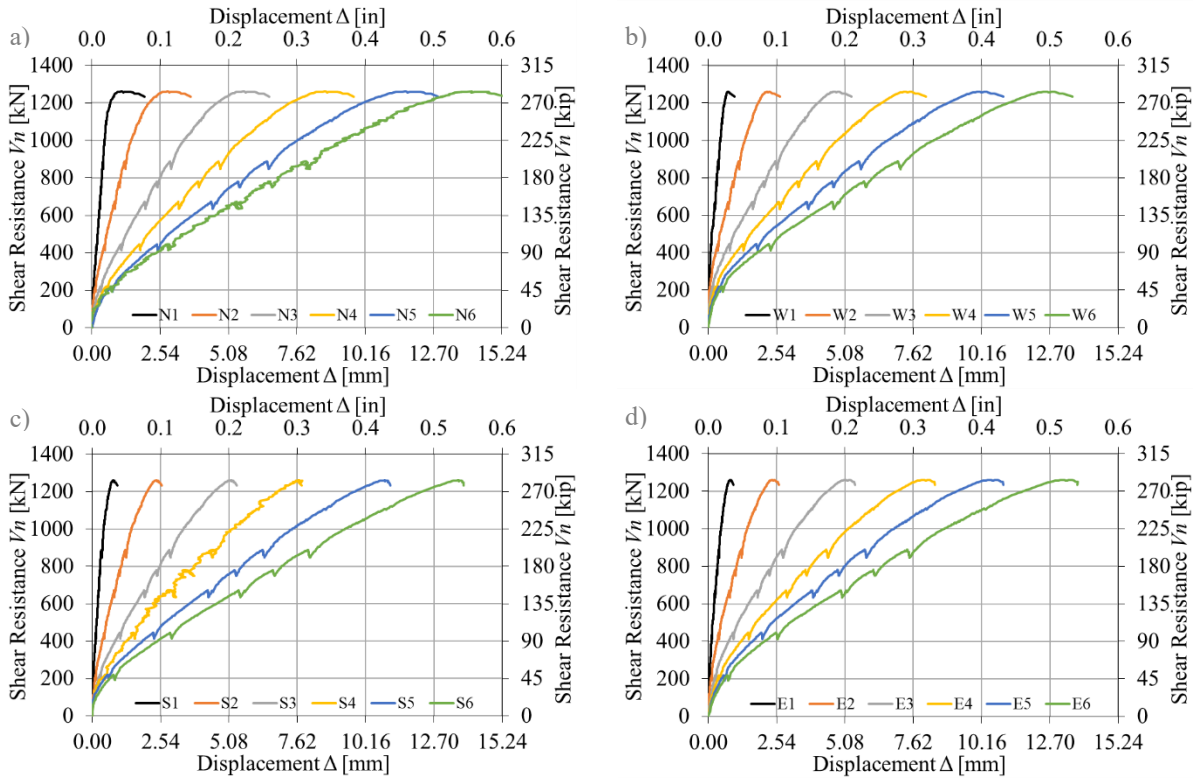

Figure 3-17: Test results for C-1.0. a), b), c) and d) displacements measured at location 1 to 6 in the fabrication direction N, W, S, and E respectively.

Figure 3-18 presents the resulting curves describing the relationship between the applied load and the rotation of the slab for each fabrication direction (N, S, W, and E). The dashed line presents the average of the four curves. As expected, it is possible to

observe that there are not great deviations and the rotations measured in the different directions are similar. As mentioned before, the apparatus used to test the specimen maintains the deflection at the locations where the point loads are applied equal, therefore, forcing the specimen to deflect symmetrically.

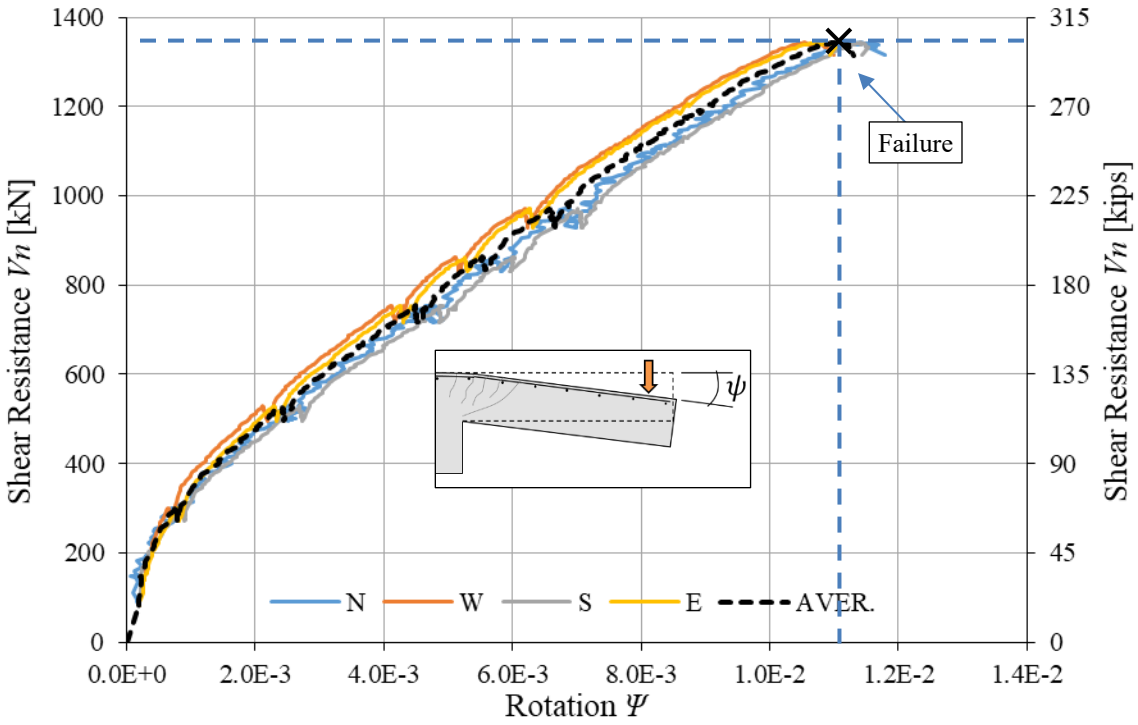

Figure 3-18: Test results for C-1.0. Shear resistance Vn vs rotation of the slab ψ.

Since the specimen sits over the load cell, the measured load does not account for its self-weight and the measured deflections are those caused by the applied load. Therefore, to obtain the actual punching shear strength of the specimen is necessary to add to the value obtained in the test, the self-weight of the slab outside the control perimeter, which is the part of the weight of the specimen that is transferred across the critical shear crack. The self-weight of the specimen is measured on the test setup using the load cell before starting the test and the value is adjusted subtracting the weight of the column by a

ratio of volumes. When the self-weight of the slab (18.5 kips) is included, the actual punching shear strength adds up to approx. 301.9 kips (1343 kN).

Additionally, as shown in Figure 3-18, the rotation observed at failure is in the order of 0.011 and the collapse of the specimen was sudden, at the moment the curve begins plateauing, failure is reached abruptly.

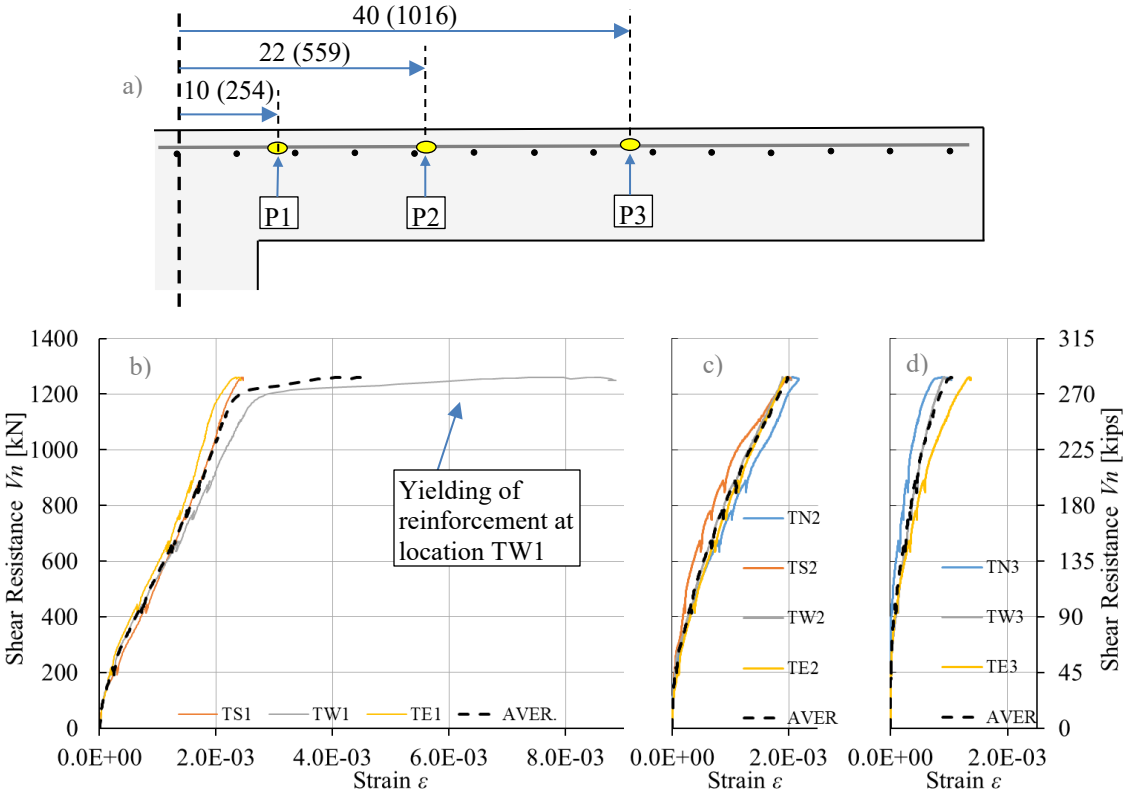

Figure 3-19: Test results for C-1.0. a) Distances from center to location of strain gauges; b), c) and d) Measured strains at locations P1, P2 and P3 respectively in all fabrication directions.

The measured strains in the longitudinal steel reinforcement at the main locations shown in the Figure 3-15 are presented in the Figure 3-19. Yielding of the hogging reinforcement was recorded when approaching the failure load at the location TW1.

A section of the slab can be seen in Figure 3-20. The failure surface presents a shape of truncated pyramid. This surface is characteristic of punching failures of flat plates without shear reinforcement.

Figure 3-20: Test results for C-1.0. Photo showing damage at failure.

Key points:

- Punching shear strength: V_n ***= 301.9 kips (1343 kN)***
- Rotation of the slab at failure: ψ ***= 0.011***
- The hogging reinforcement yields when approaching failure.

SPECIMEN #2: U-1.0

Specimen U-1.0 was nominally identical to C-1.0. This specimen was constructed with a top longitudinal steel reinforcement ratio of 1.00 %; however, was tested under distributed surface pressure loading conditions. Key properties and design details for U-1.0 are shown below in Figure 3-21.

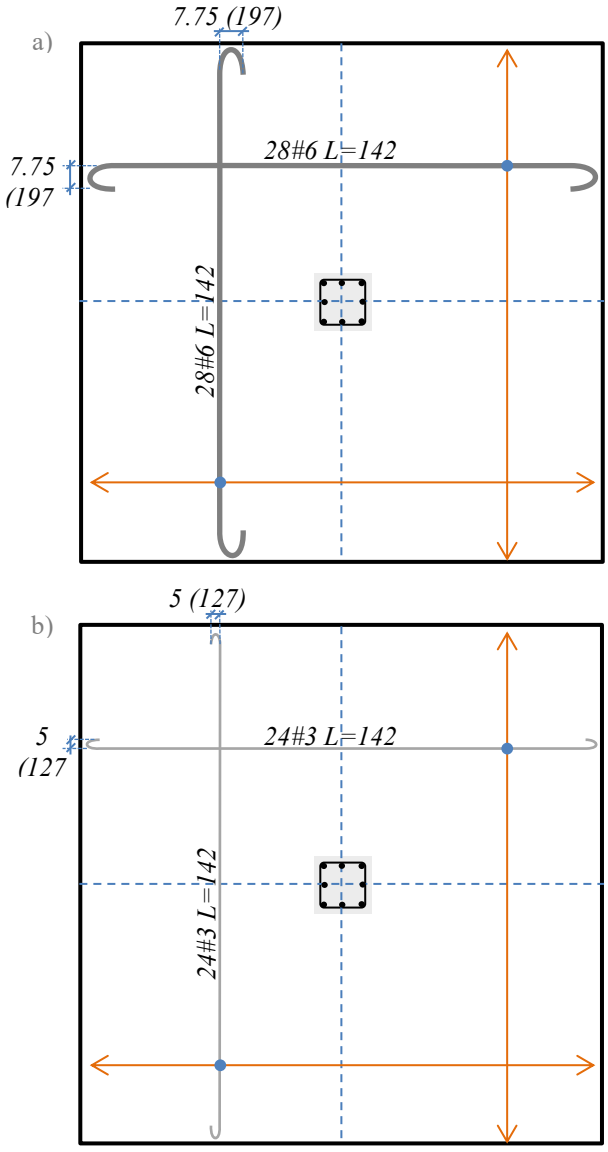

Main properties of materials:
$f_c' = 4.99\ ksi\ (34.41\ MPa)$
$f_s = 67\ ksi\ (461.95\ MPa)$
$E_s = 27{,}068\ ksi\ (186{,}627\ MPa)$

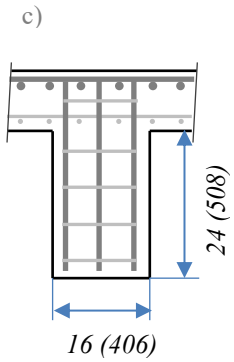

Column reinforcement:
8#7 (4.8 in^2 ~ 1.9%)
Closed stirrups #3 @ 6

Figure 3-21: Main characteristics of specimen U-1.0. Detailing of: a) Top reinforcement; b) Bottom reinforcement; c) Column reinforcement.

Summary of test results

Figure 3-22 presents the experimental data coming from the measurement of the deflection of the slab along its four fabrication directions (N, S, E, and W) as shown in Figure 3-11. The information from this plots is used to calculate the rotation of the slab at any given value of shear resistance for each fabrication direction. The rotation is taken as the slope of the trend line, computed using the method of least squares, considering the deflections measured in the LPOT devices 3 to 6.

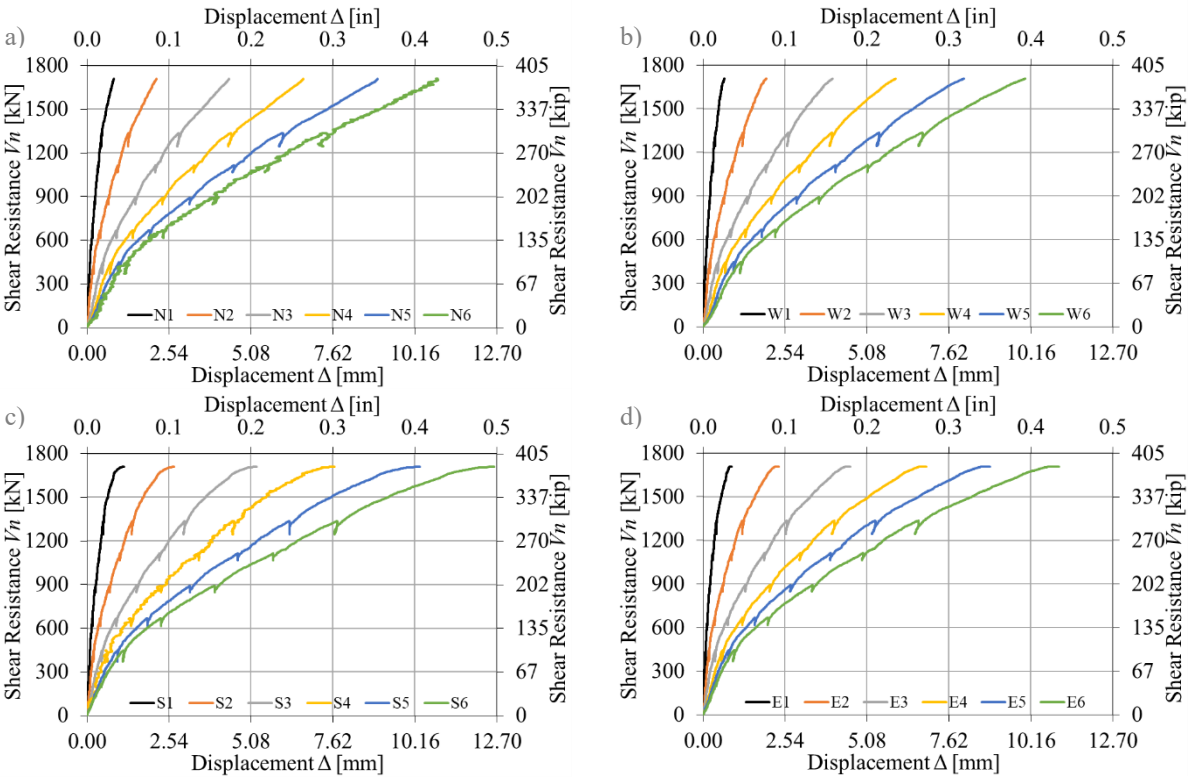

Figure 3-22: Test results for U-1.0. a), b), c) and d) displacements measured at location 1 to 6 in the fabrication direction N, W, S, and E respectively.

Figure 3-23 presents the resulting curves describing the relationship between the applied load and the rotation of the slab for each fabrication direction (N, S, W, and E). The dashed line represents the average of the four curves. When the curve is compared to

the curve of its nominally identical counterpart, C-1.0, it is possible to observe that there are larger deviations at high levels of load and the rotations measured in the different directions differ. As mentioned before, the apparatus used to test the specimen do not controls the deflection at any point, therefore, the specimen may not deflect symmetrically. As expected, the rotation measured in the N-S direction is greater than in the E-W direction in agreement with the reinforcement layout.

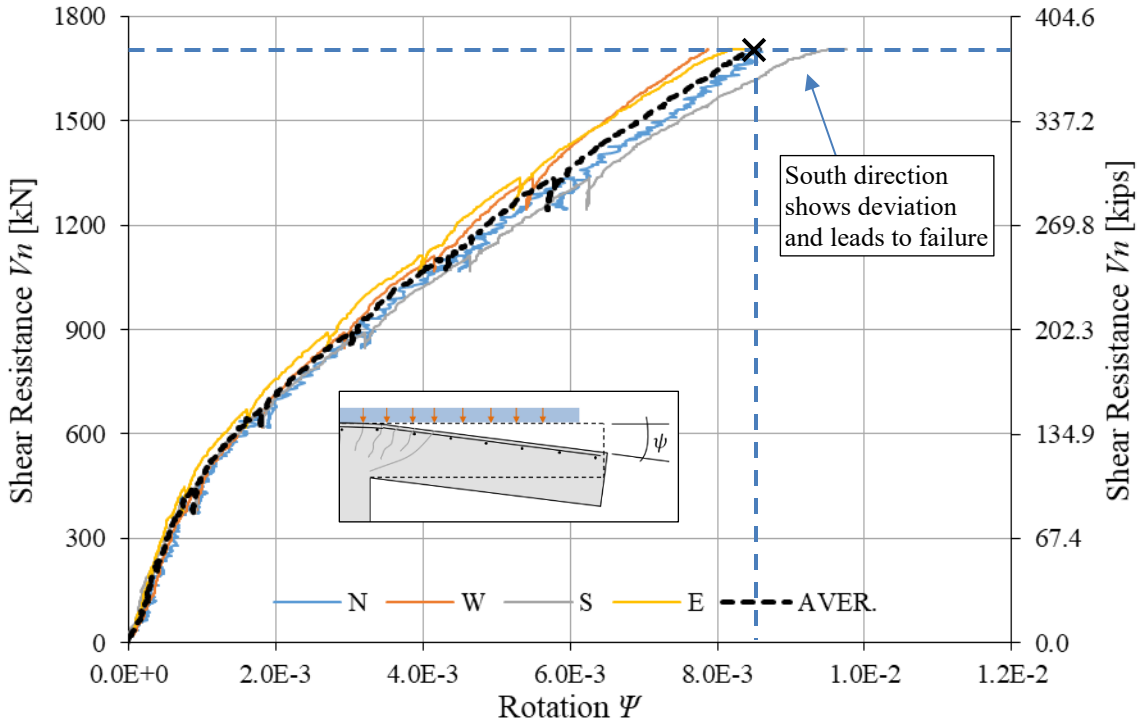

Figure 3-23: Test results for U-1.0. Shear resistance V_n vs rotation of the slab ψ.

Failure occurs on the South side, as is pointed out in Figure 3-23, being compatible to the inclination of the slab recorded. The inclination of the slab at failure is minor but it may have led to a reduced punching shear strength of the specimen.

Since the specimen sits upside down over the testing apparatus, as shown in Figure 3-8, a load equal to the self-weight must be applied for the specimen to begin to deflect

and the load cell to start to record. Therefore, it is not necessary to modify the values obtained in the test to account for self-weight.

Additionally, as shown in Figure 3-23, the rotation observed at failure is in the order of 0.0085 and the collapse of the specimen was sudden, at the moment the curve from the South direction begins plateauing, failure is reached abruptly.

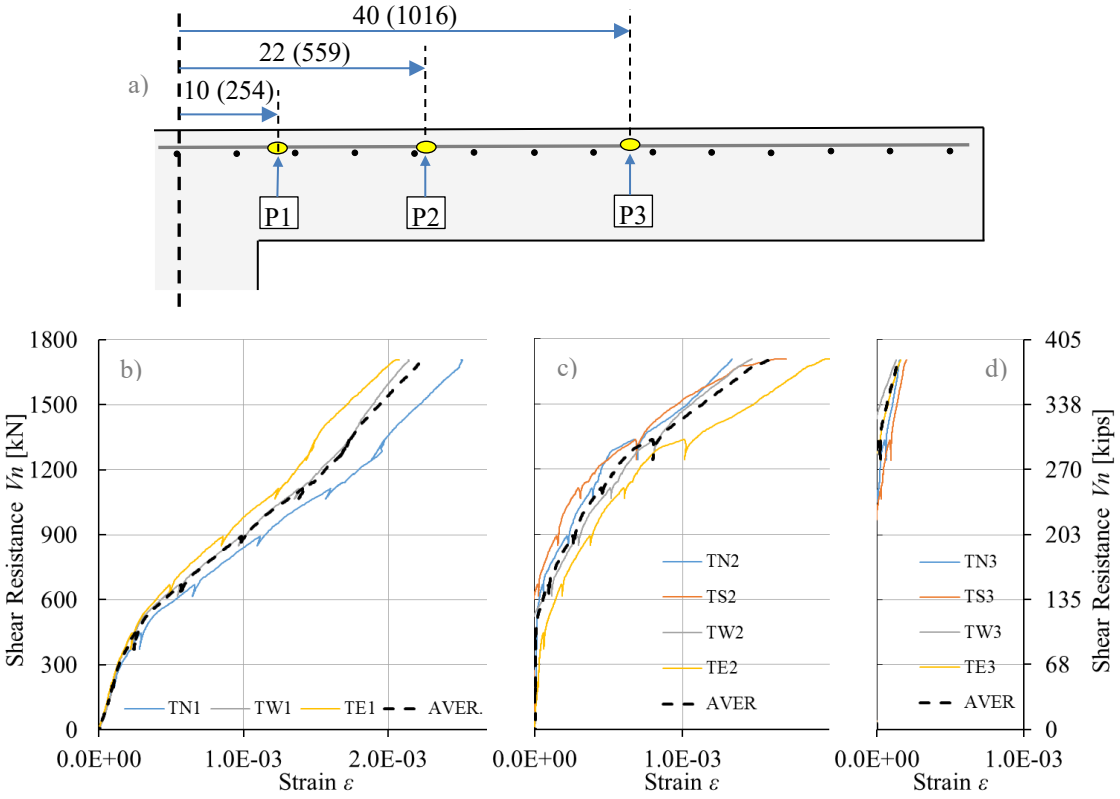

Figure 3-24: Test results for U-1.0. Measured strains. a) Distances from center to location of strain gauges; b), c) and d) Measured strains at locations P1, P2 and P3 respectively in all fabrication directions.

The measured strains in the longitudinal steel reinforcement at the main locations shown in the Figure 3-15 are presented in the Figure 3-24. Yielding of the hogging reinforcement was not recorded at any of the monitored locations, but values near the yield strain were recorded at location P1. When the measured strain at a given location is

compared to the recorded strain in the same location in the test of C-1.0, shown in Figure 3-18, the strain in the reinforcement is always smaller for any value of load.

A section of the slab can be seen in Figure 3-25. The failure surface presents a shape of truncated pyramid. This surface is characteristic of punching failures of flat plates without shear reinforcement. More damaged is observed, including buckled steel bars and spalling of concrete, which is compatible with the higher punching shear strength when compared to C-1.0.

Figure 3-25: Test results for U-1.0. Photo showing damage at failure.

Key points:

- Punching shear strength: V_n ***= 384.0 kips (1708 kN)***
- Rotation of the slab at failure: ψ ***= 0.00863***
- No yielding of the hogging reinforcement.

SPECIMEN #3: C-0.7

Specimen C-0.7 was constructed with a top longitudinal steel reinforcement ratio of 0.72 % and was tested under distributed surface pressure loading conditions. Key properties and design details for C-0.7 are shown below in Figure 3-26.

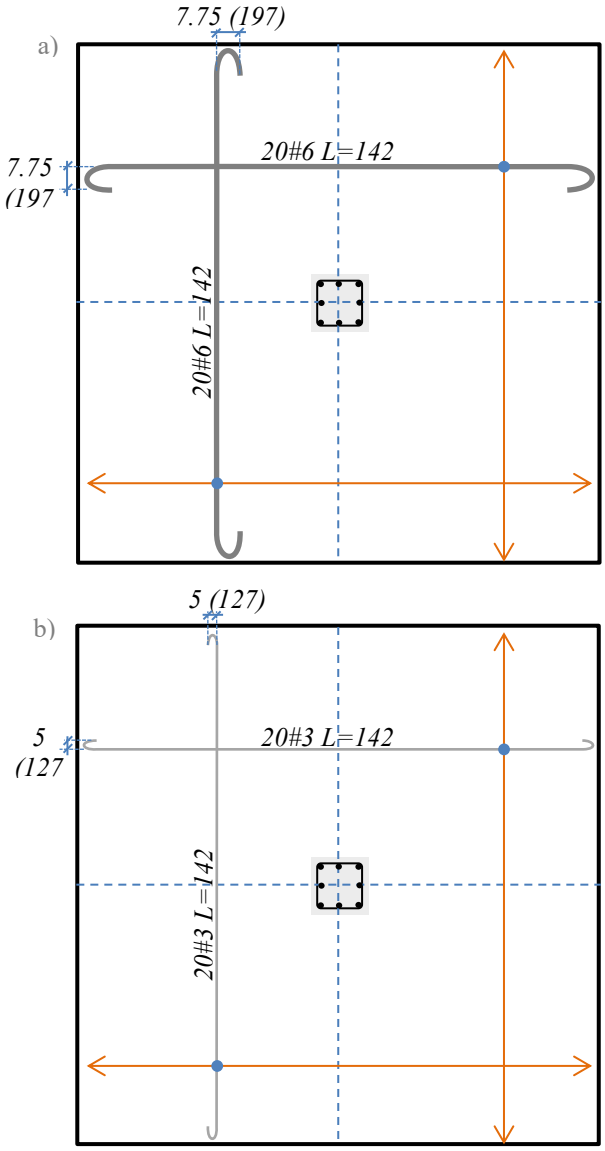

Main properties of materials:
$f_c' = 6.17\ ksi\ (42.54\ MPa)$
$f_s = 67\ ksi\ (461.95\ MPa)$
$E_s = 27{,}068\ ksi\ (186{,}627\ MPa)$

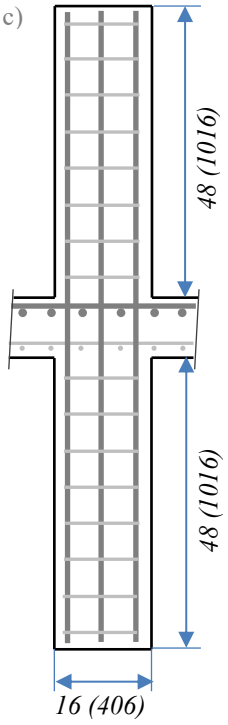

Column reinforcement:
8#7 (4.8 in^2 ~ 1.9%)
Closed stirrups #3 @ 6 in

Figure 3-26: Main characteristics of specimen C-0.7. Detailing of: a) Top reinforcement; b) Bottom reinforcement; c) Column reinforcement.

Summary of test results

Figure 3-27 presents the experimental data coming from the measurement of the deflection of the slab along its four fabrication directions (N, S, E, and W) as shown in Figure 3-11. The information from this plots is used to calculate the rotation of the slab at any given value of shear resistance for each fabrication direction. The rotation is taken as the slope of the trend line, computed using the method of least squares, considering the deflections measured in the LPOT devices 3 to 6.

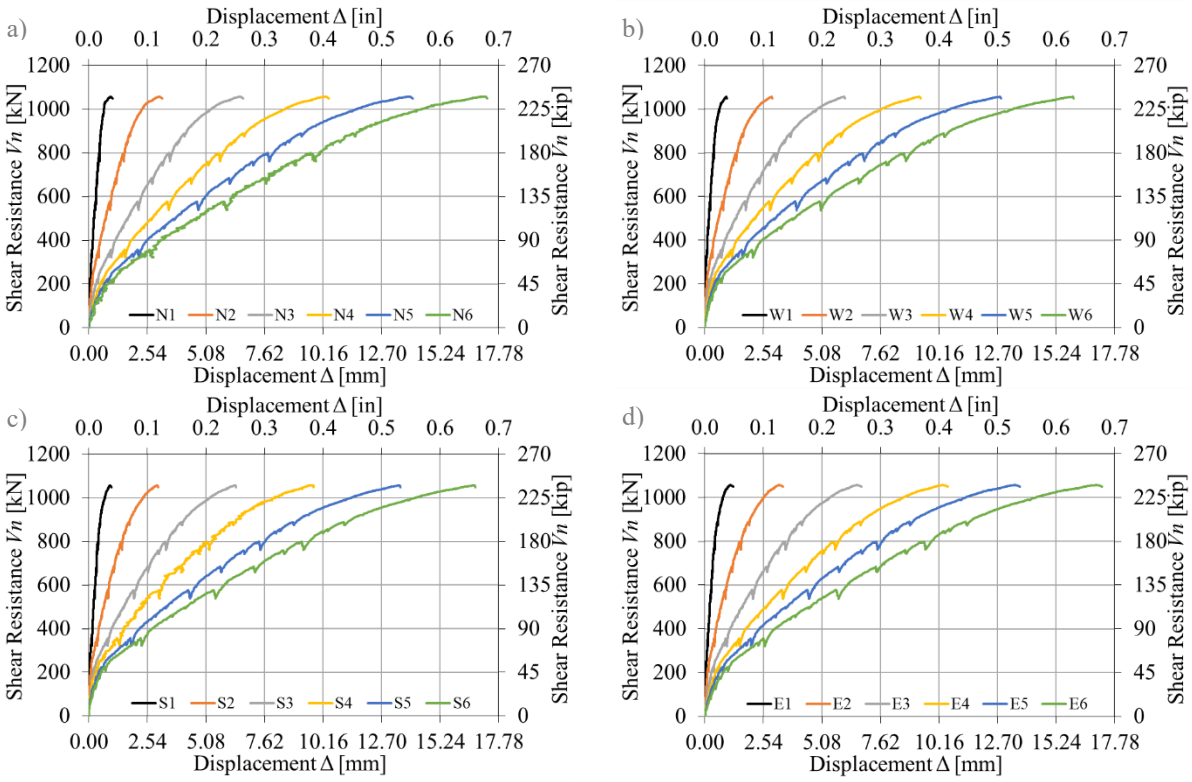

Figure 3-27: Test results for C-0.7. a), b), c) and d) displacements measured at location 1 to 6 in the fabrication direction N, W, S, and E respectively.

Figure 3-28 presents the resulting curves describing the relationship between the applied load and the rotation of the slab for each fabrication direction (N, S, W, and E). Note that the dashed represents the average of the four curves. As expected, it is possible

to observe that there are not great deviations and the rotations measured in the different directions are similar. As mentioned before, the apparatus used to test the specimen maintains the deflection at the locations where the point loads are applied equal, therefore, forcing the specimen to deflect symmetrically.

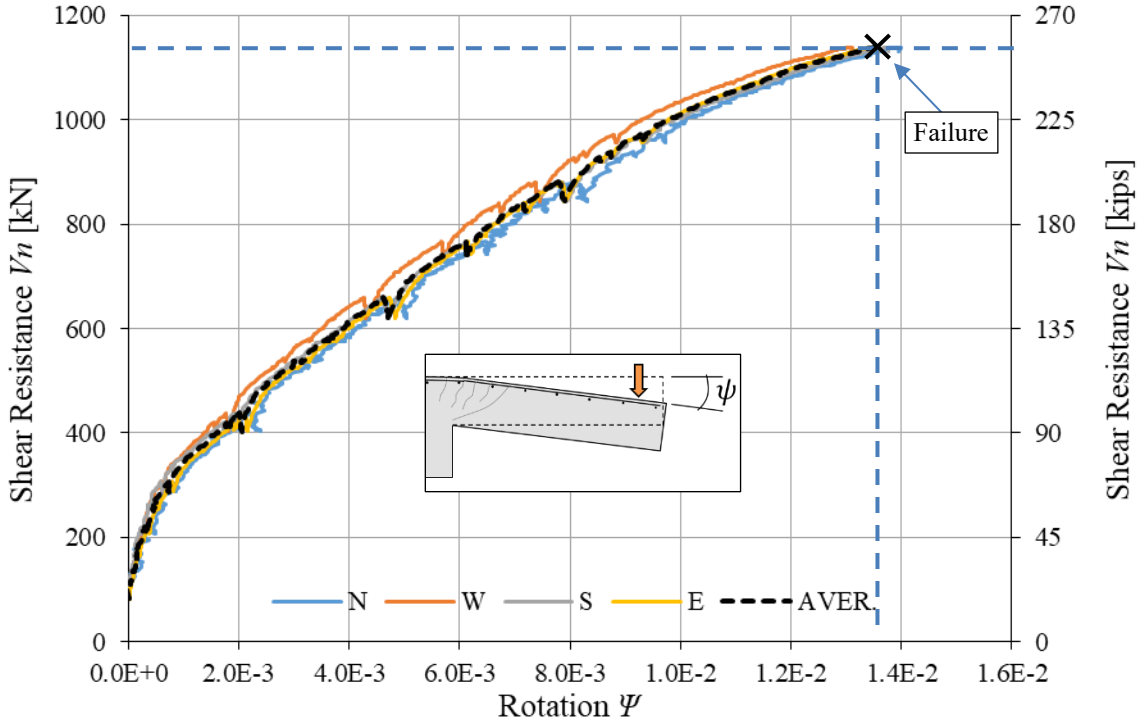

Figure 3-28: Test results for C-0.7. Shear resistance V_n vs rotation of the slab ψ.

Since the specimen sits over the load cell, the measured load does not account for its self-weight and the measured deflections are those caused by the applied load. Therefore, to obtain the actual punching shear strength of the specimen is necessary to add to the value obtained in the test, the self-weight of the slab outside the control perimeter, which is the part of the weight of the specimen that is transferred across the critical shear crack. The self-weight of the specimen is measured on the test setup using the load cell before starting the test and the value is adjusted subtracting the weight of the column by a

ratio of volumes. When the self-weight of the slab (18.4 kips) is included, the actual punching shear strength adds up to approx. 256.15 kips (1139.43 kN).

Additionally, as shown in Figure 3-28, the rotation observed at failure is in the order of 0.0136 and the collapse of the specimen was sudden, at the moment the curve begins plateauing, failure is reached abruptly. Although it is possible to see a softening of the curve when load is approaching failure.

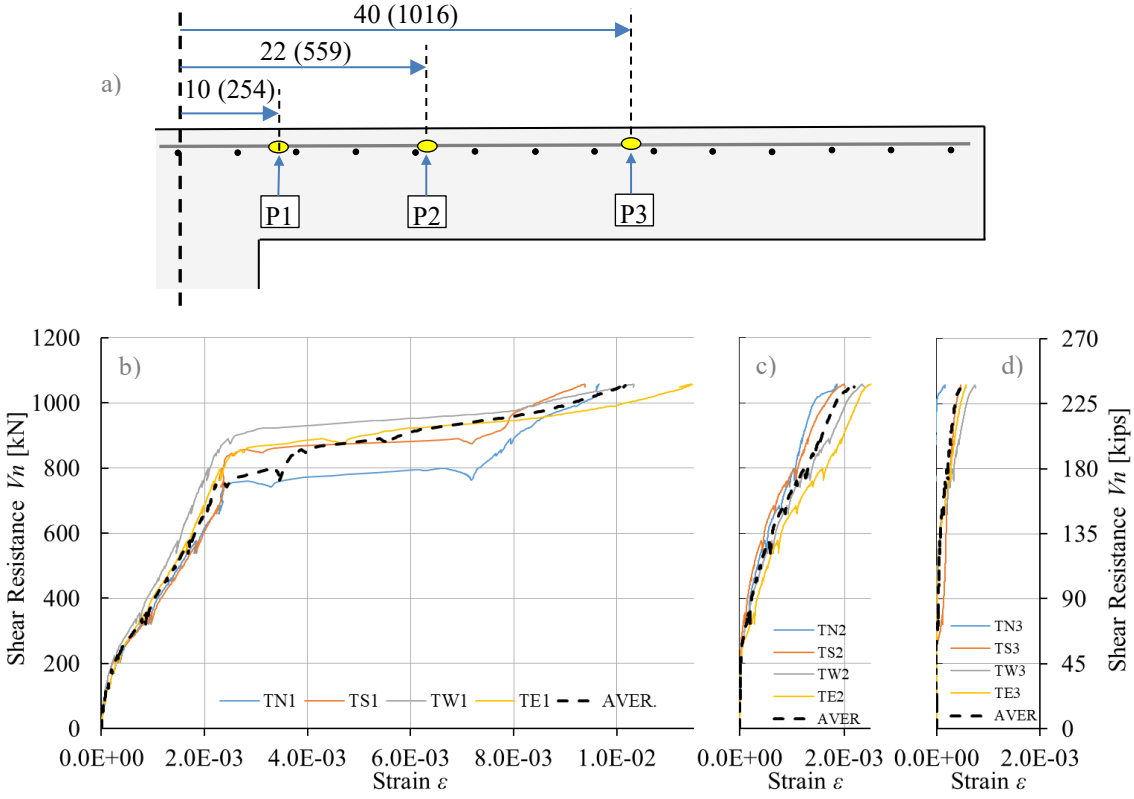

Figure 3-29: Test results for C-0.7. Measured strains. a) Distances from center to location of strain gauges; b), c) and d) Measured strains at locations P1, P2 and P3 respectively in all fabrication directions.

The measured strains in the longitudinal steel reinforcement at the main locations shown in the Figure 3-15 are presented in the Figure 3-29. Yielding of the hogging

reinforcement was recorded in all directions at location P1, and values near the yield strain were recorded in location P2.

A section of the slab can be seen in Figure 3-30. The failure surface presents a shape of truncated pyramid. This surface is characteristic of punching failures of flat plates without shear reinforcement.

Figure 3-30: Test results for C-0.7. Photo showing damage at failure.

Key points:

- Punching shear strength: V_n ***= 256.2 kips (1139 kN)***
- Rotation of the slab at failure: ψ ***= 0.0136***
- The hogging reinforcement reached yielding in all four directions of fabrication (N, S, E, and W) at location P1.

SPECIMEN #4: U-0.7

Specimen U-0.7 was nominally identical to C-0.7. This specimen was constructed with a top longitudinal steel reinforcement ratio of 0.72 %; however, was tested under distributed surface pressure loading conditions. Key properties and design details for U-0.7 are shown below in Figure 3-31.

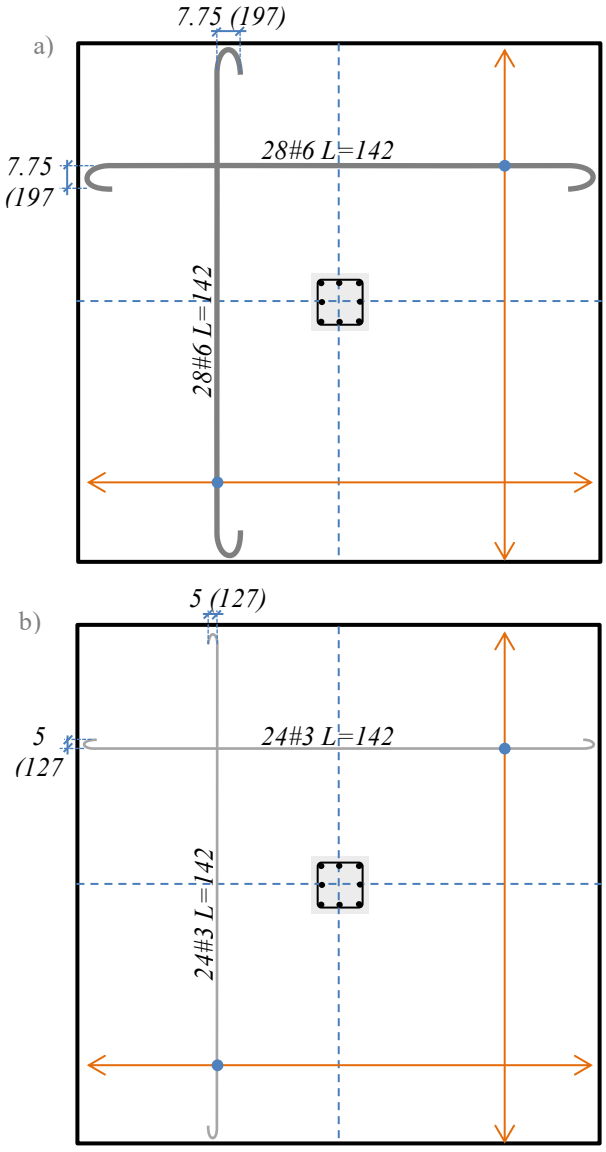

Main properties of materials:
$f_c' = 6.24\ ksi\ (43.02\ MPa)$
$f_s = 67\ ksi\ (461.95\ MPa)$
$E_s = 27{,}068\ ksi\ (186{,}627\ MPa)$

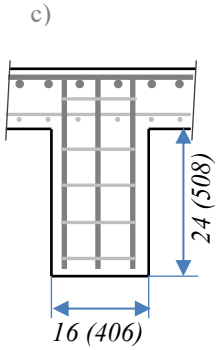

Column reinforcement:
8#7 (4.8 in^2 ~ 1.9%)
Closed stirrups #3 @ 6 in

Figure 3-31: Main characteristics of specimen U-0.7. Detailing of: a) Top reinforcement; b) Bottom reinforcement; c) Column reinforcement

Summary of test results

Figure 3-21 presents the experimental data coming from the measurement of the deflection of the slab along its four fabrication directions (N, S, E, and W), as shown in Figure 3-11. The information from this plots is used to calculate the rotation of the slab at any given value of shear resistance for each fabrication direction. The rotation is taken as the slope of the trend line, computed using the method of least squares, considering the deflections measured in the LPOT devices 3 to 6.

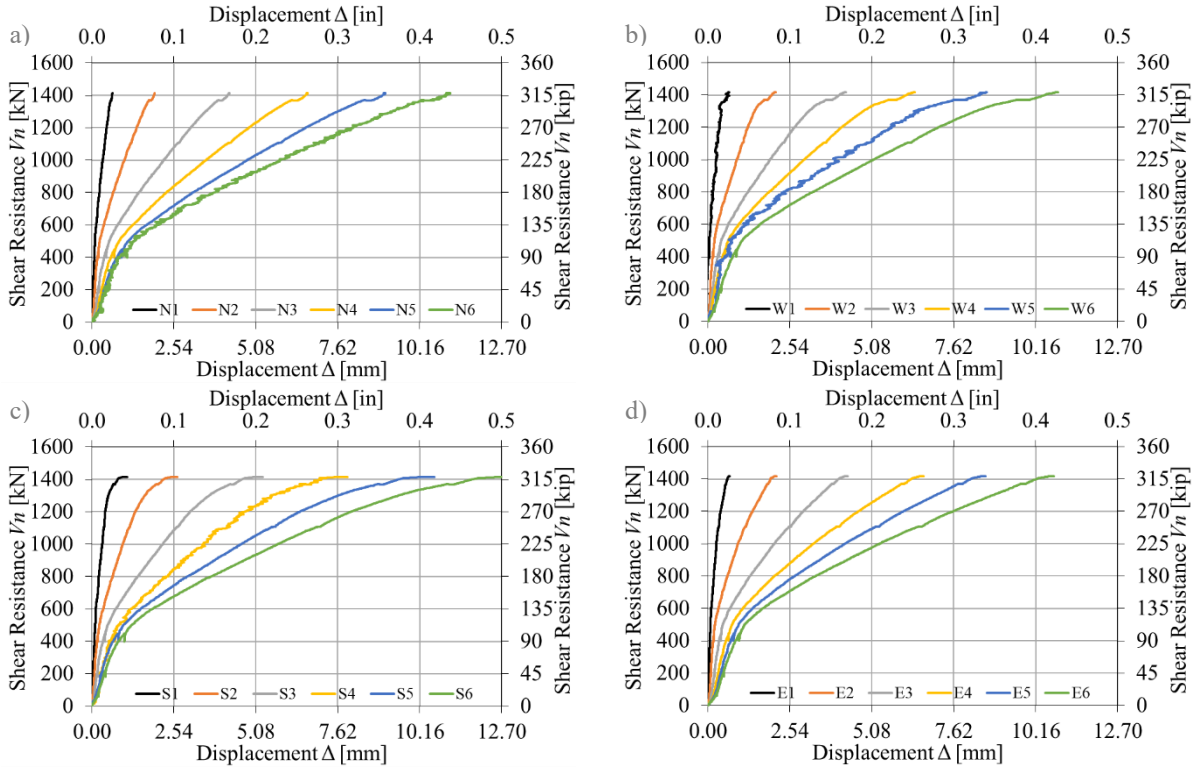

Figure 3-32: Test results for U-0.7. a), b), c) and d) displacements measured at location 1 to 6 in the fabrication direction N, W, S, and E respectively.

Figure 3-32 presents the resulting curves describing the relationship between the applied load and the rotation of the slab for each fabrication direction (N, S, W, and E). Note that the dashed line represents the average of the four curves. When the curve is

compared to the curve of its nominally identical counterpart, C-0.7, it is possible to observe that there are larger deviations at high levels of load and the rotations measured in the different directions differ. As mentioned before, the apparatus used to test the specimen do not controls the deflection at any point, therefore, the specimen may not deflect symmetrically. As expected, the rotation measured in the N-S direction is greater than in the E-W direction in agreement with the reinforcement layout.

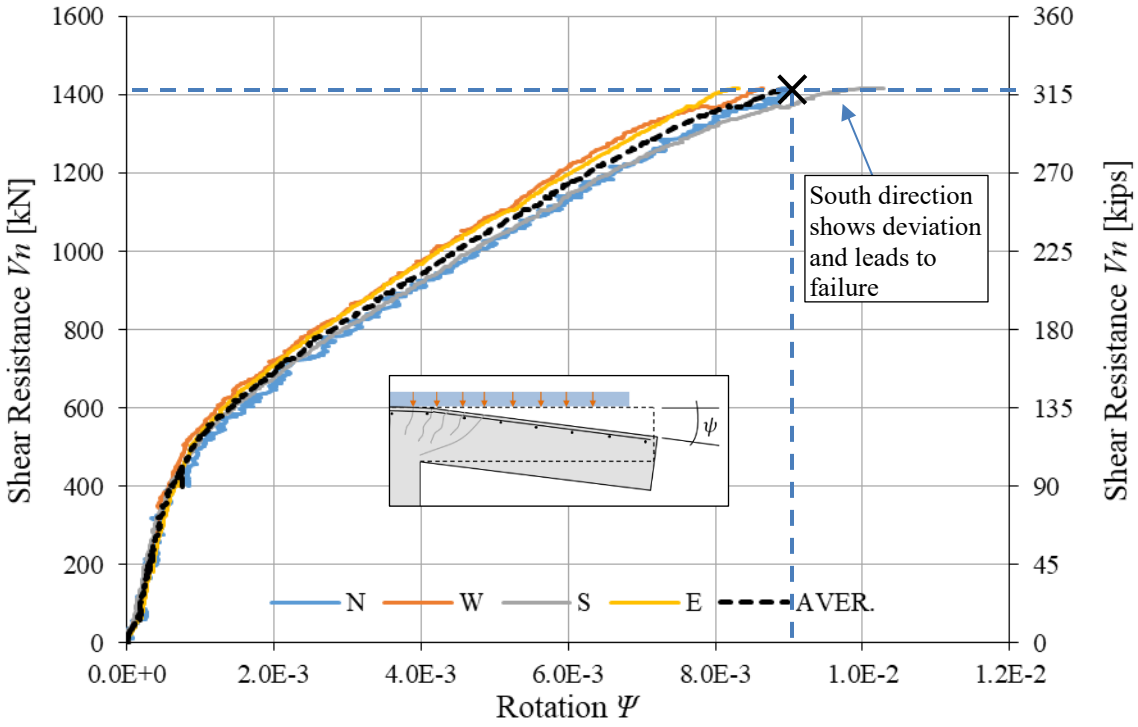

Figure 3-33: Test results for U-0.7. Shear resistance V_n vs rotation of the slab ψ.

Failure occurs on the South side, as is pointed out in Figure 3-33, being compatible to the inclination of the slab recorded. The inclination of the slab at failure may have led to a reduced punching shear strength of the specimen.

Since the specimen sits upside down over the testing apparatus, as shown in Figure 3-8, a load equal to the self-weight must be applied for the specimen to begin to

deflect and the load cell to start to record. Therefore, it is not necessary to modify the values obtained in the test to account for self-weight.

Additionally, as shown in Figure 3-33, the rotation observed at failure is in the order of 0.009 and the collapse of the specimen was sudden, at the moment the curve from the South direction begins plateauing, failure is reached abruptly.

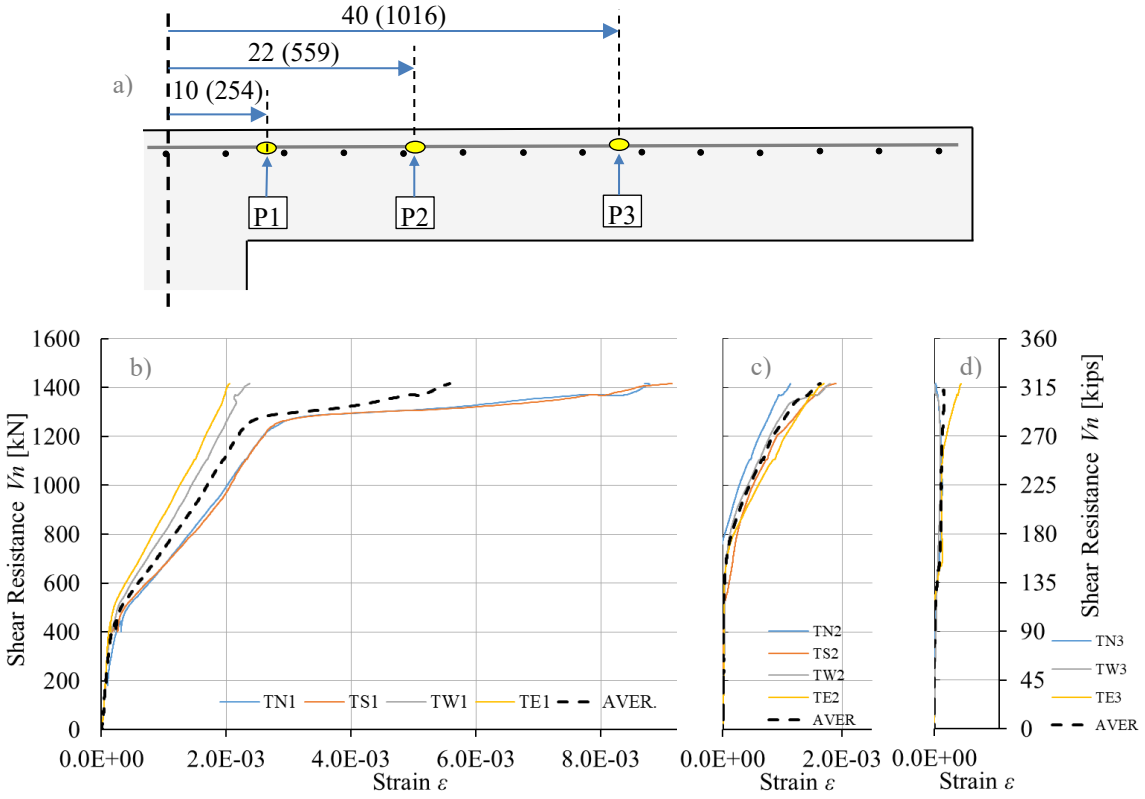

Figure 3-34: Test results for U-0.7. Measured strains. a) Distances from center to location of strain gauges; b), c) and d) Measured strains at locations P1, P2 and P3 respectively in all fabrication directions.

The measured strains in the longitudinal steel reinforcement at the main locations shown in the Figure 3-15 are presented in the Figure 3-34. Yielding of the hogging reinforcement was recorded at locations TN1 and TS1, along the direction where larger rotations were observed. When the measured strain at a given location is compared to the

recorded strain in the same location in the test of C-0.7, shown in Figure 3-28, the strain in the reinforcement is always smaller for any value of load.

A section of the slab can be seen in Figure 3-35. The failure surface presents a shape of truncated pyramid. This surface is characteristic of punching failures of flat plates without shear reinforcement. More damaged is observed, including buckled steel bars and spalling of concrete, which is compatible with the higher punching shear strength when compared to C-0.7.

Figure 3-35: Test results for U-0.7. Photo showing damage at failure.

Key points:

- Punching shear strength: V_n ***= 318.4 kips (1416 kN)***
- Rotation of the slab at failure: ψ ***= 0.00902***
- The hogging reinforcement reached yielding at the locations TN1 and TS1, along the direction where greater rotations of the slab were recorded.

COMPARISON BETWEEN EXPERIMENTS

The normalized shear resistance $V_n/\left(\sqrt{f_c'}db_0\right)$ is plotted against the rotation ψ for all specimens in Figure 3-36. From the plot it is possible to observe that tests conducted in the concentrated load (CL) apparatus reached consistently lower punching shear resistances and developed much greater rotations for all normalized shear load levels when compared with the data obtained from the tests conducted using the uniformly distributed load (UL) apparatus.

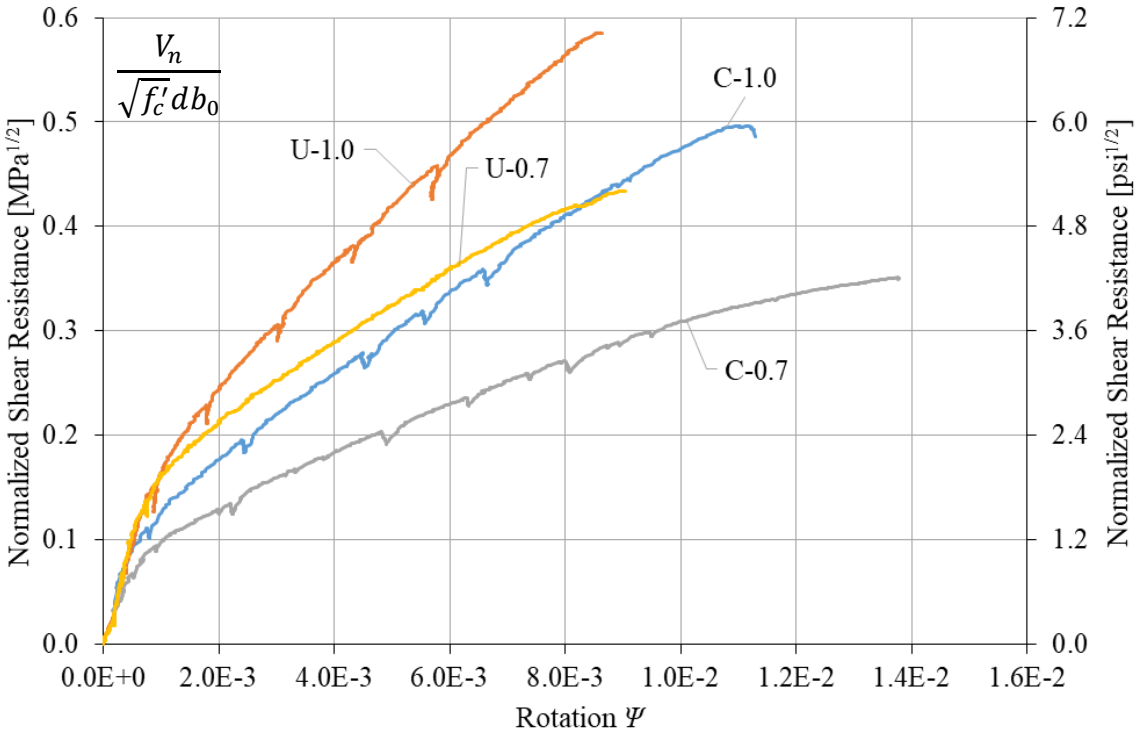

Figure 3-36: Comparison between tests. Normalized shear resistance vs Rotation

Note that in Figure 3-36, curves for CL test specimens (C-1.0 & C-0.7) have been adjusted to account for the self-weight and the self-weight induced rotation of the slab using the measured rotation in UL specimens at a load level equal to the self-weight. Only the part of the isolated slab element adding to shear stress resistance was considered in the self-weight adjustment.

Formulations/provisions to estimate punching shear strength presented in Chapter 2 of this thesis (ACI 318-14, Eurocode 2, *fib* Model Code 2010, and Critical Crack Shear Theory) are fitted from experiments performed using testing procedures that have typically been similar in concept to the Concentrated Load test setup used to test specimens #1 and #3 (C-1.0 & C-0.7) of the experimental program presented in this thesis. Given the findings in Figure 3-36, differences between the results obtained from the specimens tested in the UL test setup (U-1.0 & U-0.7) and those tested in the CL test setup (C-1.0 & C-0.7), is arguable if having a static/constant procedure for all loading scenarios is rational. Moreover, in real-world cases, depending on the structure employed in the field, one test setup may be more representative than the other.

As noted in Table 2-4 and discussed in Chapter 2, the North-American building code provisions, ACI 318-14, do not account for the longitudinal steel reinforcement ratio ρ_l to assess the punching shear resistance of slab-column connections, however, Eurocode 2 and *fib* Model Code 2010 do. As is possible to observe from the results presented in Figure 3-36, the approach taken by the American standard is not capable of capturing the trend clearly shown in the test data pertaining to the increase in punching resistance as a result of increased longitudinal steel reinforcement ratio. This observation has been made by many others in the past (Guandalini and Muttoni et al. 2009); however, all of these prior testing programs employed more conventional concentrated load testing procedures. Thus, it is interesting to note that this well-established trend was observed in both loading scenarios and, as such, was found to be independent of the loading condition employed in the test. More on this topic is discussed in Chapter 4 where the tests results are compared with numerical models.

Chapter 4: Numerical Simulations

In this chapter the results obtained from a series of numerical analyses are presented. The numerical models were built to represent the specimens comprising the experimental program and the analyses were carried out to compare the results, assert the validity of the computer simulation as a good representation of the reality and extend the analyses to other cases. In all cases, the overall dimensions, the longitudinal steel reinforcement conditions, the materials properties, and the applied loading conditions were nominally-identical to that comprising the slab specimens and employed in the testing program.

VecTor4, a nonlinear finite element analysis program from the *VecTor Analysis Group* and dedicated to the analysis of three-dimensional reinforced concrete structures, was employed to perform the nonlinear analyses.

MATERIAL MODELS

The models specified into the program to describe the behavior of the RC in the slab-column connections are listed in Table 4-1.

Table 4-1: Models describing the mechanical behavior of RC

Compression Base Curve:	Hognestad	***Steel Hysteresis:***	Seckin (w/ Bauschinger)
Compression Post-Peak:	Park-Kent (mod)	***Rebar Dowel Action:***	Tassios (Crack Slip)
Compression Softening:	Vecchio 1992-A	***Rebar Buckling:***	Dhakal-Maekawa (mod)
Tension Stiffening:	Modified Bentz	***Crack Spacing:***	CEB-FIP 1978 – Def.
Tension Softening:	Bilinear	***Slip Distortion:***	Walraven
Confinement Strength:	*Kupfer/Richart*	*Among others*	

More information regarding the material models used, and their implementation within the *VecTor* analysis software can be found elsewhere (Wong, Vecchio, and Trommels 2013).

MODELS CHARACTERISTICS

Test specimen characteristics and testing procedures were discussed in Chapter 3. For each specimen, a quarter-slab model, as shown in Figure 4-1, was considered and restraints were provided along the edges of the model to enforce symmetry conditions. The quarter-slab modeling approach was done to reduce computation times required for the analyses.

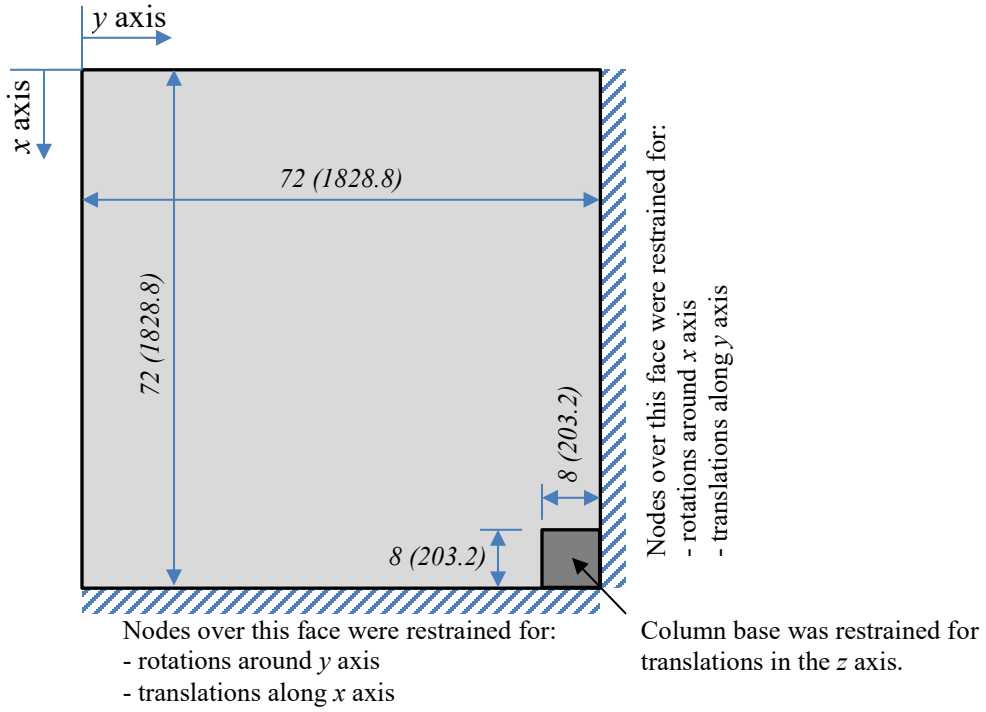

Figure 4-1: General dimensions and restraint conditions adopted for the numerical models [in (mm)]

The steel reinforcing bars used in the construction of the slabs was modeled discretely, using truss bar finite elements. Two types of steel reinforcement materials were

specified for the truss elements, corresponding to US No. 3 and No. 6 reinforcing bars with mechanical properties provided in Table 3-3.

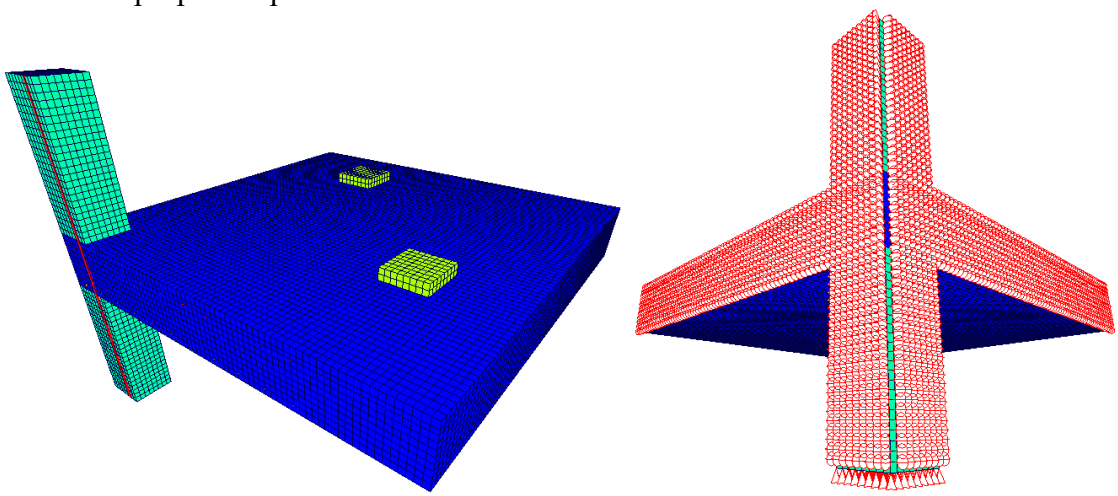

Figure 4-2: Capture of the model for CL specimens showing created mesh, material assignments and nodal retrains.

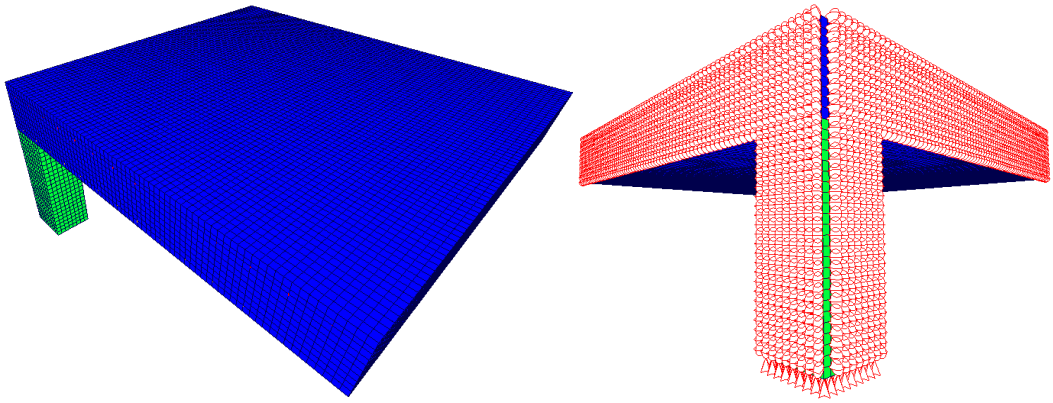

Figure 4-3: Capture of the model for UL specimens showing created mesh, material assignments and nodal retrains.

The tension mat of reinforcement was modeled using the exact effective depths of the reinforcing bars provided in the *x* and *y* directions of the slab. However, for the compressive mat of reinforcement, the truss bar finite elements used to represent the

compression reinforcing bars were placed at the mean value of the (flexural) effective depth for the x and y directions.

Two concrete materials were used in the models, one to represent the slab concrete and the other to represent the column concrete. The two concrete material types had the same mechanical properties, listed in Table 3-2 for each specimen; however, the material type created to represent the column was modeled with smeared reinforcement to include column reinforcement contributions.

A common meshing strategy was used to model the slab regions for all analyses performed. The slab was divided into 10 linear brick finite elements through the depth and a brick element aspect ratio of approximately 1.0. This element sizing required 72 brick elements in each orthogonal direction and resulted in the use of 51,840 solid elements to represent the slab regions of the testing specimens.

Load was applied to simulate the conditions employed in the two different testing scenarios. For specimens tested using the UL apparatus, point loads were applied to every node on the top surface of the slab within the loaded area shown in Figure 3-8. Note that uniformly distributed loads are not supported in the version of the software used. For specimens tested in the CL apparatus, two rigid plates were added to the model at the locations where the vertical support struts are provided to distribute forces and avoid local punching failures from developing. However, in this case, prescribed vertical displacements were applied at the locations of the supports and the base of the intersecting column was restrained.

SPECIMEN #1: C-1.0

The displaced shape obtained from the analysis of C-1.0 is presented in Figure 4-4. Note that the displaced shown corresponds to a load level of 71 % of ultimate (i.e., $0.7 \cdot V_u$). As seen in the image and corroborated by way of calculated displacements, the model is computed to deform symmetrically as a result of the prescribed displacement loading protocol employed in the analysis.

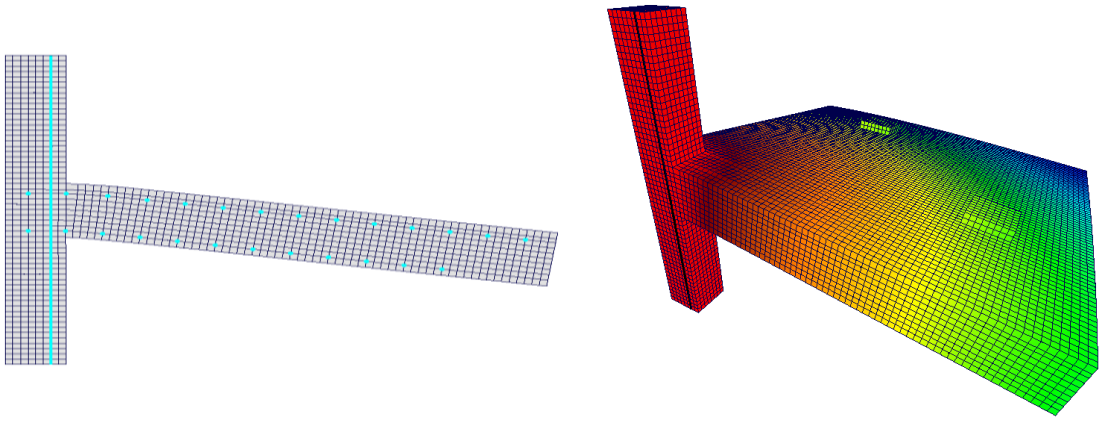

Figure 4-4: Displaced shape of the numerical model for specimen C-1.0 under a load level of $0.7 \cdot V_u$ (x 30 magnification of displacements shown)

The numerical model was found to provide reasonable estimates of the load-rotation response of the slabs, as shown in Figure 4-5. The first stretch of the curve is identical for both the model and the test; however, the stiffness of the computed response does not starts to decline until the shear reaches approximately 90 kips (400 kN), while the stiffness of the test specimen exhibited softening much earlier at a value of shear around 45 kips (200 kN). After the shear resistance surpassed 180 kips (800 kN) the model showed a loss of stiffness, the curve gently plunged below the experimental data and reached failure at an inferior value of load and rotation when compared to test. The differences can be attributed to the variability in the values to determine the concrete mechanical properties, most importantly in the tests to obtain the tensile strength and the strain at peak of the

compressive strength, which could have influenced the resistance in the model. Also it is important to keep in mind that the numerical model is been contrasted with the results of a single test rather than an average of several identical tests.

In Figure 4-6, the strains in the tension reinforcement at several different monitored locations are plotted against the two-way shear resistance Vn. It is possible to observe good agreement between the experimental data and the model. In Figure 4-6d, the labels of the monitored locations imply that the strain observed at that point is comparable to the data recorded in two locations of the test, i.e. the location TNS1 in the model is analogous to the locations TN1 and TS1 in the tested specimen (refer to Figure 3-15).

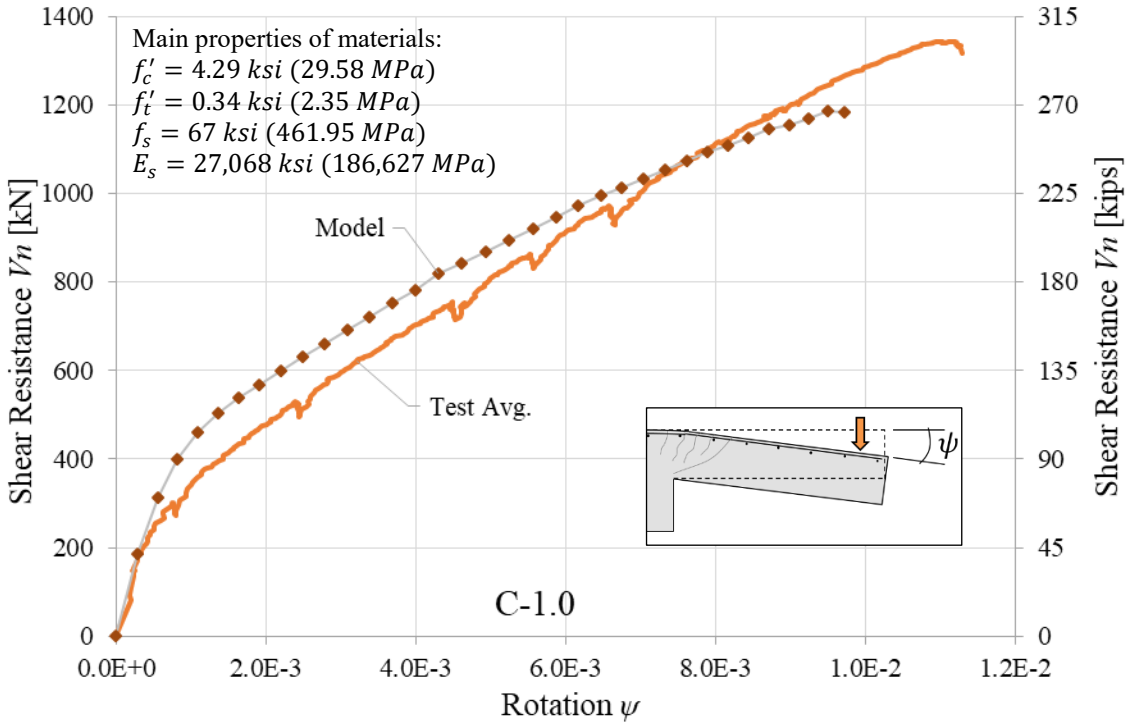

Figure 4-5: Results from numerical model of the specimen C-1.0. Shear resistance V_n vs rotation of the slab ψ

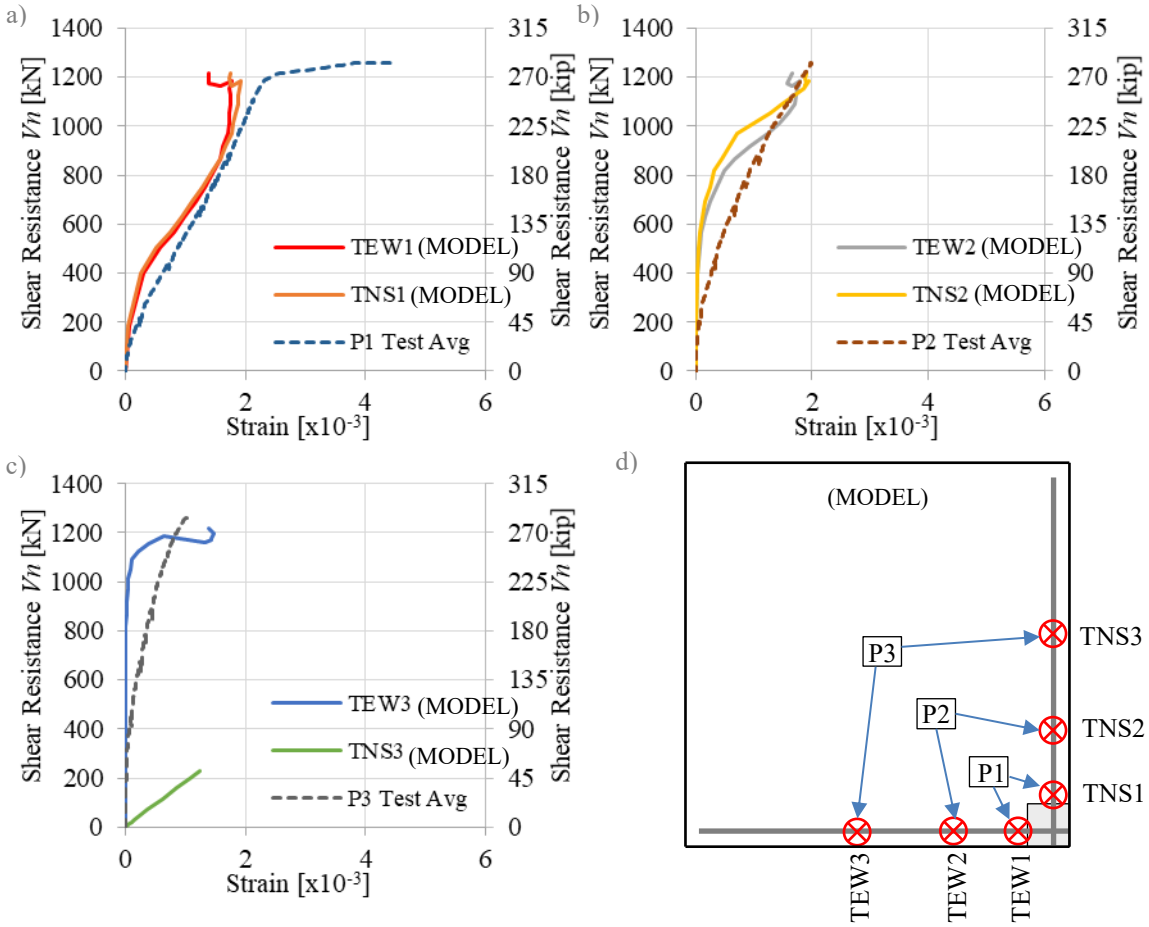

Figure 4-6: a), b) and c) Average strain in the steel reinforcement measured at P1, P2 and P3 in the test (Refer to Figures 3-15 and 3-19) contrasted with their analogous position in the model, d) Monitored locations in the model in correspondence with monitored locations in the test.

In Table 4-2, key points from the test and the numerical model are compared.

Table 4-2: Comparison between key points from the model and test of C-1.0

	TEST	*MODEL*
Shear at failure	1343 kN (302 kips)	1186 kN (267 kips)
Rotation of slab at failure	0.0110	0.0095

SPECIMEN #2: U-1.0

The displaced shape obtained from the analysis of U-1.0 is presented in Figure 4-7. Note that the displaced shown corresponds to a load level of 68 % of ultimate (i.e., $0.68 \cdot V_u$). As corroborated by way of calculated displacements, the model does not deform symmetrically in agreement with the loading conditions and the reinforcement layout considering the difference in effective depth in the x- and y-directions.

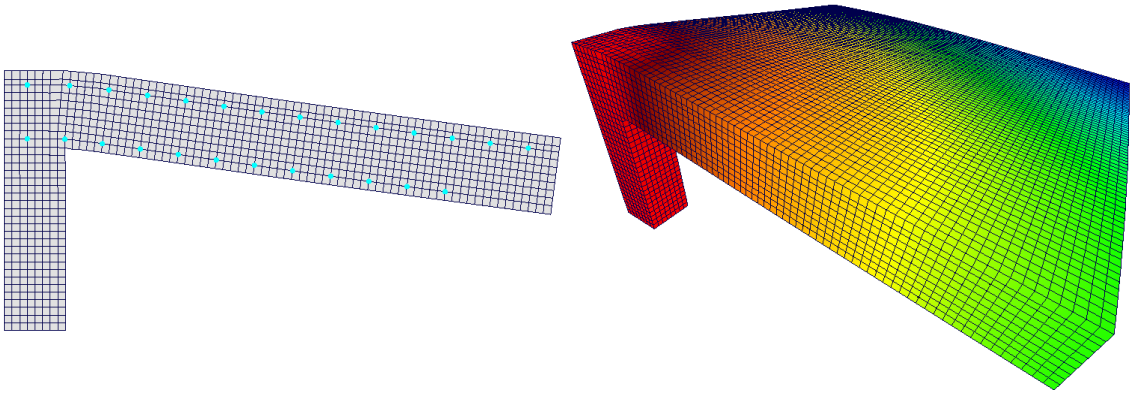

Figure 4-7: Displaced shape of the numerical model for specimen U-1.0 under a load level of $0.68 \cdot V_u$ (x 30 magnification of displacements shown)

The numerical model was found to provide reasonable estimates of the load-rotation response of the slabs, as shown in Figure 4-8. The model shows a slightly higher initial stiffness and reaches slightly superior values of shear resistance for any rotation of the slab. The model curve approaches the experimental data at higher values of load; however, the experiment fails sooner. A comparative analysis is provided in the following section related to the possible causation of this difference which seems to be pertaining to slab-column connections tested with surface pressure loading conditions. Additionally, as mentioned before, the numerical model is been contrasted with the results of a single test rather than an average of several identical tests.

In Figure 4-9, the strains in the tension reinforcement at several different monitored

locations are plotted against the two-way shear resistance Vn. Again, it can be seen good agreement between the experimental data and the model. In Figure 4-9.d) the labels of the monitored locations imply that the strain observed at that point is comparable to the data recorded in two locations of the test, i.e. the location TNS1 in the model is analogous to the locations TN1 and TS1 in the tested specimen (refer to Figure 3-15).

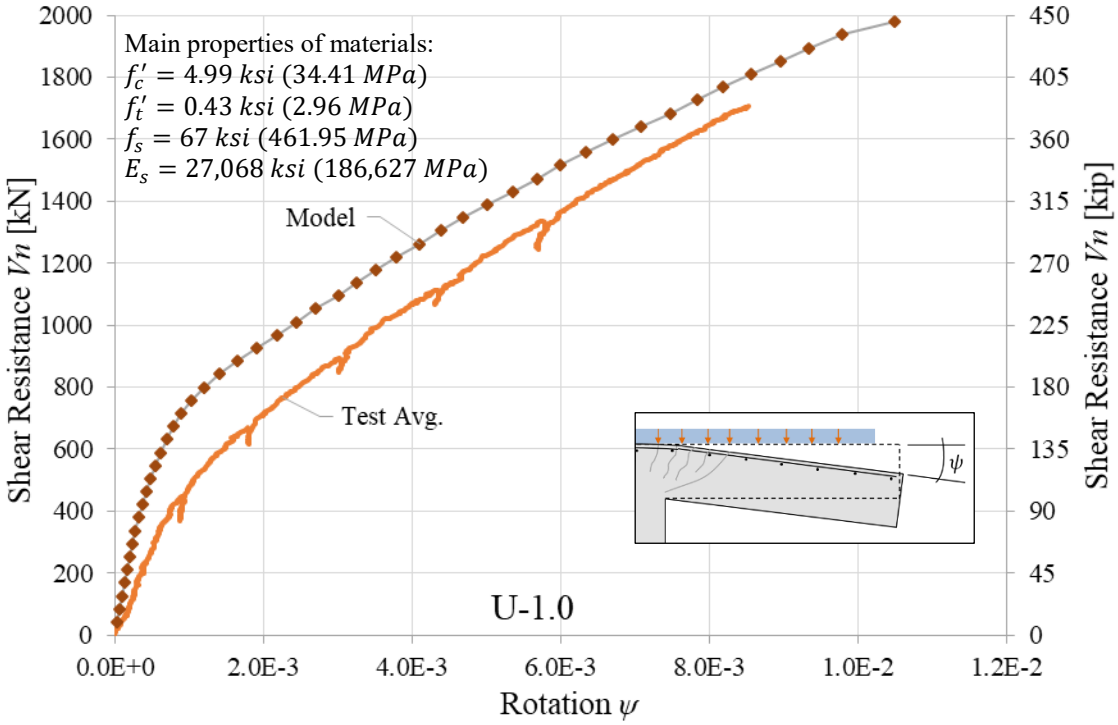

Figure 4-8: Results from numerical model of the specimen U-1.0. Shear resistance V_n vs rotation of the slab ψ

In Table 4-3, key points from the test and the numerical model are compared.

Table 4-3: Comparison between key points from the model and test of U-1.0

	TEST	*MODEL*
Shear at failure	1708 kN (384 kips)	1978 kN (445 kips)
Rotation of slab at failure	0.0086	0.0105

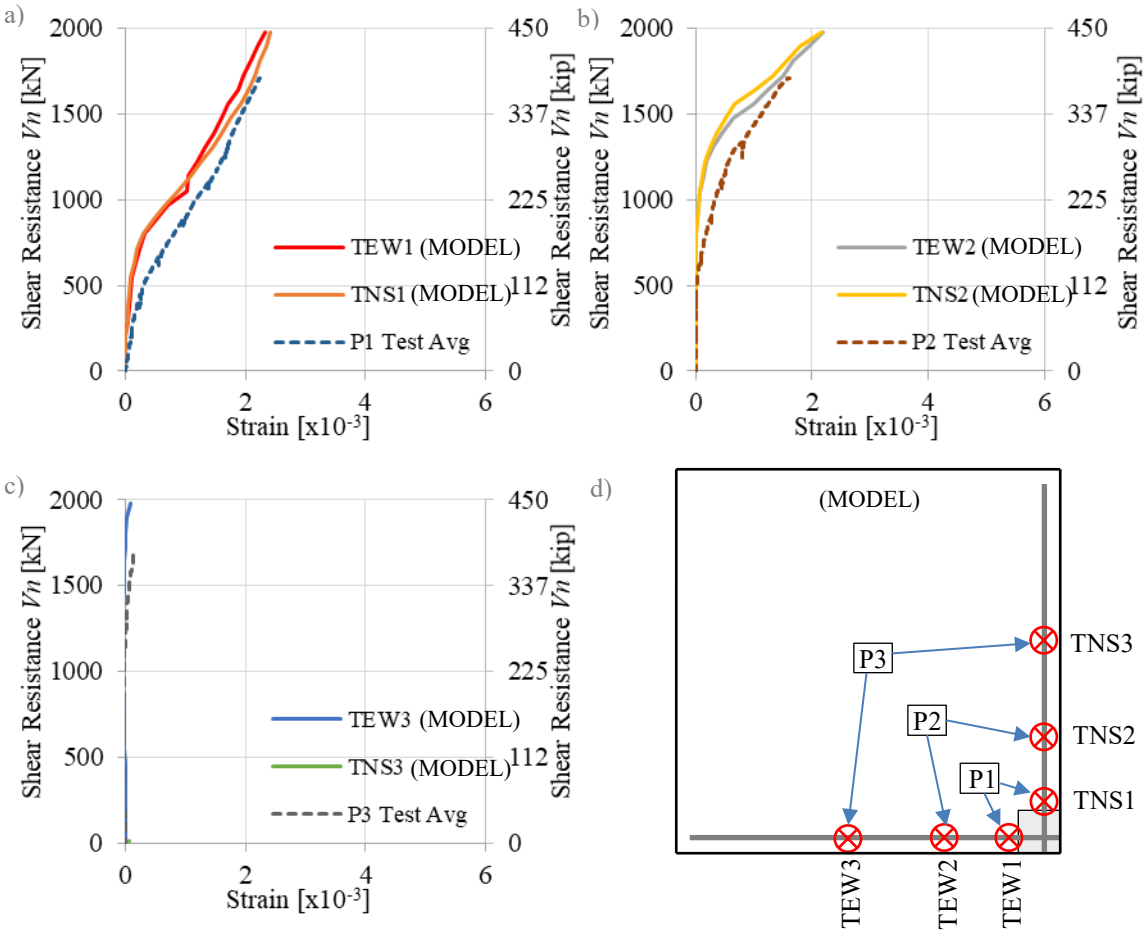

Figure 4-9: a), b) and c) Average strain in the steel reinforcement measured at P1, P2 and P3 in the test (Refer to Figures 3-15 and 3-24) contrasted with their analogous position in the model, d) Monitored locations in the model in correspondence with monitored locations in the test.

SPECIMEN #3: C-0.7

The displaced shape obtained from the analysis of C-0.7 is presented in Figure 4-4. Note that the displaced shown corresponds to a load level of 68 % of ultimate (i.e., $0.68 \cdot V_u$). As seen in the image and corroborated by way of calculated displacements, the model is computed to deform symmetrically as a result of the prescribed displacement loading protocol employed in the analysis.

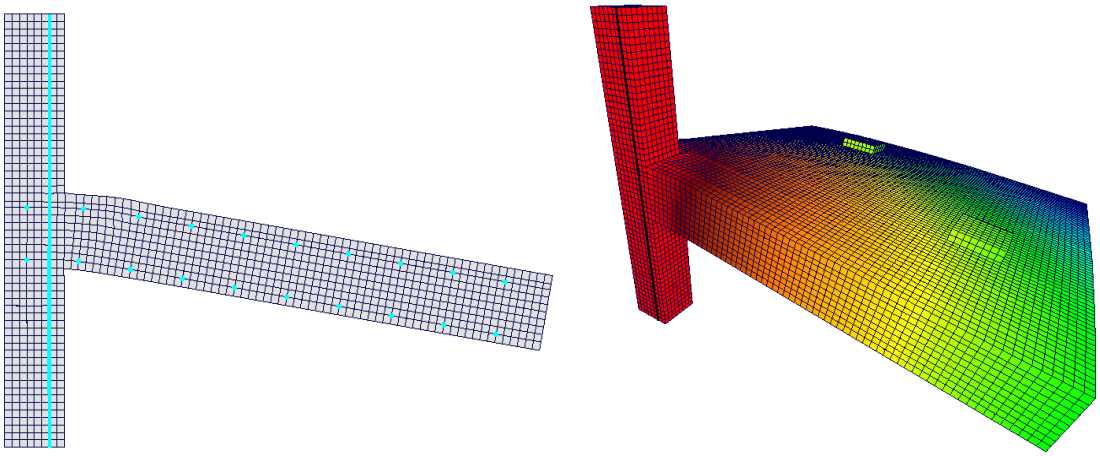

Figure 4-10: Displaced shape of the numerical model for specimen C-0.7 under a load level of $0.68 \cdot V_u$ (x 30 magnification of displacements shown)

The numerical model was found to provide reasonable estimates of the load-rotation response of the slabs, as shown in Figure 4-11; however, the model can resist more load at same rotation. This characteristic was found in other plots, but at low levels of load. In other models, at higher values of resistance, the curve tends to gently approach the experimental data, feature not found in this case. The difference can be attributed to the variability in the values to determine the concrete mechanical properties, most importantly in the tensile strength of concrete, which could add up to the resistance in the model. Additionally, note that the numerical model is been contrasted with the results from a single test rather than an average of several identical tests.

The load-rotation relationship derived from the numerical model presents a sudden loss of stiffness at around the same value of rotation of the slab at which the specimen reaches failure in the test (0.0135). The curve becomes nearly horizontal for a few load steps before regaining some stiffness and finally reaching collapse. It would be possible to expect collapse of the specimen at this point.

In Figure 4-12, the strains in the tension reinforcement at several different locations are plotted against the two-way shear resistance *Vn*. Good agreement is found between the experimental data and the model considering the differences in Figure 4-11. In Figure 4-12.d), the labels of the monitored locations imply the strain observed is comparable to the data recorded in two locations of the test, i.e. the location TNS1 in the model is analogous to the locations TN1 and TS1 in the tested specimen (refer to Figure 3-15).

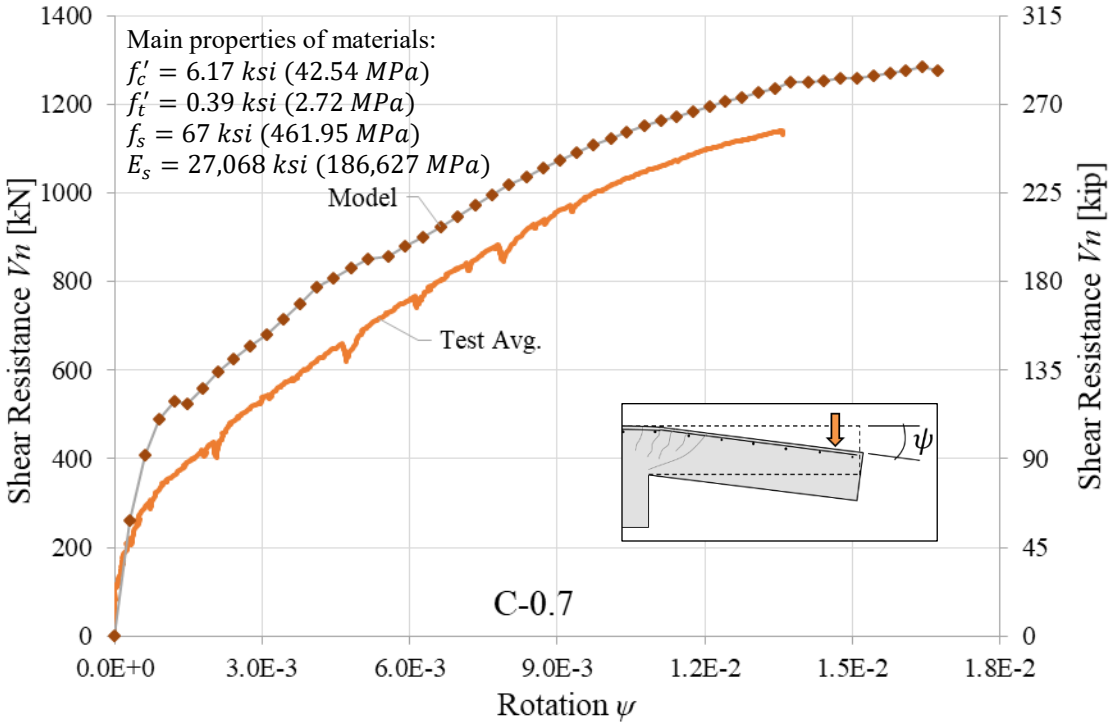

Figure 4-11: Results from numerical model of the specimen C-0.7. Shear resistance V_n vs rotation of the slab ψ

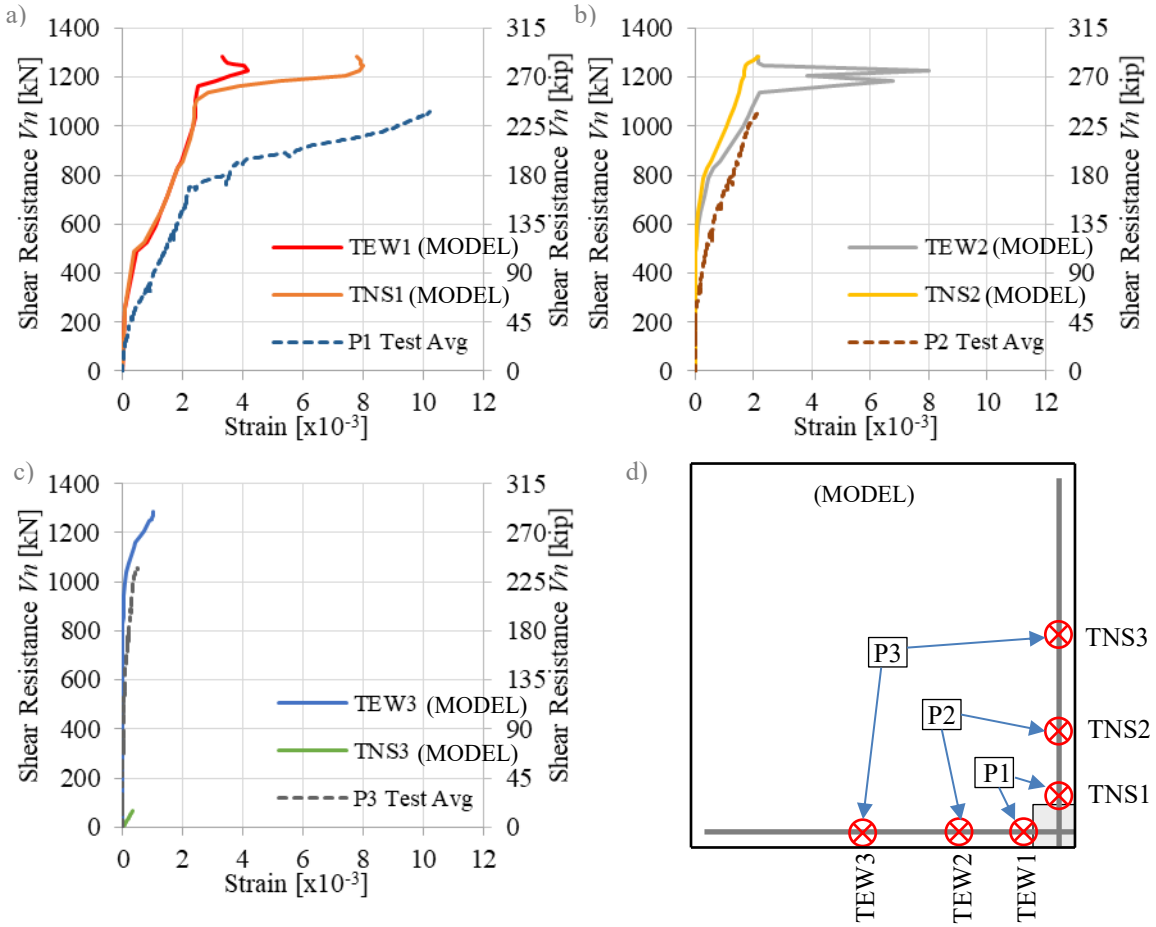

Figure 4-12: a), b) and c) Average strain in the steel reinforcement measured at P1, P2 and P3 in the test (Refer to Figures 3-15 and 3-29) contrasted with their analogous position in the model, d) Monitored locations in the model in correspondence with monitored locations in the test.

In Table 4-4, key points from the test and the numerical model are compared.

Table 4-4: Comparison between key points from the model and test for C-0.7.

	TEST	*MODEL*
Shear at failure	1139 kN (256 kips)	1285 kN (289 kips)
Rotation of slab at failure	0.0136	0.0165

SPECIMEN #4: U-0.7

The displaced shape obtained from the analysis of U-0.7 is presented in Figure 4-13. Note that the displaced shown corresponds to a load level of 71 % of ultimate (i.e., $0.71 \cdot V_u$). As corroborated by way of calculated displacements, the model does not deform symmetrically in agreement with the loading conditions and the reinforcement layout considering the difference in effective depth in the x- and y-directions.

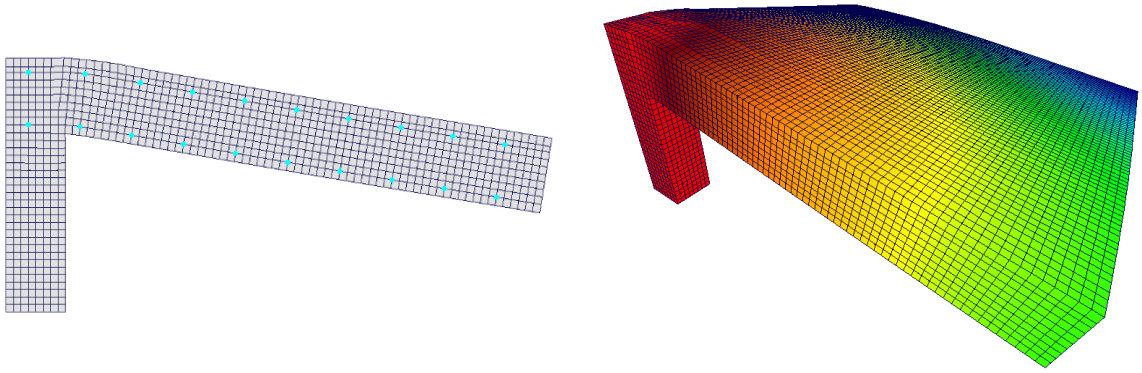

Figure 4-13: Displaced shape of the numerical model for specimen U-0.7 under a load level of $0.71 \cdot V_u$ (x 30 magnification of displacements shown)

The numerical model was found to provide reasonable estimates of the load-rotation response of the slabs, as shown in Figure 4-14. The model shows a slightly higher initial stiffness and reaches superior values of shear resistance for any rotation of the slab. This is also a characteristic found in other plot, C-0.7 (refer to Figure 4-11). The models presenting this feature have high compressive strength of concrete. The difference can be attributed to the variability in the values to determine the concrete mechanical properties, most importantly in the tensile strength of concrete, which could add up to the resistance in the model. Additionally, the numerical model is been contrasted with the results of a single test rather than an average of several identical tests.

The slab-column connection fails sooner in the experiment showing a shear strength

much lower than the obtained in the model. Failure in the tested specimen occurs at the rotation when the model starts to loose stiffness. A comparative analysis is provided in the following section related to the possible causation of this difference which seems to be pertaining to slab-column connections tested with surface pressure loading conditions.

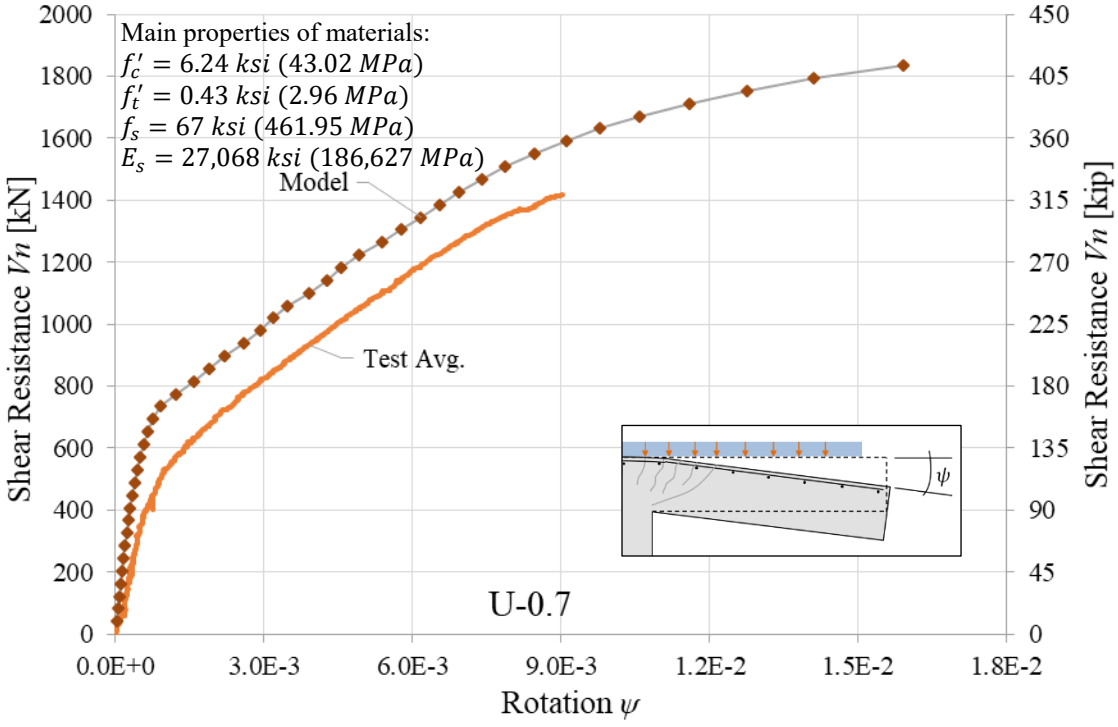

Figure 4-14: Results from numerical model of the specimen U-0.7. Shear resistance V_n vs rotation of the slab ψ

In Figure 4-15, the strains in the tension reinforcement at several different monitored locations are plotted against the two-way shear resistance Vn. Good agreement is shown between the experimental data and the model. In Figure 4-15.d) the labels of the monitored locations imply that the strain observed at that point is comparable to the data recorded in two locations of the test, i.e. the location TNS1 in the model is analogous to the locations TN1 and TS1 in the tested specimen (refer to Figure 3-15).

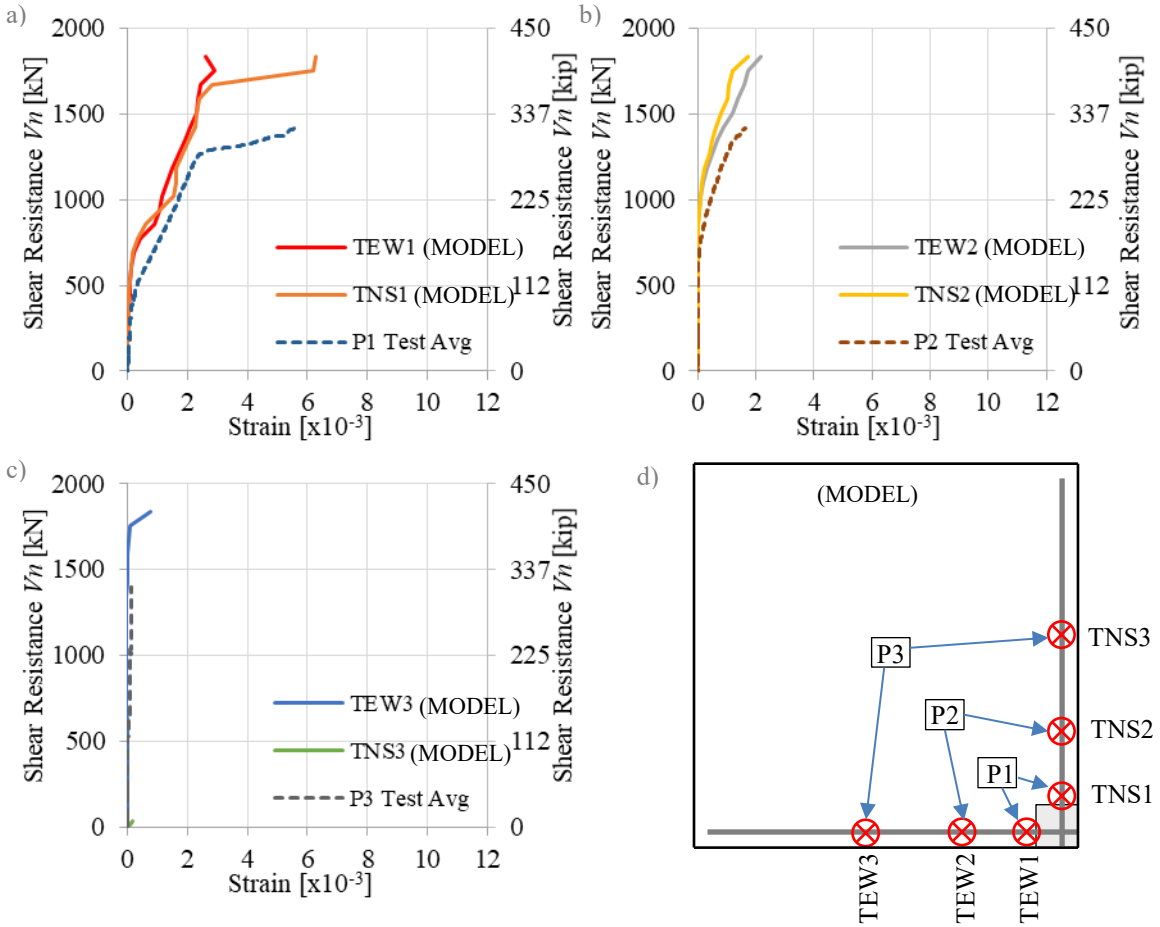

Figure 4-15: a), b) and c) Average strain in the steel reinforcement measured at P1, P2 and P3 in the test (Refer to Figures 3-15 and 3-34) contrasted with their analogous position in the model, d) Monitored locations in the model in correspondence with monitored locations in the test.

In Table 4-5, key points from the model and test of U-0.7 can be found.

Table 4-5: Comparison between key points from the model and test of U-0.7.

	TEST	*MODEL*
Shear at failure	1416 kN (318 kips)	1835 kN (412 kips)
Rotation of slab at failure	0.0090	0.0159

DISCUSSION OF RESULTS

Comparison between Experiments and Numerical models

The normalized shear resistance $V_n/\left(\sqrt{f_c'}db_0\right)$ versus rotation ψ response obtained from all numerical models and tests is presented in Figure 3-31.

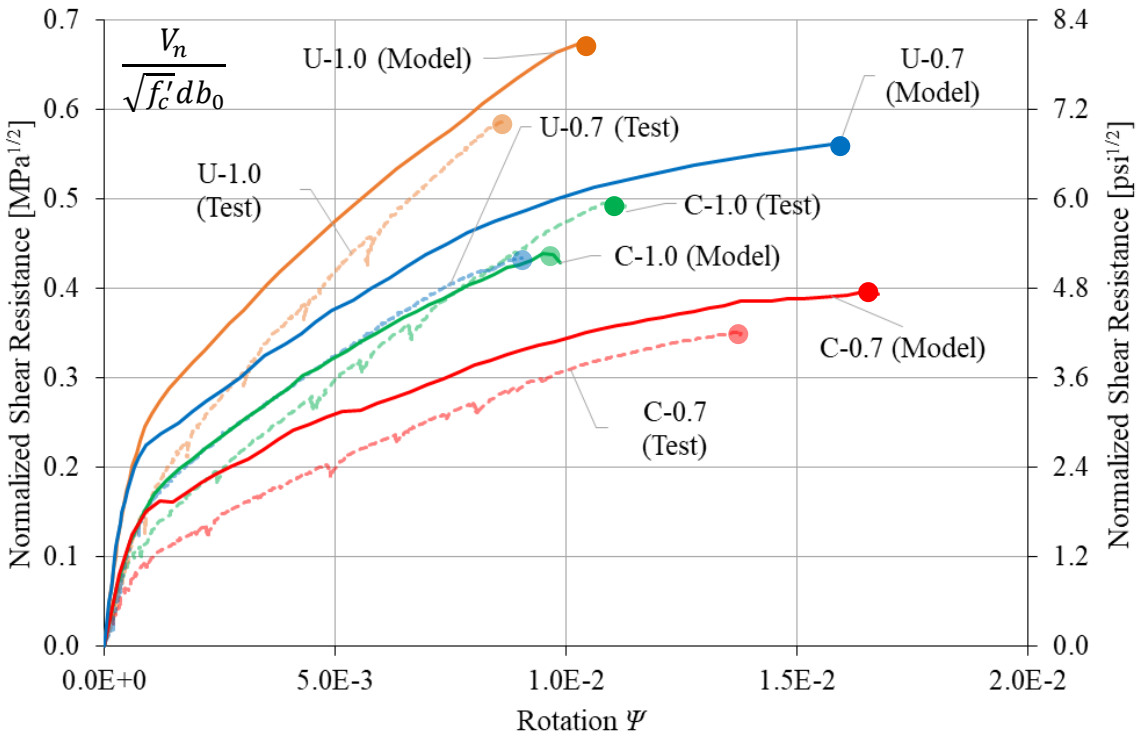

Figure 4-16: Normalized shear resistance $V_n/\left(\sqrt{f_c'}db_0\right)$ versus rotation ψ responses

The numerical models for the CL specimens, C-1.0 and C-0.7, reasonably captured the measured experimental responses. While typically overestimating slab stiffness, particularly in the initial cracking phase of the response, the shear resistances and the rotations of the slabs at failure are estimated with levels of accuracy that can typically be deemed suitable for slabs exhibiting brittle shear-controlled behaviors. Discrepancies in the response estimates may likely be attributed to the variability in the mechanical properties, more specifically the tensile strength of concrete which plays an important role

in the computation of post-cracking shear resisting response. The numerical models presented significant sensitivity to the variation of this parameter.

The numerical models of the UL specimens, U-1.0 and U-0.7, do not capture the experimental responses with the same degree of accuracy. The overall computed behaviors seem to be in-line with those measured; however, the tests failed with significantly lower shear resistances than those estimated by way of the numerical models.

When comparing the numerical model developed for a CL specimen with its nominally-identical counterpart tested on the UL apparatus (i.e., C-1.0 with U-1.0 and C-0.7 with U-0.7 respectively), it can be observed that failure occurs at around the same value of rotation, approximately 0.015 for models with hogging reinforcement ratios of 0.72 % and 0.011 for those with 1.00 %. However, as expected, models of UL specimens achieve much higher failure loads due to the combination of bending moment and out-of-plane shear applied to the slab-column connection.

Punching shear strength from tests, numerical models and other formulations

In this section, the punching shear strength of the tested specimens is compared with the estimations from the numerical simulations shown in this chapter and the formulations described in Chapter 2 (ACI 318-14; Eurocode 2; *fib* Model Code 2010 and CSCT). The results are presented in Table 4-5 and in Figure 4-17. Note that all code-based shear strength estimates were done without the use of resistance or safety factors.

Both *fib* Model Code 2010 and CSCT were found to be the most accurate analytical models to predict punching shear strength consistently following the trends observed in the experimental data. CSCT provided the most accurate shear strength estimates; however, it did marginally over-predict the punching shear strength of specimens with low reinforcement ratios (by up to 7 % in the case of U-0.7). For the calculation of the punching

shear strength by CSCT, as can be seen in detail in Appendix A, the failure criterion is compared to a load-rotation response obtained from a non-linear elastic numerical model. This method is comparable to a *level of approximation IV* according to *fib* Model Code 2010 provisions. In the case other methods were used to determine the load-rotation response, i.e. yield line method, the punching shear resistance obtained would have been lower.

Table 4-6: Punching Shear Capacities Obtained from Tests, Numerical Simulation, and Code/Analysis Procedures

SOURCE	SPECIMENS								Avg. V_n/V_t (COV)
	C-1.0		***U-1.0***		***C-0.7***		***U-0.7***		
	Kip (kN)	V_n/V_t	*Kip (kN)*	V_n/V_t	*Kip (kN)*	V_n/V_t	*Kip (kN)*	V_n/V_t	
TEST	302 (1343)	-	384 (1708)	-	256 (1139)	-	318 (1415)	-	-
Numerical	262 (1167)	0.87	435 (1934)	1.13	280 (1247)	1.10	399 (1776)	1.25	1.09 (0.146)
CSCT	266 (1182)	0.88	339 (1509)	0.88	268 (1194)	1.05	339 (1508)	1.07	0.97 (0.107)
fib 2010	218 (968)	0.72	283 (1260)	0.74	203 (902)	0.79	268 (1192)	0.84	0.77 (0.070)
ACI 318	218 (971)	0.72	235 (1047)	0.61	262 (1164)	1.02	263 (1171)	0.83	0.80 (0.22)
EC2	231 (1025)	0.76	243 (1079)	0.63	233 (1035)	0.91	234 (1039)	0.73	0.77 (0.183)

Eurocode 2 was found to provide good estimates for shear strength capacity, especially considering the simplicity of the formulation. However, it is apparent that the Eurocode 2 procedure was unable to capture the influence of the different loading

conditions developed in the test specimens comprising the experimental program (i.e., the influence of the different M/V ratios developed by way of the two different test setups).

Lastly, ACI 318-14 mistakenly estimates that the punching shear strength will be larger for specimens with lower hogging reinforcement ratios leading towards unconservative shear strength estimates for the slab reinforced with 0.72 % flexural reinforcement. This result is reached given the difference in compressive strength of concrete between the specimens and by the fact that ACI 318-14 does not account for the hogging reinforcement ratio in its formulation.

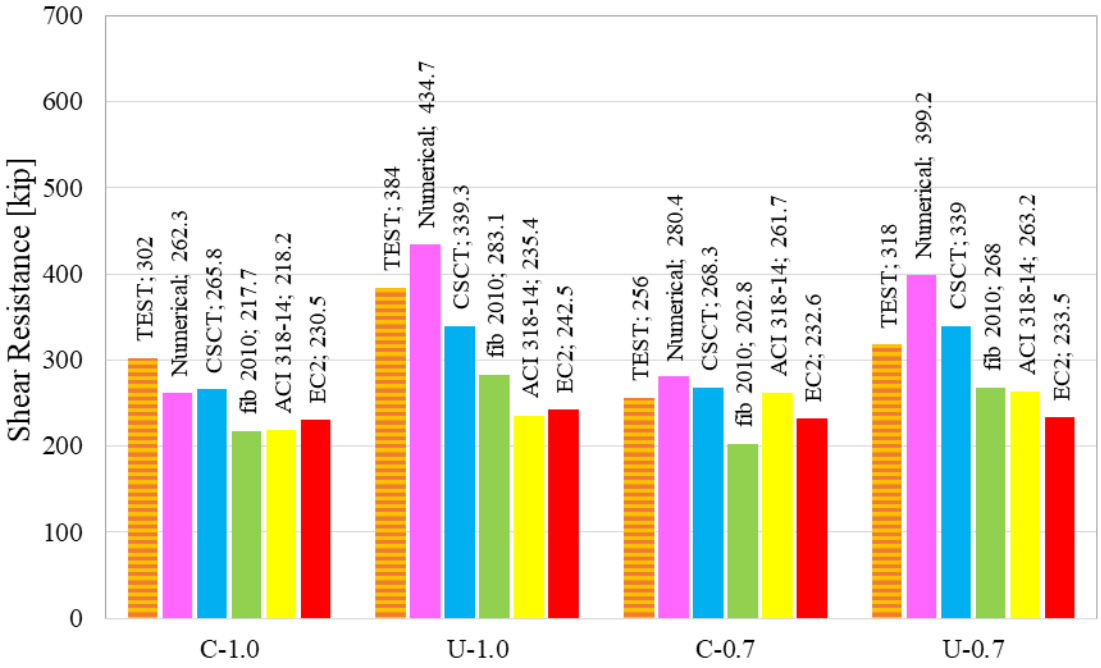

Figure 4-17: Test results vs the different estimations obtained for the punching shear strength for each specimen

The limitations of ACI 318-14 in its ability to accurately estimate punching shear strength of slab-column connections are at plain sight. Contrary to the trend observed in the tests, where the punching shear capacity increases with increasing reinforcement ratio, ACI 318 predicts the opposite: punching shear strength for the test specimens with low

reinforcement ratios is greater. This results are obtained due to the lower compressive strength of concrete found in the test specimens with high hogging reinforcement ratios. This inconsistency may actually produce designs with limited conservatism, as was the case for specimen C-0.7 (refer to Table 4-5). This is starkly contrasts finding made by others (Alexander and Hawkins 2005) who have indicated that the main asset of ACI 318 provisions was to foster safe and serviceable structures and not to produce accurate estimates of results from tests.

Influence of the longitudinal tension reinforcement ratio

In Figure 4-18, the normalized punching shear stress at the critical section of a prototype slab-column connection obtained from numerical models for the two loading conditions, concentrated and uniformly distributed load, is plotted for a wide range of longitudinal reinforcement ratios. In Figure 4-19, and from the same series of analyses, the rotation at failure is plotted as a function of the hogging reinforcement ratio. The results are gathered in several curves and contrasted with the results from the tests. For reference, curves made with estimations from the application of CSCT are added to the plots.

The prototype connection shares the main geometric parameters with the tested specimens: without shear reinforcement and with a 16 in. (406 mm) square column, 10 in. (254 mm) slab thickness, and 8.5 in. (216 mm) effective depth. Typical values are adopted for the material properties: 60 ksi (420 MPa) yield strength of the steel reinforcement and 4350 psi (30 MPa) specified compressive strength of concrete. The rest of the concrete's material properties are adopted as default, calculated with the expressions found in the software's user manual (Wong, Vecchio, and Trommels 2013). Note that the tensile strength of concrete in the models is 0.26 ksi (1.81 MPa), therefore, a ratio $f_t'/\sqrt{f_c'}$ of approximately 4 is considered in all cases, associated with the uniaxial tension test.

Punching shear strength as a function of the longitudinal reinforcement ratio

In Figure 4-18, there is agreement between the results obtained from CSCT and the numerical simulations, the mentioned curves follow the same trend.

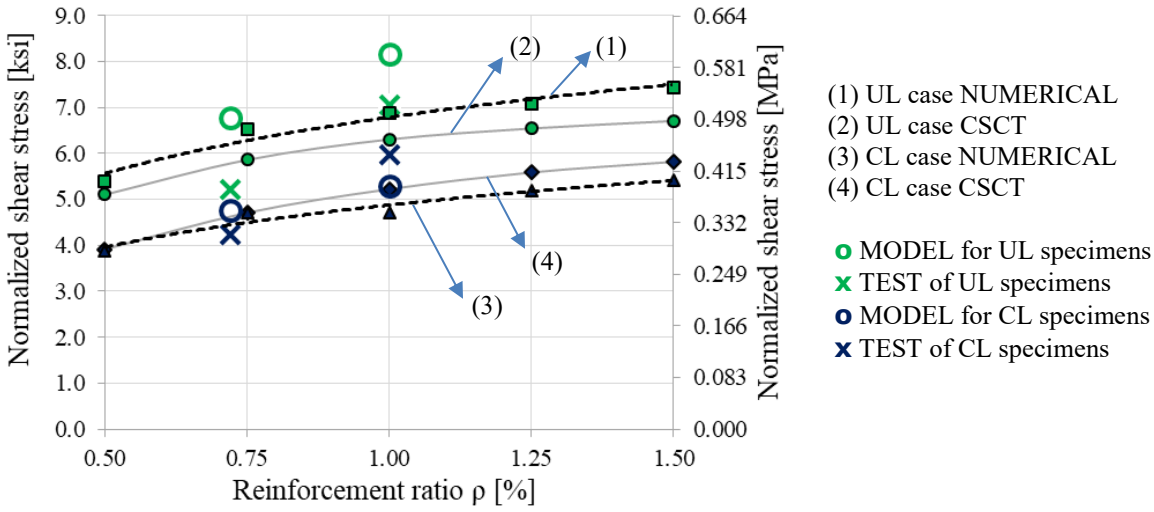

Figure 4-18: Punching shear strength *vs* longitudinal tension reinforcement ratio

For the case of slab-column connections subjected to concentrated loading conditions (CL specimens), the two-way shear resistance estimations by way of the CSCT are, in all cases, slightly higher than the estimations obtained from the numerical models. Moreover, the results from the numerical simulations for the tested specimens are in agreement with these curves. However, the punching shear strength obtained from the tests, C-0.7 and C-1.0, and the values obtained from the numerical models for the same specimens are comparable only for C-0.7, and in the case of C-1.0, the strength reported in the test is significantly higher. Moreover, the computed punching shear strength in the models presents little divergence from curve (3) in Figure 4-18. Note that the ratios of $f_t'/\sqrt{f_c'}$ for C-0.7 and C-1.0 are approximately 5.0 and 5.2 respectively, around 25 % larger in average than the value computed for the models.

For the connections subjected to surface pressure loading conditions (UL specimens), the estimations made using the CSCT were found to be lower. The two-way

shear resistances measured in the tests are significantly lower than the predicted values in the numerical models for specimens U-0.7 and U-1.0. Moreover, the values obtained from the models present significant divergence from curve (1) in Figure 4-18. Note that the ratios of $f_t'/\sqrt{f_c'}$ for U-0.7 and U-1.0 are approximately 6.1 and 5.4 respectively, much larger than the values computed from the models.

Rotation at failure as a function of the longitudinal reinforcement ratio

In Figure 4-19, it is noted that a larger dispersion of the estimated slab rotations was obtained as compared to the estimation of the punching shear strength. The rotation at failure seems to be a parameter that is more difficult to evaluate with precision. However, despite the deviation, the curves made from CSCT and numerical models follow the same trend. Given the nature of the governing failure criterion, CSCT did not provide good estimates of the rotation at failure for slab-column connections tested on the UL test setup. Larger rotations at failure are observed for numerical models simulating conventional testing conditions (CL specimens). Significant inconsistencies are observed for U-0.7 that lead to the possibility of errors during the test.

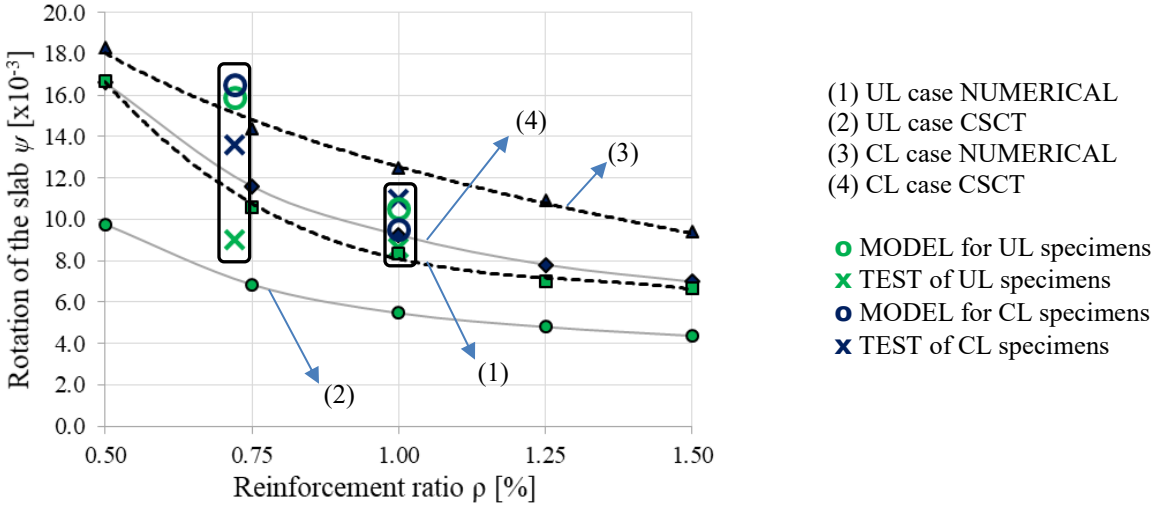

Figure 4-19: Rotation at failure *vs* longitudinal tension reinforcement ratio

Punching shear strength as a function of the rotation of the slab

The normalized shear strength $V_n/\left(\sqrt{f_c'}db_0\right)$ is plotted against the rotation of the slab at failure in Figure 4-20.

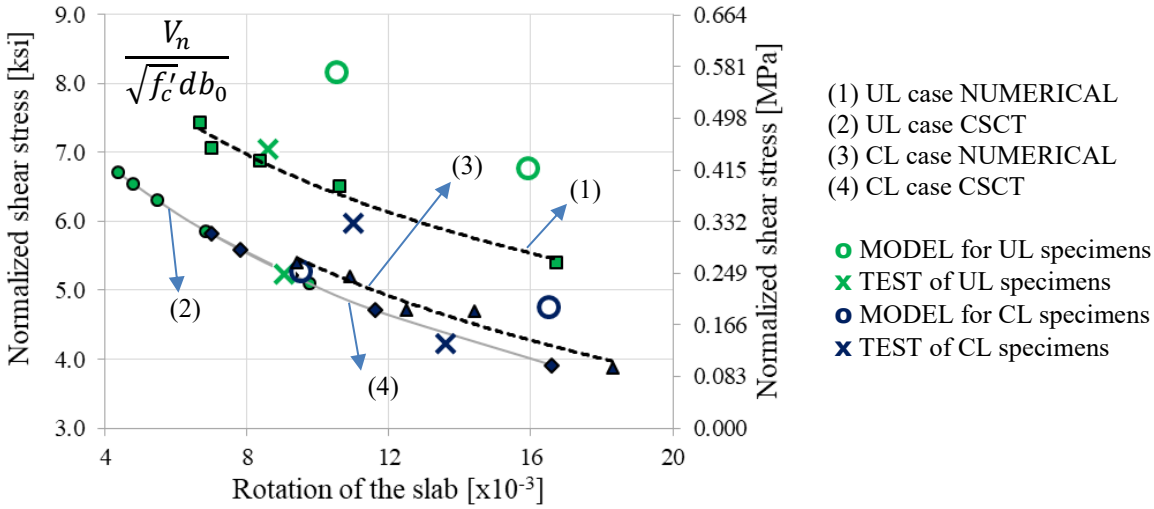

Figure 4-20: Punching Shear Strength vs Rotation at Failure - criterions for CL and UL specimens

As expected, the estimations with CSCT, curves (2) and (4), fall over the CSCT failure criterion. The curve (3), failure criterion for CL numerical models, is adjacent to the CSCT failure criterion. Moreover, the punching shear strength reported in the tests of specimens C-1.0 and C-0.7, and the estimations computed from numerical models for the same connections, fall near or above the failure criterion defined by Muttoni (2008).

The curve (1), failure criterion for UL numerical models, is displaced upwards from curve (3). Thus, the use of a single failure criterion to determine the two-way shear strength of slab-column connections for all loading scenarios, as found in CSCT or *fib* MC 2010, may not reasonable. The test data and the simulations made of the experiments confirms that with exception of the specimen C-0.7 and suggest the occurrence of errors during testing. CSCT related failure criteria have been proposed in the past by others (Einpaul et al. 2016) to account for alternative loading scenarios.

Chapter 5: Conclusions

Many conclusions can be drawn regarding the influence of the loading conditions of isolated slab-column test specimens:

- Building codes, like ACI 318-14 and Eurocode 2, do not take into account loading condition or distribution. Usually, these codes are being used to design slabs with an ultimate shear stress derived from the hypothesis that the slab is supporting a uniformly distributed load.
- The Critical Shear Crack Theory (CSCT) formulation, or the interpretation made of it in the *fib* Model Code 2010, do take into account the applied load condition but only to determine the flexural capacity of the slab. The failure criterion employed by these models was developed from experiments done on isolated specimens where the testing conditions were generally consistent, point loads applied along the perimeter representing the line of contraflexure. Therefore, as expected, this formulations gave better estimates for the specimens tested in the conventional type of testing apparatus.
- The American standard (ACI 318) does not take into account the hogging reinforcement nor the size effect. Clear deficiencies that consistently do not follow the clear trends observed in the experiments and lead to questionable results in some cases, estimations made with ACI 318-14 for slab-column connections with low reinforcement ratios were shown to not provide conservative results (refer to Table 4-5). These parameters are considered in the other formulations presented in this thesis, which offered better estimates for shear capacity.
- An increase in the punching resistance as a result of increased longitudinal tension reinforcement ratio was observed in both loading scenarios, concentrated and

surface pressure loading conditions, and, as such, was found to be independent of the loading condition employed in the test.

- The isolated slab-column connection specimens subjected to uniformly distributed load, reached higher shear capacities but exhibited more brittle responses. Thus, the slab shear stress capacities computed by way of code formulations that have been fitted from more conventional testing techniques, may often be highly conservative.
- CSCT and numerical models give similar results and offer the best estimates for the punching shear strength. However, for the case of the computer simulation made for the tested slab-column connection U-0.7 it predicted higher resistances than the observed in the tests. Furthermore, the relationship shear resistance and slab rotation derived from the numerical model is in the line of the results obtained in the experiments, but the tests seem to reach failure at lower values of shear. This could be attributed to an error in the testing of the slab or to the emergence of another failure mode (somehow not captured in the numerical modeling) that limits the punching shear strength of the specimen.
- The loading conditions considered in this thesis, concentrated forces versus distributed surface pressure, produce different combinations of slab bending moments and out-of-plane shear forces which was found to affect the punching shear strength of the slab-column connections. Thus, the application of a single failure criterion, as employed in the CSCT or *fib* MC 2010, for all loading scenarios may not sufficient.
- Only two slab-column connections were subjected to uniformly distributed loading in this testing program. From the results obtained, it is evident that more testing is necessary to assess the validity of the data and to establish definitive trends.

Appendix A: Example calculations of punching shear resistance

This appendix shows the calculations made for the specimens U-1.0 and C-0.7 to estimate their punching shear strength according to *fib* Model Code 2010, ACI 318-14, Eurocode 2, and the Critical Shear Crack Theory.

ESTIMATIONS FOR SPECIMEN #2: U-1.0

- Main material properties:

Compressive strength of concrete: $f_c' = 4.99\ ksi = 34.4\ MPa$

Yield Strength of the reinforcement: $f_y = 67\ ksi = 462\ MPa$

Modulus of Elasticity of the reinforcement: $E_s = 27{,}068\ ksi = 186{,}627\ MPa$

fib Model Code 2010

- Shear-resisting control perimeter (b_0):

$$b_0 = k_e \cdot b_{1,red} \qquad \text{Eq. 2-9}$$

According to the Figure 7.3-21of *fib* Model Code 2010, and considering the dimensions of the column's cross-section ($c = 16" = 406\ mm$) and the average effective depth of the slab ($d = 8.5" = 216\ mm$), the basic control perimeter (b_1) shall be:

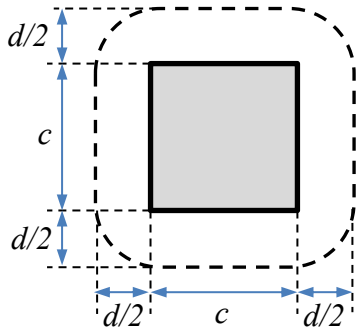

$$b_1 = 4c + \pi d$$
$$b_1 = 4 \cdot 16\ in + \pi \cdot 8.5\ in$$
$$b_1 = 90.7\ in = 2304\ mm$$

Figure A-1: Basic control perimeter (b_1) according to *fib* MC 2010 for U-1.0.

b_1 is not to be reduced since there is no presence of openings, pipes or inserts: $b_{1,red} = b_1$

The value of k_e shall be taken as 1.0 since there is no eccentricity.

Replacing the values into the eq. (7.3-58) from *fib* MC 2010:

$b_0 = 1.0 \cdot b_1 = 90.7\ in = 2304\ mm$

- Parameter for size effect (k_{dg}):

$$k_{dg} = \frac{32}{16 + d_g} \geq 0.75 \qquad \text{Eq. 2-13}$$

Considering that the maximum specified aggregate size is $d_g = 1.0" = 25.4\ mm$:

$$k_{dg} = \frac{32}{16 + d_g} = \frac{32}{16 + 25.4\ mm} = 0.77 \geq 0.75$$

It is also permitted to use $k_{dg} = 1.0$.

Using Level II approximation:

$$\psi = 1.5 \cdot \frac{r_s}{d} \cdot \frac{f_{yd}}{E_s} \cdot \left(\frac{m_{Ed}}{m_{Rd}}\right)^{1.5} \qquad \text{Eq. 2-15}$$

Since: $m_{Ed} = V_{Ed}/8$ and $V_{flex} \cong 8m_{Rd}$. The given expression for ψ can be rewritten as follows:

$$\psi = 1.5 \cdot \frac{r_s}{d} \cdot \frac{f_y}{E_s} \cdot \left(\frac{V}{V_{flex}}\right)^{3/2} \qquad \text{Eq. 2-25}$$

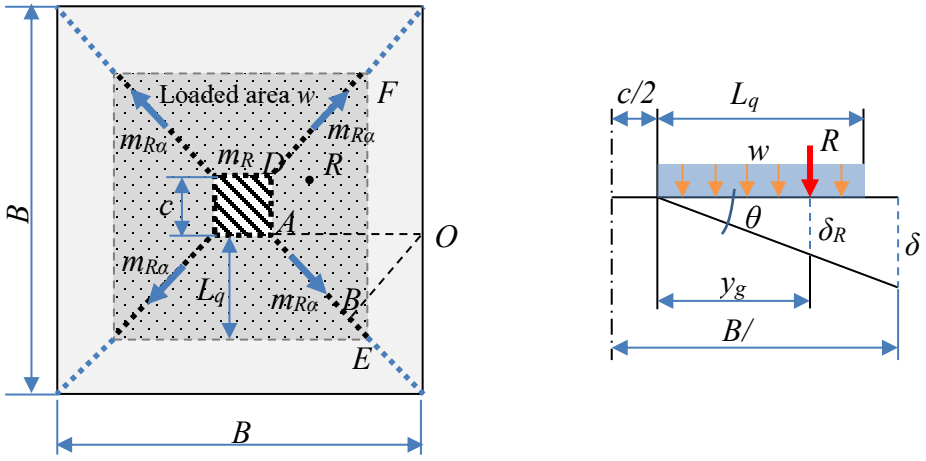

Figure A-2: Yield-line sketch for calculation of V_{flex} for UL specimens.

The flexural strength V_{flex} of the slab can be estimated using the yield-line method (Muttoni 2008). The proposed mechanism to determine V_{flex} is shown in Figure A-2.

Considering the following aspects and applying the principle of virtual work:

- For the case where the same reinforcement is provided in each direction, the slab has the same resistance per unit length regardless of the orientation of the yield line.
- m_R is achieve along the yield line up to the edge of the loaded area and from there to the edge of the slab decreases linearly to zero.

$$W_{ext} = W_{INT}$$

$$4 \cdot R \cdot \delta_R = m_R \cdot 4 \cdot c \cdot \theta + m_R \cdot 4 \cdot \sqrt{2} \cdot L_q \cdot \alpha + 4 \cdot m_R/2 \cdot \left(\frac{(B-c)}{\sqrt{2}} - \sqrt{2} \cdot L_q\right) \cdot \alpha$$

$$w \cdot A \cdot y_g \theta = m_R \cdot \left[c \cdot \theta + \sqrt{2} \cdot L_q \cdot \alpha + \frac{\alpha}{2} \cdot \left(\frac{(B-c)}{\sqrt{2}} - \sqrt{2} \cdot L_q\right)\right]$$

Where, A is the area of the trapezius ADEF, y_g is the distance from the face of the column to center of gravity of the trapezius ADEF, r_y is the radius of the yielded zone, r_c is the radius of the column ($2c/\pi$), m_R is the nominal moment capacity and α is the rotation of the slab in the direction BO.

$$A = (c + L_q) \cdot L_q \quad \& \quad y_g = \frac{L_q}{6} \cdot \frac{3c + 4L_q}{c + L_q}$$

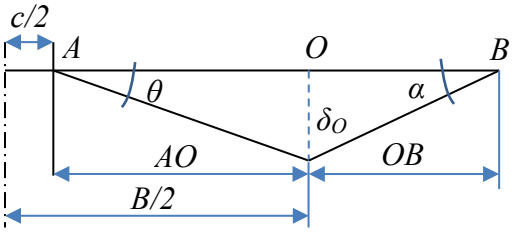

$$AO = \frac{(B-c)}{2} \quad \& \quad OB = \frac{(B-c)}{2\sqrt{2}}$$

$$\delta_O = AO \cdot \theta = OB \cdot \alpha$$

$$\alpha = \frac{AO}{OB} \cdot \theta = \sqrt{2} \cdot \theta$$

Replacing into the virtual work equation:

$$w \cdot (c + L_q) \cdot \frac{{L_q}^2}{6} \cdot \frac{3c + 4L_q}{c + L_q} \cdot \theta = m_R \cdot \left[c \cdot \theta + 2 \cdot L_q \cdot \theta + \frac{\theta}{\sqrt{2}} \cdot \left(\frac{(B-c)}{\sqrt{2}} - \sqrt{2} \cdot L_q\right)\right]$$

$$w \cdot \frac{{L_q}^2}{6} \cdot (3c + 4L_q) = m_R \cdot (L_q + {}^{B}/_{2} + {}^{c}/_{2})$$

$$w = \frac{6 \cdot m_R \cdot \left(L_q + {}^{B}/_{2} + {}^{c}/_{2}\right)}{{L_q}^2 \cdot (3c + 4L_q)} \leftarrow V_{flex} = w4A$$

$$V_{flex} = \frac{6 \cdot m_R \cdot \left(L_q + {}^{B}/_{2} + {}^{c}/_{2}\right)}{{L_q}^2 \cdot (3c + 4L_q)} \cdot 4 \cdot (c + L_q) \cdot L_q$$

Simplifying the latter equation, V_{flex} shall be:

$$V_{flex} = \frac{24 \cdot m_R \cdot \left(L_q + {}^{B}/_{2} + {}^{c}/_{2}\right) \cdot (c + L_q)}{L_q \cdot (3c + 4L_q)} \qquad \text{Eq. A-1}$$

Where L_q is the distance from the face of the column to the outer edge of the loaded area (50 in) and m_R is the nominal moment capacity as follows:

$$m_R = \rho_l \cdot f_{yd} \cdot d^2 \cdot \left(1 - \frac{\rho_l \cdot f_{yd}}{2 \cdot f_{ck}}\right) \qquad \text{Eq. 2-16}$$

$$m_R = 0.01 \cdot 462\ MPa \cdot (216\ mm)^2 \cdot \left(1 - \frac{0.01 \cdot 462\ MPa}{2 \cdot 34.4\ MPa}\right)$$

$$m_R = 200.9\ kN.m/m = 45.2\ kip.in/in$$

Replacing m_R into equation Eq. A-1, the flexural strength is:

$$V_{flex} = \frac{24 \cdot 45.2\ kip.in/in \cdot \left(50" + {}^{144"}/_{2} + {}^{16"}/_{2}\right) \cdot (16" + 50")}{50" \cdot (3 \cdot 16" + 4 \cdot 50")} = 750\ kip = 3336\ kN$$

- Rotation of the slab (ψ):

Assuming $V = 283\ kip = 1259\ kN$

$$\psi = 1.5 \cdot \frac{r_s}{d} \cdot \frac{f_y}{E_s} \cdot \left(\frac{V}{V_{flex}}\right)^{3/2} = 1.5 \cdot \frac{1664\ mm}{216\ mm} \cdot \frac{462\ MPa}{186627\ MPa} \cdot \left(\frac{1259\ kN}{3336\ kN}\right)^{3/2} = 0.0066$$

- Parameter related to the rotation of the slab (k_ψ):

$$k_\psi = \frac{1}{1.5 + 0.9 \cdot k_{dg} \cdot \psi \cdot d} \qquad \text{Eq. 2-12}$$

$$k_\psi = \frac{1}{1.5 + 0.9 \cdot 0.77 \cdot 0.0066 \cdot 216\ mm} = 0.402$$

- Punching shear strength attributed to concrete ($V_{Rd,c}$):

$$V_{Rd,c} = \alpha_c \cdot k_\psi \cdot \sqrt{f_{ck}} \cdot b_0 \cdot d_v/\gamma_c \qquad \text{Eq. 2-11}$$

$V_{Rd,c} = 1.074 \cdot 0.402 \cdot \sqrt{34.4\ MPa} \cdot 2304\ mm \cdot 216\ mm$

$V_{Rd,c} = 1259\ kN = 283\ kip$

- Punching shear strength (V_{Rd}):

$V_{Rd} = V_{Rd,c} + V_{Rd,s}$ Eq. 2-10

Since there is no shear reinforcement: $V_{Rd,s} = 0$

Thus, $\boxed{V_{Rd} = V_{Rd,c} = 283\ kip = 1259\ kN}$ = Assumed $V \Longrightarrow OK$

ACI 318-14 Building Code

- Critical section (b_0):

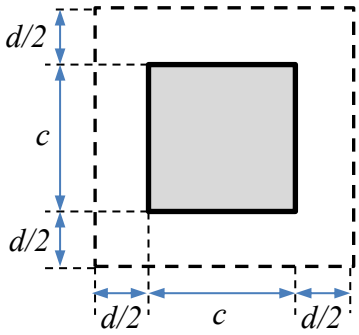

$b_0 = 4 \cdot (c + d)$
$b_0 = 4 \cdot (16\ in + 8.5\ in)$
$b_0 = 98\ in = 2489\ mm$

Figure A-3: Critical section (b_0) according to ACI 318-14 for U-1.0.

- Shear strength provided by concrete (v_C):

  According to Table 2-1, v_C shall be:

$$v_C\ the\ least\ of \begin{cases} 4\lambda\sqrt{f_c'} = 4\sqrt{4990\ psi} = 283\ psi \\ \left(2 + \frac{4}{\beta}\right)\lambda\sqrt{f_c'} = \left(2 + \frac{4}{1}\right)\sqrt{4990\ psi} = 424\ psi \\ \left(2 + \frac{\alpha_s d}{b_0}\right)\lambda\sqrt{f_c'} = \left(2 + \frac{40 \cdot 8.5"}{98"}\right)\sqrt{4990\ psi} = 386\ psi \end{cases}$$

$\Longrightarrow v_C = 283\ psi$

- Nominal shear strength (v_n) and punching shear strength (V_n):

$v_n = v_c + v_s$ Eq. 2-1

Since there is no shear reinforcement: $v_s = 0 \Longrightarrow v_n = v_c = 282.6\ psi$

$V_n = v_n \cdot b_0 \cdot d = 283\ psi \cdot 98\ in \cdot 8.5\ in$

$\boxed{V_n = 235\ kip = 1047\ kN}$

Eurocode 2

- Basic control perimeter (u_1):

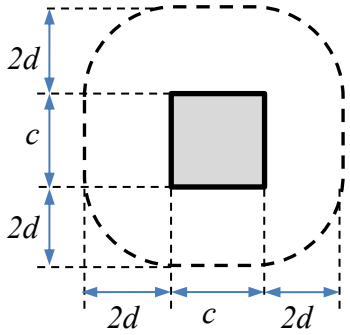

$u_1 = 4c + \pi 4 d_{eff}$
$u_1 = 4 \cdot 16\ in + \pi \cdot 4 \cdot 8.5\ in$
$u_1 = 170.8\ in = 4339\ mm$

Figure A-4: Basic control perimeter (u_1) according to EC2 for U-1.0.

- Punching shear resistance for slab without shear reinforcement (V_{Rd}):

$v_{Rd,c} = C_{Rd,c} k \cdot (100 \rho_l f_{ck})^{1/3} + k_1 \sigma_{cp} \geq v_{min} + k_1 \sigma_{cp}$ Eq. 2-5

Since the slab is nonprestressed and only gravity load is being considered $\Longrightarrow \sigma_{cp} = 0$

From Eq. (6.3N) $\Longrightarrow v_{min} = 0.035 \cdot k^{1.5} \cdot f_{ck}^{0.5}$

Considering $k = 1 + \sqrt{200/d} = 1 + \sqrt{200/215.9\ mm} = 1.96 \leq 2.0$ and $C_{Rd,c} = 0.18$

Replacing values into Eq. (6.47) from EC 2:

$v_{Rd,c} = C_{Rd,c} k \cdot (100 \rho_l f_{ck})^{1/3} \geq 0.035 \cdot k^{1.5} \cdot f_{ck}^{0.5}$

$v_{Rd,c} = 0.18 \cdot 1.96 \cdot (100 \cdot 0.01 \cdot 34.4\ MPa)^{1/3} \geq 0.035 \cdot 1.96^{1.5} \cdot (34.4\ MPa)^{0.5}$

$v_{Rd,c} = 1.151\ MPa \geq 0.564\ MPa \rightarrow OK$

$V_{Rd} = V_{Rd,c} = v_{Rd,c} \cdot u_1 \cdot d_{eff} = 1.151\ MPa \cdot 4339\ mm \cdot 216\ mm$

$\boxed{V_{Rd} = 1079\ kN = 243\ kip}$

Critical Shear Crack Theory

The relationship between the slab rotation ψ and the total applied load V was obtained from a nonlinear numerical simulation using *VecTor4*, a nonlinear finite element analysis (NLFEA) program for reinforced concrete shells and plates subjected to quasi-static load conditions (Hrynyk and Vecchio 2015). The shell element model was conceived using the same approach described for the solids-based models in Chapter 4 but, in this case, shear deformations were intentionally not accounted for.

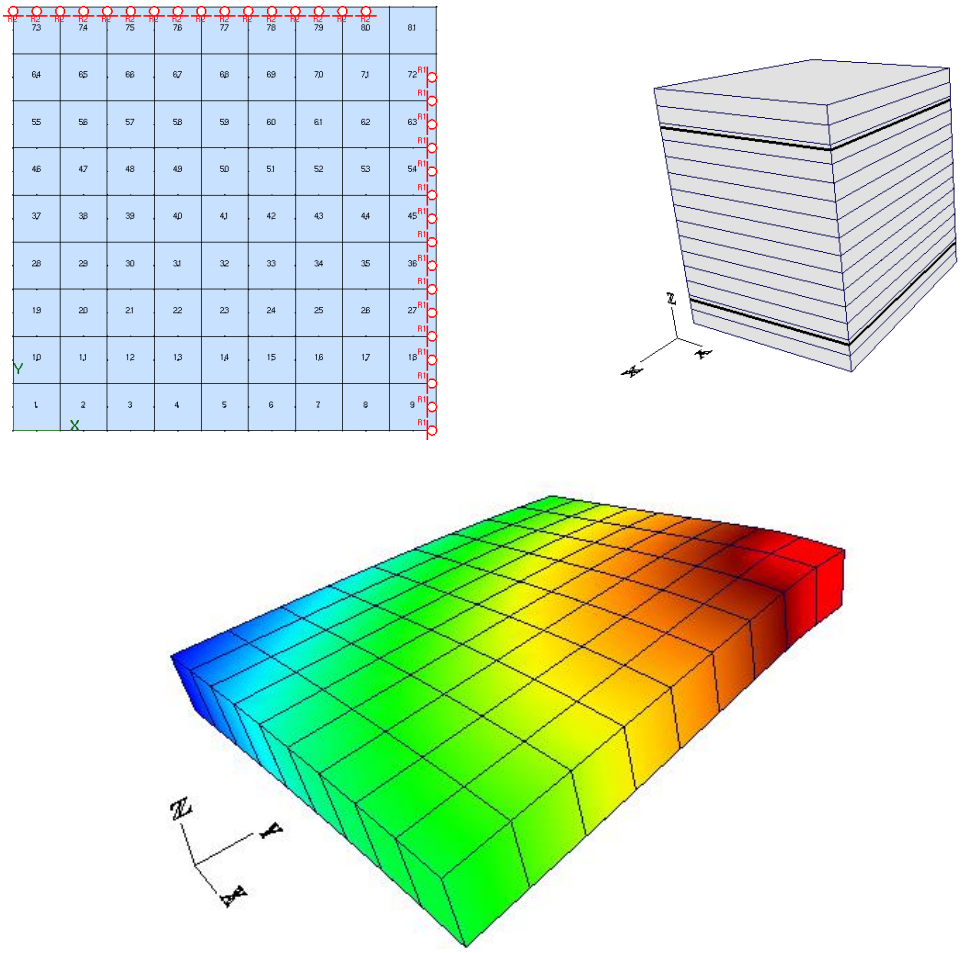

Figure A-5: Shell model for specimen U-1.0: top view (upper-left); single element showing concrete layers (15) and reinforcement layers considered (4) (upper-right); deformed shape for a given load step (bottom-middle).

The rotation was computed based on the registered vertical displacements of the nodes at the restrained edges as the slope of the trend line obtained by linear regression.

The load versus rotation curve was plotted together with the CSCT failure criterion from where the punching shear strength of the slab-column connection was obtained:

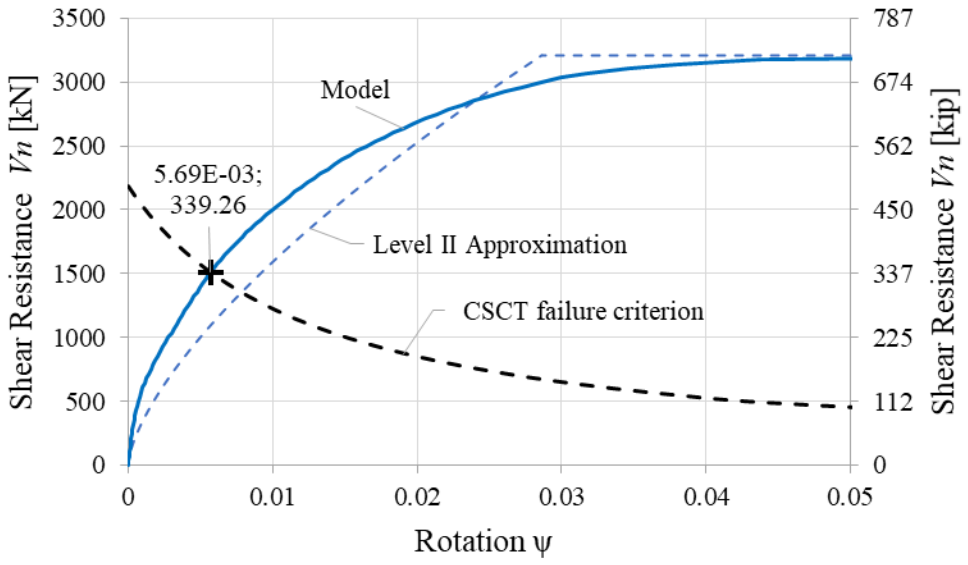

Figure A-6: Shear resistance vs rotation from nonlinear numerical simulation plotted against the CSCT failure criterion for specimen U-1.0.

Thus, calculating the point where the load vs rotation response intersects the CSCT failure criterion, the punching shear strength for the slab-column connection results:

$$V_{Rd} = 1509\ kN = 339\ kip$$

Summary of results

Table A-1: Punching shear capacity estimations for U-1.0.

U-1.0	*fib (LII)*	*ACI*	*EC2*	*CSCT*	*TEST*
V_n [kip (kN)]	283 (1259)	235 (1047)	242 (1079)	339 (1509)	384 (1708)
V_n/V_{test}	0.74	0.61	0.63	0.88	-

ESTIMATIONS FOR SPECIMEN #3: C-0.7

- Main material properties:

Compressive strength of concrete: $f_c' = 6.17\ ksi = 42.5\ MPa$

Yield strength of the reinforcement: $f_y = 67\ ksi = 462\ MPa$

Modulus of elasticity of the reinforcement: $E_s = 27{,}068\ ksi = 186{,}627\ MPa$

***fib* Model Code 2010**

- Shear-resisting control perimeter (b_0):

$$b_0 = k_e \cdot b_{1,red} \qquad \text{Eq. 2-9}$$

According to the Figure 7.3-21of *fib* Model Code 2010, and considering the dimensions of the column's cross-section ($c = 16" = 406\ mm$) and the average effective depth of the slab ($d = 8.5" = 216\ mm$), the basic control perimeter (b_1) shall be:

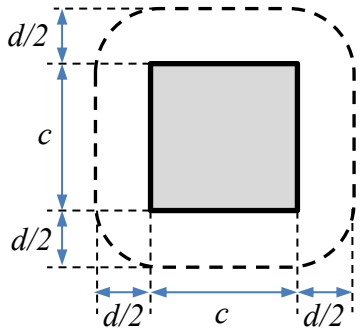

$$b_1 = 4c + \pi d$$
$$b_1 = 4 \cdot 16\ in + \pi \cdot 8.5\ in$$
$$b_1 = 90.7\ in = 2304\ mm$$

Figure A-7: Basic control perimeter (b_1) according to *fib* MC 2010 for C-0.7.

b_1 is not to be reduced since there is no presence of openings, pipes or inserts: $b_{1,red} = b_1$

The value of k_e shall be taken as 1.0 since there is no eccentricity.

Replacing the values into the eq. (7.3-58) from *fib* MC 2010:

$b_0 = 1.0 \cdot b_1 = 90.7\ in = 2304\ mm$

- Parameter for size effect (k_{dg}):

$$k_{dg} = \frac{32}{16 + d_g} \geq 0.75 \qquad \text{Eq. 2-13}$$

Considering that the maximum specified aggregate size is $d_g = 1.0" = 25.4\,mm$:

$$k_{dg} = \frac{32}{16 + d_g} = \frac{32}{16 + 25.4\,mm} = 0.77 \geq 0.75$$

It is also permitted to use $k_{dg} = 1.0$.

Using Level II approximation:

$$\psi = 1.5 \cdot \frac{r_s}{d} \cdot \frac{f_{yd}}{E_s} \cdot \left(\frac{m_{Ed}}{m_{Rd}}\right)^{1.5} \qquad \text{Eq. 2-15}$$

Since: $m_{Ed} = V_{Ed}/8$ and $V_{flex} \cong 8m_{Rd}$. The given expression for ψ can be rewritten as follows:

$$\psi = 1.5 \cdot \frac{r_s}{d} \cdot \frac{f_y}{E_s} \cdot \left(\frac{V}{V_{flex}}\right)^{3/2} \qquad \text{Eq. 2-25}$$

The flexural strength V_{flex} of the slab can be estimated by the yield-line method.

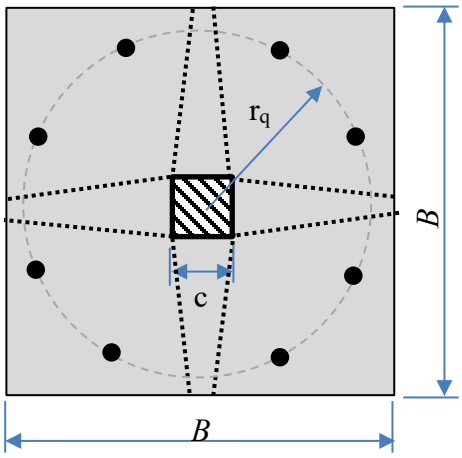

Figure A-8: Yield-line sketch for calculation of V_{flex} for CL specimens.

For this case the expression for V_{flex} was derived by Muttoni (2008):

$$V_{flex} = \frac{4m_R}{r_q[\cos(\pi/8) + \sin(\pi/8)] - c} \cdot \frac{B^2 - Bc - c^2/4}{B - c} \qquad \text{Eq. A-2}$$

Where r_q is the distance from the central axis of the column to the bearing plate (61 in) and m_R is the nominal moment capacity as follows:

$$m_R = \rho_l \cdot f_{yd} \cdot d^2 \cdot \left(1 - \frac{\rho_l \cdot f_{yd}}{2 \cdot f_{ck}}\right)$$ Eq. 2-16

$$m_R = 0.072 \cdot 462\ MPa \cdot (216\ mm)^2 \cdot \left(1 - \frac{0.072 \cdot 462\ MPa}{2 \cdot 42.5\ MPa}\right)$$

$$m_R = 148.8\ kN.m/m = 33.4\ kip.in/in$$

The flexural strength results:

$$V_{flex} = \frac{4 \cdot 33.4\ kip.in/in}{61"[\cos(\pi/8) + \sin(\pi/8)] - 16"} \cdot \frac{144"^2 - 144" \cdot 16" - \frac{(16")^2}{4}}{144" - 16"}$$

$$V_{flex} = 302\ kip = 1345\ kN$$

- Rotation of the slab (ψ):

Assuming $V = 203\ kip = 902\ kN$

$$\psi = 1.5 \cdot \frac{r_s}{d} \cdot \frac{f_y}{E_s} \cdot \left(\frac{V}{V_{flex}}\right)^{3/2} = 1.5 \cdot \frac{1664\ mm}{216\ mm} \cdot \frac{462\ MPa}{186627\ MPa} \cdot \left(\frac{902\ kN}{1345\ kN}\right)^{3/2} = 0.0157$$

- Parameter related to the rotation of the slab (k_ψ):

$$k_\psi = \frac{1}{1.5 + 0.9 \cdot k_{dg} \cdot \psi \cdot d}$$ Eq. 2-12

$$k_\psi = \frac{1}{1.5 + 0.9 \cdot 0.77 \cdot 0.0157 \cdot 216\ mm} = 0.259$$

- Punching shear strength attributed to concrete ($V_{Rd,c}$):

$$V_{Rd,c} = \alpha_c \cdot k_\psi \cdot \sqrt{f_{ck}} \cdot b_0 \cdot d_v/\gamma_c$$ Eq. 2-11

$$V_{Rd,c} = 1.074 \cdot 0.259 \cdot \sqrt{42.5\ MPa} \cdot 2304\ mm \cdot 216\ mm$$

$$V_{Rd,c} = 902.3\ kN = 203\ kip$$

- Punching shear strength (V_{Rd}):

$$V_{Rd} = V_{Rd,c} + V_{Rd,s}$$ Eq. 2-10

Since there is no shear reinforcement: $V_{Rd,s} = 0$

Thus, $\boxed{V_{Rd} = V_{Rd,c} = 203\ kip = 902\ kN}$ = Assumed $V \Longrightarrow OK$

ACI 318-14 Building Code

- Critical section (b_0):

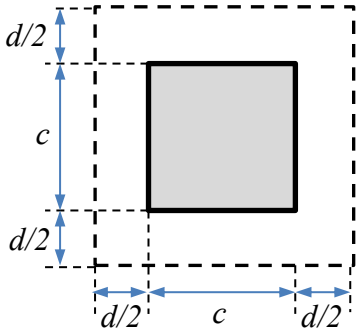

$$b_0 = 4 \cdot (c + d)$$
$$b_0 = 4 \cdot (16\ in + 8.5\ in)$$
$$b_0 = 98\ in = 2489\ mm$$

Figure A-9: Critical section (b_0) according to ACI 318-14 for C-0.7.

- Shear strength provided by concrete (v_c):

  According to Table 2-1, v_c shall be:

$$v_c\ the\ least\ of \begin{cases} 4\lambda\sqrt{f_c'} = 4\sqrt{6170\ psi} = 314\ psi \\ \left(2 + \frac{4}{\beta}\right)\lambda\sqrt{f_c'} = \left(2 + \frac{4}{1}\right)\sqrt{6170\ psi} = 471\ psi \\ \left(2 + \frac{\alpha_s d}{b_0}\right)\lambda\sqrt{f_c'} = \left(2 + \frac{40 \cdot 8.5"}{98"}\right)\sqrt{6170\ psi} = 430\ psi \end{cases}$$

$$\Longrightarrow v_c = 314\ psi$$

- Nominal shear strength (v_n) and punching shear strength (V_n):

$$v_n = v_c + v_s \qquad \text{Eq. 2-1}$$

Since there is no shear reinforcement: $v_s = 0 \Longrightarrow v_n = v_c = 314\ psi$

$$V_n = v_n \cdot b_0 \cdot d = 314\ psi \cdot 98\ in \cdot 8.5\ in$$

$$\boxed{V_n = 262\ kip = 1164\ kN}$$

Eurocode 2

- Basic control perimeter (u_1):

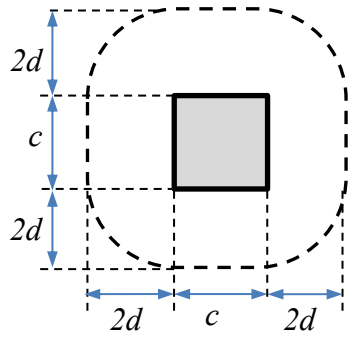

$$u_1 = 4c + \pi 4 d_{eff}$$
$$u_1 = 4 \cdot 16\ in + \pi \cdot 4 \cdot 8.5\ in$$
$$u_1 = 170.8\ in = 4339\ mm$$

Figure A-10: Basic control perimeter (u_1) according to EC2 for U-1.0.

- Punching shear resistance for slab without shear reinforcement (V_{Rd}):

$$v_{Rd,c} = C_{Rd,c} k \cdot (100 \rho_l f_{ck})^{1/3} + k_1 \sigma_{cp} \geq v_{min} + k_1 \sigma_{cp} \qquad \text{Eq. 2-5}$$

Since the slab is nonprestressed and only gravity load is being considered $\Longrightarrow \sigma_{cp} = 0$

From Eq. (6.3N) $\Longrightarrow v_{min} = 0.035 \cdot k^{1.5} \cdot f_{ck}^{0.5}$

Considering $k = 1 + \sqrt{200/d} = 1 + \sqrt{200/216\ mm} = 1.96 \leq 2.0$ and $C_{Rd,c} = 0.18$

Replacing values into Eq. (6.47) from EC 2:

$$v_{Rd,c} = C_{Rd,c} k \cdot (100 \rho_l f_{ck})^{1/3} \geq 0.035 \cdot k^{1.5} \cdot f_{ck}^{0.5}$$

$$v_{Rd,c} = 0.18 \cdot 1.96 \cdot (100 \cdot 0.0072 \cdot 42.5\ MPa)^{1/3} \geq 0.035 \cdot 1.96^{1.5} \cdot (42.5\ MPa)^{0.5}$$

$$v_{Rd,c} = 1.104\ MPa \geq 0.63\ MPa \rightarrow OK$$

$$V_{Rd} = V_{Rd,c} = v_{Rd,c} \cdot u_1 \cdot d_{eff} = 1.104\ MPa \cdot 4339\ mm \cdot 216\ mm$$

$$\boxed{V_{Rd} = 1035\ kN = 233\ kip}$$

Critical Shear Crack Theory

The relationship between the slab rotation ψ and the total applied load V was obtained from a nonlinear numerical simulation using *VecTor4*, a nonlinear finite element analysis (NLFEA) program for reinforced concrete shells and plates subjected to quasi-static load conditions (Hrynyk and Vecchio 2015). The shells model was conceived using the same approach described for the solids-based models in Chapter 4, but in this case shear deformations were intentionally not accounted for.

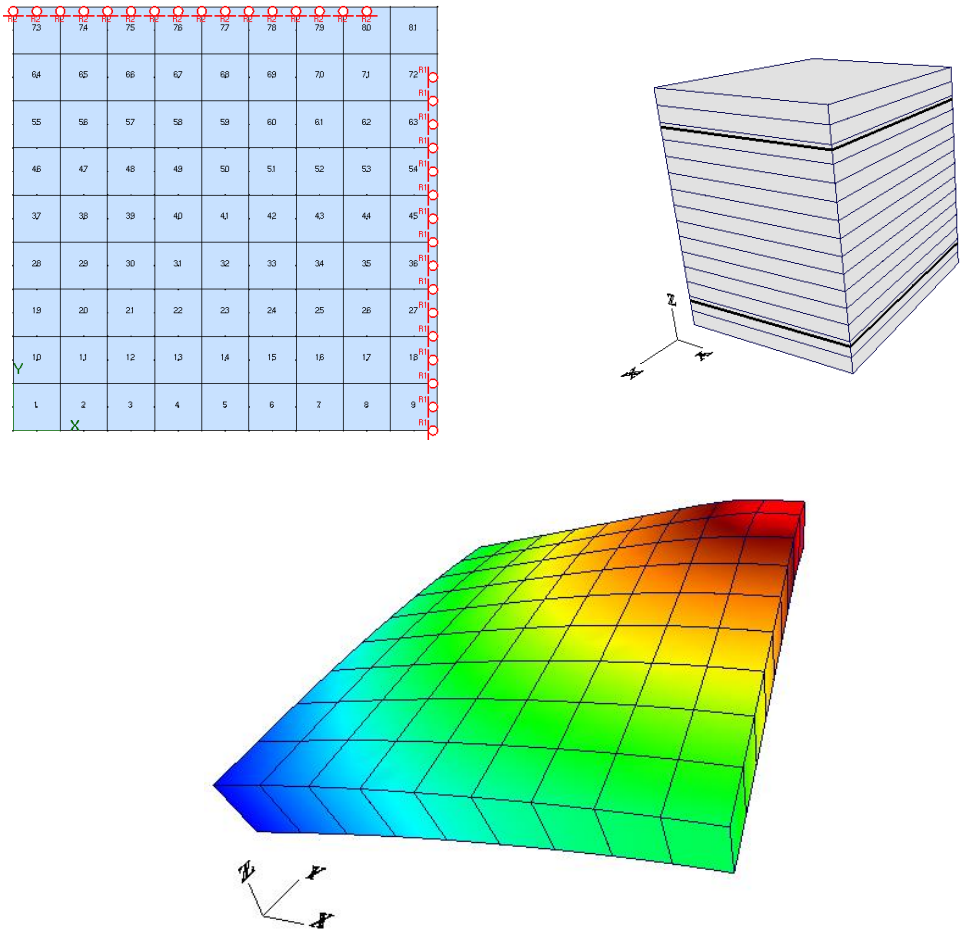

Figure A-11: Shell model for specimen C-0.7: top view (upper-left); single element showing concrete layers (15) and reinforcement layers considered (4) (upper-right); deformed shape for a given load step (bottom-middle).

The rotation was computed based on the registered vertical displacements of the nodes at the restrained edges as the slope of the trend line obtained by linear regression.

The load versus rotation curve was plotted together with the CSCT failure criterion from where the punching shear strength of the slab-column connection was obtained:

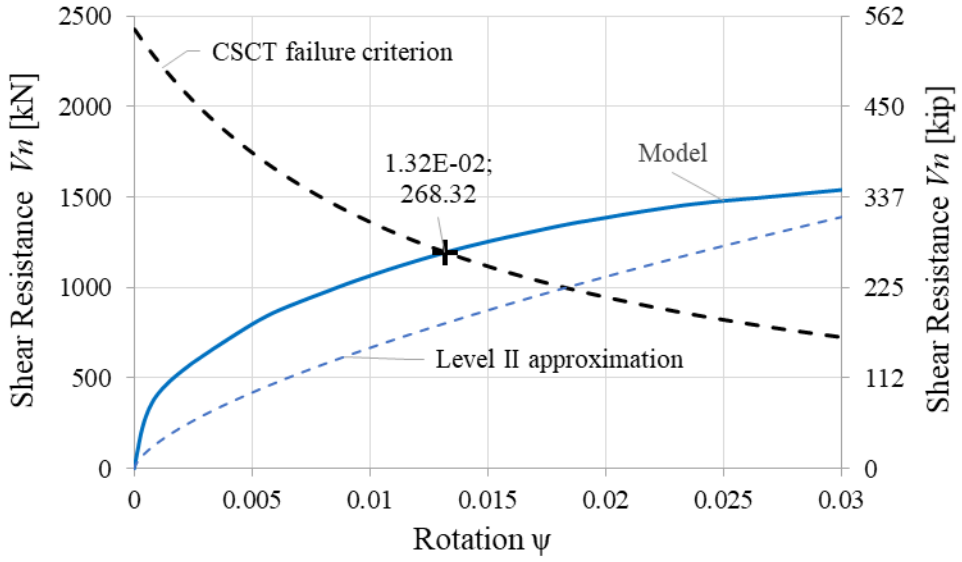

Figure A-12: Shear resistance vs rotation from nonlinear numerical simulation plotted against the CSCT failure criterion for specimen C-0.7.

Thus, calculating the point where the load vs rotation response intersects the CSCT failure criterion, the punching shear strength for the slab-column connection results:

$$V_{Rd} = 1194\ kN = 268\ kip$$

Summary of results

Table A-2: Punching shear capacity estimations for C-0.7.

C-0.7	*fib (LII)*	*ACI*	*EC2*	*CSCT*	*TEST*
V_n [kip (kN)]	203 (902)	262 (1164)	232 (1035)	268 (1194)	258 (1148)
V_n/V_{test}	0.79	1.02	0.90	1.04	-

Appendix B: Material Properties

CONCRETE PROPERTIES

For each slab-column connection listed in the experimental program, at least 18 cylindrical test samples of size 4 × 8-in (102 × 203-mm), 3 prismatic specimens of size 6 × 6 × 18-in (152 × 152 × 457-mm), and 3 "dog-bone" shaped specimens with a central cross-section of 4 × 4-in (102 × 102-mm), were sampled during casting and stored in the laboratory following the standardized procedure in compliance with ASTM C 31.

This specimens were tested to determine the properties listed in Chapter 3 for the concrete used in each slab-column connection. In the case of the cylindrical test specimens, they were used to perform the compressive strength test according to ASTM C39 and the split tension test according ASTM C496. In the case of the prism specimens, they were tested to assess the modulus of rupture according to ASTM C78. Finally, the "dog-bone" shaped specimens were used in the direct tension test for which there is no standard available.

In this appendix, all the results from the aforementioned tests will be presented in a summarized manner as a supplement to the values listed in Chapter 3.

Table B-1: Compressive strength test data for all specimens.

#	*Designation*	*Compressive strength [psi,(MPa)]*				
		#1	*#2*	*#3*	*Avg.*	*COV*
1	*C-1.0*	4423 (30.5)	4298 (29.6)	4163 (28.7)	4295 (29.6)	0.030
2	*U-1.0*	5087 (35.1)	4940 (34.1)	4947 (34.1)	4991 (34.4)	0.017
3	*C-0.7*	6433 (44.4)	5964 (41.1)	6111 (42.1)	6169 (42.5)	0.039
4	*U-0.7*	6181 (42.6)	6196 (42.7)	6338 (43.7)	6238 (43.0)	0.014

Table B-2: Modulus of rupture test data for all specimens.

#	Designation	*Modulus of rupture [psi,(MPa)]*				
		#1	*#2*	*#3*	*Avg.*	*COV*
1	*C-1.0*	692 (4.77)	734 (5.06)	666 (4.59)	697 (4.81)	0.049
2	*U-1.0*	763 (5.26)	637 (4.39)	583 (4.02)	661 (4.56)	0.139
3	*C-0.7*	501 (3.45)	630 (4.34)	672 (4.63)	601 (4.14)	0.148
4	*U-0.7*	705 (4.86)	771 (5.32)	711 (4.90)	729 (5.03)	0.050

Table B-3: Split tension test data for all specimens.

#	Designation	*Tensile strength from split tension test [psi,(MPa)]*				
		#1	*#2*	*#3*	*Avg.*	*COV*
1	*C-1.0*	640 (4.41)	641 (4.42)	626 (4.32)	636 (4.38)	0.014
2	*U-1.0*	877 (6.05)	753 (5.19)	713 (4.92)	781 (5.38)	0.110
3	*C-0.7*	802 (5053)	709 (4.89)	758 (5.23)	756 (5.21)	0.061
4	*U-0.7*	685 (4.72)	628 (4.33)	647 (4.46)	653 (4.51)	0.045

Table B-4: Direct tension test data for all specimens.

#	Designation	*Tensile strength from direct tension test [psi,(MPa)]*				
		#1	*#2*	*#3*	*Avg.*	*COV*
1	*C-1.0*	388 (2.68)	332 (2.29)	302 (2.08)	341 (2.35)	0.128
2	*U-1.0*	443 (3.05)	410 (2.82)	435 (2.99)	429 (2.96)	0.041
3	*C-0.7*	428 (2.95)	418 (2.88)	335 (2.31)	394 (2.71)	0.129
4	*U-0.7*	447 (3.08)	431 (2.97)	443 (3.05)	433 (2.99)	0.019

Table B-5: Strain at peak from direct tension test data for all specimens.

#	Designation	*Strain at peak tensile strength from direct tension test [$\times 10^{-3}$]*				
		#1	*#2*	*#3*	*Avg.*	*COV*
1	*C-1.0*	0.142	0.066	0.038	0.082	0.662
2	*U-1.0*	0.091	0.069	0.094	0.085	0.164
3	*C-0.7*	0.060	0.098	0.083	0.080	0.236
4	*U-0.7*	0.079	0.094	0.100	0.091	0.121

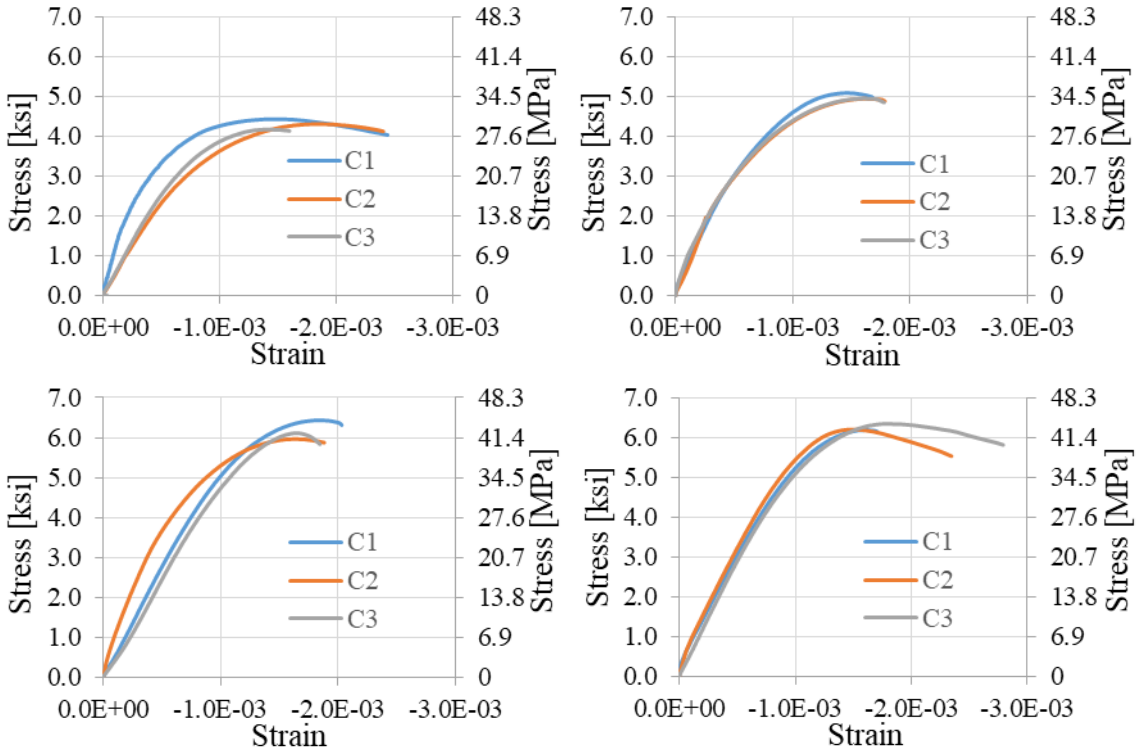

Figure B-1: Stress *vs* strain curves from tested cylindrical specimens. From left to right and top to bottom, results from specimens C-1.0, U-1.0, C-0.7 and U-0.7 respectively.

STEEL BARS PROPERTIES

The mechanical properties of the steel bars used as reinforcement in the specimens, which are listed in Chapter 3, were obtained from the testing of coupons.

Table B-6: Yield strength from test data for all coupons.

Size	*Yield strength F_y [ksi,(MPa)]*				
	#1	*#2*	*#3*	*Avg.*	*COV*
US No. 3	64.5 (444.7)	63.6 (438.5)	63.3 (436.4)	63.8 (439.9)	0.01
US No. 6	69.0 (475.7)	69.0 (475.7)	62.3 (429.5)	66.6 (459.2)	0.058

Table B-7: Ultimate tensile strength from test data for all coupons.

Size	*Ultimate strength F_u [ksi,(MPa)]*				
	#1	*#2*	*#3*	*Avg.*	*COV*
US No. 3	97.5 (672.2)	95.8 (660.9)	96.2 (663.1)	96.5 (665.3)	0.009
US No. 6	111.1(766.1)	109.2(752.9)	104.6(721.2)	108.3(746.7)	0.031

Table B-8: Modulus of elasticity from test data for all coupons.

Size	*Modulus of Elasticity E_s [ksi,(MPa)]*				
	#1	*#2*	*#3*	*Avg.*	*COV*
US No. 3	28982 (199823)	28330 (195328)	29299 (202009)	28871 (199058)	0.017
US No. 6	27380 (188778)	27096 (186820)	26727 (184276)	27068 (186627)	0.012

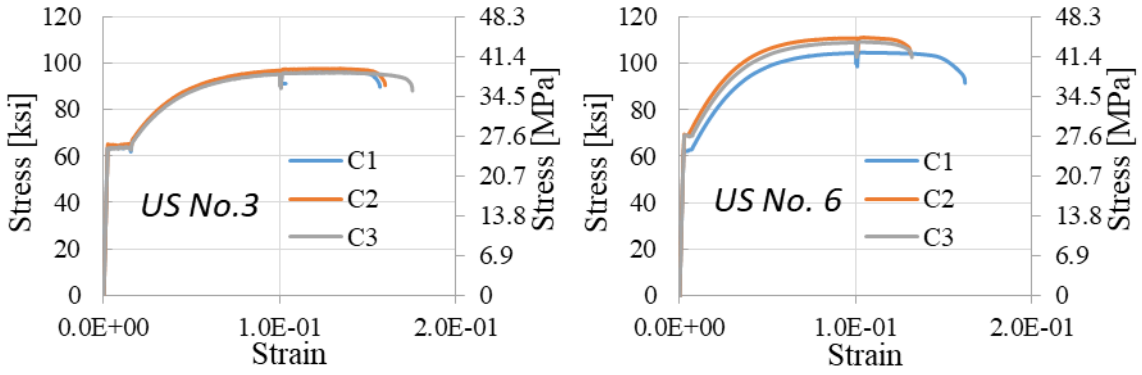

Figure B-1: Stress *vs* strain curves from tested coupons: bar size US No. 3 and US No. 6.

Appendix C: Tests results

This appendix presents figures showing the cracking observed at failure.

Figure C-1: Cracking observed at failure for test specimen #1: C-1.0

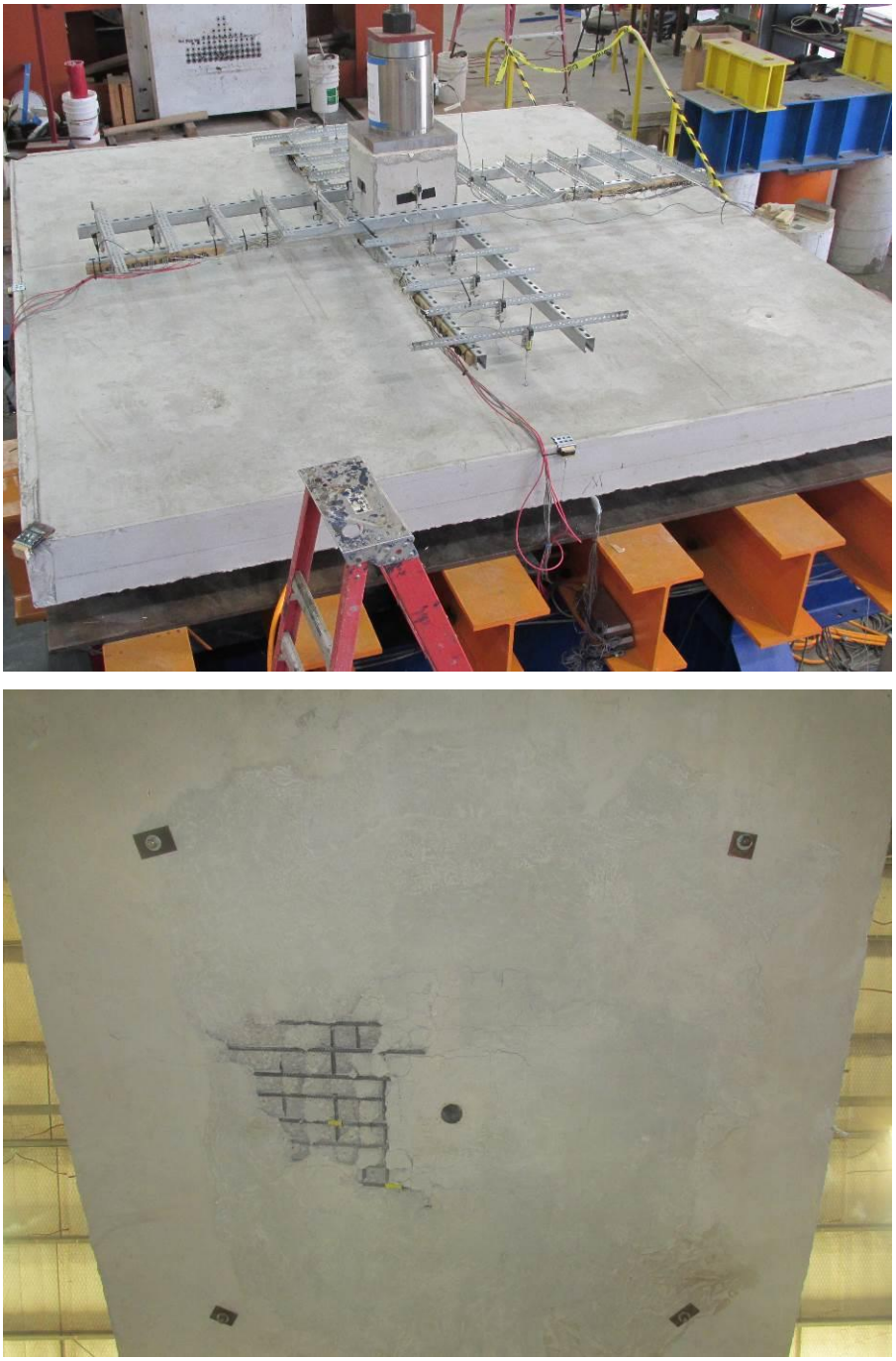

Figure C-2: Cracking observed at failure for test specimen #2: U-1.0

Figure C-3: Cracking observed at failure for test specimen #3: C-0.7

Figure C-4: Cracking observed at failure for test specimen #4: U-0.7

References

American Concrete Institute. "ACI 318-14: Building Code Requirements for Structural Concrete and Commentary." (2008).

Alexander, S. D. B., and N. M. Hawkins. "A Design Perspective on Punching Shear." Special Publication 232 (2005): 97-108.

Bayrak, Oguzhan, and James O. Jirsa. "Two-way shear strength of slab-column connections: Reexamination of ACI 318 provisions." ACI Structural Journal 106.2 (2009): 160.

Birkle, Gerd, and Walter H. Dilger. "Influence of slab thickness on punching shear strength." *ACI Structural Journal* 105.2 (2008): 180.

Einpaul, Jürgen, Carlos E. Ospina, Miguel Fernández Ruiz, and Aurelio Muttoni. "Punching shear capacity of continuous slabs." *ACI Structural Journal* 113, no. 4 (2016): 861.

European Committee for Standardization. “Eurocode 2: Design of Concrete Structures”. (2004)

Gardner, N. J. "ACI 318-05, CSA A23. 3-04, Eurocode 2 (2003), DIN 1045-1 (2001), BS 8110-97 and CEB-FIP MC 90 Provisions for Punching Shear of Reinforced Concrete Flat Slabs." *Special Publication* 232 (2005): 1-22.

Glikman, Mario, Gabriel Polo, Oguzhan Bayrak, and Trevor D. Hrynyk. "Application of an Inclined Shear Reinforcing Assembly for Slab-Column Connections." *Special Publication*321 (2017): 7-1.

Goh, Chong Yik M., and Trevor D. Hrynyk. "Toward Practical Modelling of Reinforced Concrete Flat Slab Systems." IABSE Symposium Report. Vol. 109. No. 51. International Association for Bridge and Structural Engineering, 2017.

Guandalini, Stefano, Olivier L. Burdet, and Aurelio Muttoni. "Punching tests of slabs with low reinforcement ratios." ACI Structural Journal 106.1 (2009): 87.

Hawkins, Neil M., and Denis Mitchell. "Progressive collapse of flat plate structures." Journal Proceedings. Vol. 76. No. 7. 1979.

Code, Model. "Fib model code for concrete structures 2010." *Document Competence Center Siegmar Kästl eK, Germany* (2010).

Joint ACI-ASCE Committee 352. "Recommendations for Design of Beam-Column Connections in Monolithic Reinforced Concrete Structures (ACI 352R-02)." Farmington Hills, Michigan: American Concrete Institute, 2002.

Moehle, Jack P., Michael E. Kreger, and Roberto Leon. "Background to recommendations for design of reinforced concrete slab-column connections." Structural Journal 85.6 (1988): 636-644.

Muttoni, Aurelio. "Punching shear strength of reinforced concrete slabs without transverse reinforcement." ACI structural Journal 105.EPFL-ARTICLE-116123 (2008): 440-450

Wong, P. S., F. J. Vecchio, and H. Trommels. "Vector2 & Formworks user's manual second edition." (2013).

Vita

Leandro Sebastian Montagna was born in Santa Fe, Argentina, on November 8th 1987. During his undergraduate studies at Universidad Tecnologica Nacional (UTN), he was awarded with a scholarship from the German Service for Academic Exchange (DAAD) and assisted the Technische Universität Dresden. After receiving his Bachelor of Science's degree in Civil engineering from UTN, he worked as a structural design engineer for two (2) years before being awarded with the Fulbright Scholarship to pursue graduate studies in the United States. Soon after that, he entered The University of Texas at Austin, where he received his Master of Science in Engineering's degree (Structural engineering focused) in May 2018.

Email Address: leandrosm87@hotmail.com

This thesis was typed by the author.